Instituto Tecnológico y de Estudios Superiores de Monterrey

Campus Monterrey

School of Engineering and Sciences

Assessment of nitrate and sulfate contamination in groundwater using isotopic and hydrogeochemical tools in three aquifer systems of Northern Mexico

A dissertation presented by

Juan Antonio Torres Martínez

Submitted to the
School of Engineering and Sciences
in partial fulfillment of the requirements for the degree of

Doctor of Philosophy

In

Engineering Science

Major in Environmental Systems

Monterrey Nuevo León, December 1st, 2020

Dedicatoria

A mi compañera de vida, Tania, por ser mi soporte e ir de la mano día a día, siempre juntos, siempre fuertes.

A Emma, por llegar a mi vida y darme el último empujón cuando las cosas fueron complicadas, mi luz al final del día.

Acknowledgements

First of all, I would like to express my sincere thanks to my advisors Dr. Jürgen Mahlknecht and Dr. Abrahan Mora, for trusting me in this great adventure and having their continued support despite the ups and downs during my Ph.D. studies. For all the time, patience, motivation, and immense knowledge that you shared with me. All your guidance helped me throughout the research and writing of this thesis.

Besides my advisors, I would like to thank the rest of my thesis committee: Dr. Ismael Aguilar Barajas, Dr. Aldo I. Ramirez, and Dr. Peter Knappett for their insightful comments and encouragement to keep growing with each review.

Muchas gracias a mi familia por apoyarme mamá, papá, hermana, por estar ahí, lejos en el espacio, pero cerca de corazón.

Gracias a Lupita, sin quien el camino hubiera sido más difícil terminar de recorrer.

Gracias a mis amigos, Homero porque fue mi "si tú no te bajas del barco, yo tampoco" durante las horas de plática a pesar de la distancia y el horario, a Nadx, Bernardo y Héctor, porque las risas no faltaron. A Lucas y Amayrani por su apoyo incondicional en la distancia.

My sincere thanks to all the people who motivated me not to give up on the Water Center for Latin America and the Caribbean. To Cristina for her support and hours of conversation in the office, to Álvaro, Rogelio, Mary, and Bolor for all their support.

My acknowledgment to Tecnológico de Monterrey and CONACyT for their support in doctoral scholarships, without which this research would not have been possible.

Gracias a todos los que, en algún momento, me desearon un buen cierre de ciclo, que es hoy.

A todos, gracias, das lo que recibes y espero reciban lo mejor.

Assessment of nitrate and sulfate contamination in groundwater using isotopic and hydrogeochemical tools in three aquifer systems of Northern Mexico

By

Juan Antonio Torres Martínez

Abstract

Nitrate and sulfate comprise a significant portion of ionic charge in most natural waters. Groundwater pollution from nitrate is one of the most prevalent environmental problems. Over the past decades, groundwater quality has deteriorated worldwide due to the intensive use of fertilizers in agriculture, the release of untreated urban sewage and industrial wastewater (e.g., mining, smelting, steel manufacturing, kraft pulp, paper mills, and flue gas desulphurization circuits), and natural sources (natural fertilization, bacterial production, atmospheric deposition). These pollution sources contributed to adverse human and biota effects. Furthermore, arid or semi-arid areas are mainly dependent on groundwater resources, which, together with accelerated population growth, generates water stress and often leads to groundwater quality deterioration. To assess these issues, the origin and biogeochemical transformations of nitrate and sulfate in groundwater have been widely studied since the 1970s. A successful tool for tracing pollution sources is the use of the dual-stable isotopic compositions of nitrate ($\delta^{15}N_{NO3}$ and $\delta^{18}O_{NO3}$) and sulfate ($\delta^{34}S_{SO4}$ and $\delta^{18}O_{SO4}$). Unfortunately, despite the ability of the dual-isotope plot to trace the origin of NO_3^- and SO_4^{2-} contamination, uncertainties remain because two or more sources may sometimes overlap, hindering the correct differentiation of the origin.

For this reason, this Ph.D. research aims to identify and quantify nitrate and sulfate sources in groundwater within three semi-arid areas of Northern Mexico with multiple potential sources using a multi-tracer approach combined with a Bayesian isotope mixing model. The study cases were a highly urbanized industrial area (Monterrey Metropolitan Area), an intensive livestock-agricultural area (Comarca Lagunera Region), and a coastal agricultural aquifer (La Paz aquifer). The approach followed in this research is a useful tool for estimating the contribution of different nitrate and sulfate sources, allowing establishing effective pollution management strategies in contaminated aquifers.

Contents

Chapter 1: General introduction

Water is an essential component that is needed to support life and the ecosystem's health. However, water resources are irregularly distributed in space and time or under high pressure due to the combination of naturally occurring conditions and anthropogenic actions (Thomas and Gibbons, 2018). Groundwater is the largest freshwater reservoir for human use (~ two-thirds of global freshwater resources). However, in arid and semi-arid regions, water scarcity is a natural condition, where groundwater becomes the most important source (Bajaj et al., 2019). This shortage has been intensified by rapid population growth and economic development in the industrial and agricultural sectors. These economic activities increase water resource pressure, modifying their natural water balance (Pereau et al., 2019; Thomas and Gibbons, 2018). Therefore, they generate an environmental concern creating new challenges in controlling water contamination to preserve its quality (Boretti and Rosa, 2019).

Groundwater is widely used because it is relatively technically feasible to access and inexpensive to use due to natural filtration processes that remove surface-derived contaminants (Aeschbach-Hertig and Gleeson, 2012). Globally, approximately 70% of groundwater extraction is used for agriculture (Boretti and Rosa, 2019; Fienen and Arshad, 2016). Following agriculture, the next two most significant water-consuming sectors are industry (19%), followed by domestic water supply (11%; Ritchie and Rose, 2020). Following the global trend, in Mexico, the greatest water-consuming sector is agriculture (76%), followed by domestic water supply (14.4%) and industry (9%). In terms of water source, 36% of the total volume used by irrigation and industry is derived from groundwater, whereas around 60% for domestic water supply (CONAGUA, 2018).

Due to the increased competition for water demand, it is necessary to improve water protection and management and create effective policies. If aquifers are not managed carefully, several consequences commonly result from the overexploitation of groundwater as well as economic activities polluting the land surface and, therefore, water infiltrating into the aquifers (Boretti and Rosa, 2019). Specifically, these consequences include the depletion of groundwater levels, land subsidence, change in flow pattern promoting seawater intrusion, water pollution generated by heavy metals' discharge, organic contaminants, and emerging pollutants in urban environments.

Northern Mexico has an arid climate with frequent droughts. Rare precipitation events are typically derived from hurricanes. Consequently, surface water resources are limited, and cities are highly dependent on aquifers. This region is highly productive economically in the agricultural, livestock, and industrial sectors. Due to the intense anthropogenic pressures on groundwater resources, identifying different contamination sources, including the different biogeochemical transformations of NO_3^- and SO_4^{2-} contamination, is highly necessary, intending to preserve limited resources.

There are different techniques to identify sources of contamination, of which the application of a multi-isotope approach stands out. This approach can describe groundwater mixing processes with different origins and chemical composition, influencing hydrochemistry, and isotope relationships in groundwater. Furthermore, suppose they are correctly applied and combined with Bayesian mixing models. In that case, it is possible to discriminate between the different potential sources to evaluate the biogeochemical processes present in the study area and quantify the contribution of either nitrate or sulfate to groundwater contamination.

Nevertheless, in Mexico, there is only a pair of studies that employed nitrate and sulfate isotopes (Horst et al., 2011; Pastén-Zapata et al., 2014) to differentiate the origin of pollution sources and transformations that affect the composition of groundwater. To our knowledge, this is the first investigation that uses a Bayesian isotope mixing approach for identifying the sources and their contributions to sulfate groundwater pollution. Results derived from this research could be applied by decision-makers or water managers to better understand sources of nitrate and sulfate pollution in aquifers to the scale of nitrate and sulfate's contribution in the watershed and, consequently, integrate this knowledge in the development of groundwater management plans.

1.1 Problem statement

Water in nature (surface or groundwater) is never free of pollution. Typically it contains dissolved solids resulting from water-rock interactions or organic materials. The principal causes of anthropogenic groundwater contamination can be classified as agricultural, industrial, and urban. Human activities produce changes in the groundwater quality of the

different flow systems by introducing pollutants from different sources. This results in three typical water quality issues: 1) land and aquifer salinization processes, 2) mobilization of naturally occurring contamination (As, Fe, F⁻, among others), and 3) pollution derived from chemicals or microorganisms by anthropogenic activities. Anthropogenic groundwater pollution is the consequence of inadequate protection of vulnerable aquifers against the intensification of agricultural cultivation and livestock farming, and discharges and leachates from urban, industrial, and mining activities (Fienen and Arshad, 2016).

1.1.1   Nitrate in groundwater

1.1.1.1   Nitrogen cycle

To better understand the nitrate problem, it is necessary to know the nature of the nitrogen cycle. This is achieved by identifying the different nitrogen sources and the transformations involved throughout their transport in different media. Nitrogen (N) is a biologically active element that participates in many important reactions for the life of ecosystems, which affect water quality. N can be found in the environment in different oxidation states. These different oxidation states are partly owed to a wide variety of sources. N can be found as nitrate (NO_3^-), nitrite (NO_2^-), ammonia (NH_4^-), organic compounds of N (N_{org}), among others.

The N biogeochemical cycle involves different N forms and, therefore, different transformations by which they enter the environment. The main transformations that can typically be identified in the environment are fixation, volatilization, assimilation (uptake by plants, immobilization in soil), mineralization, nitrification, heterotrophic and autotrophic denitrification, dissimilatory nitrate reduction to ammonium (DNRA), and anammox (**Table 1.1**). Most of these processes are realized by microbes and directly affect N availability and the organic matter pool. N's behavior in the environment is closely linked to the redox cycle of C, S, P, and trace elements such as Fe and Mn.

Table 1.1. Biogeochemical transformations in the nitrogen cycle

Reaction	Formula	O_2 environment
Fixation	$N_2 \rightarrow N_{org}$	Aerobic
Mineralization	$N_{org} \rightarrow NH_3, NH_4$	Both
Nitrification	$NH_4 \rightarrow NO_2 \rightarrow NO_3$	Aerobic
Immobilization	$NO_3, NH_4 \rightarrow N_{org}$	Aerobic
Denitrification	$NO_3 \rightarrow NO_2 \rightarrow N_2$	Anaerobic
Annamox reaction	$NO_2, NH_4 \rightarrow N_2$	Anaerobic

Source: adapted from Bernhard, 2010; and Stein and Klotz, 2016

1.1.1.2 Groundwater nitrate pollution

Nitrogen is one of the primary nutrients for the survival of all organisms (Bernhard, 2010); however, there has been a substantial increase in nitrate concentrations in surface water (e.g., Lassaletta et al., 2009; Xia et al., 2018) and groundwater (e.g., Ducci et al., 2019; Serhal et al., 2009) worldwide. This increase is mainly associated with the intensive use of fertilizers in agriculture, untreated industrial wastewater, urban sewage, or natural sources (natural fertilization, bacterial production, and atmospheric deposition).

Exceeding the maximum permitted limit of nitrate in water for human consumption (50 mg/L as NO_3^-) established by the World Health Organization (WHO) (WHO, 2017) produces considerable impacts on public health. Some of these consequences are methemoglobinemia in children under six months of age (blue-baby syndrome), congenital disabilities result from ingesting during pregnancy, colorectal cancer, thyroid disease, and neural tube defects (Leslie and Lyons, 2018; Ward et al., 2018).

1.1.2 Sulfate in groundwater

1.1.2.1 Sulfur cycle

Sulfur (S), similar to nitrogen, is a biologically active element involved in different essential activities in the environment (Valiente et al., 2017). S could be found in the environment in different oxidation states and, because of a wide variety of potential sources, it could be found as hydrogen sulfide (H_2S), sulfate (SO_4^{2-}), sulfite (SO_3^{2-}), among others. Human activities have an essential effect on the global sulfur cycle. For example, the burning of coal, natural gas, or other fossil fuels has increased the amount of S in the atmosphere, resulting in the entire S cycle.

The global sulfur cycle also includes transformations of the different sulfur species through oxidation states. Furthermore, these transformations play an important role in geological and biological processes. The most critical processes in this cycle are organic sulfur mineralization, hydrogen sulfide oxidation, dissimilative reduction, desulfurization, or bacterial sulfate reduction. Almost all of these processes are carried out by plants, fungi, or bacteria and are closely related to the carbon cycle.

1.1.2.2   Groundwater sulfate pollution

Sulfate is another ubiquitous element dissolved in water bodies, arising as a pollutant of surface and groundwater. The origin of this pollution could be derived from natural processes such as water-rock interaction, atmospheric deposition, geothermal processes, or seawater intrusion; however, another important source is the result of different anthropogenic activities as domestic wastewater, industrial waste, or agrochemical sources (Fernando et al., 2018; Galhardi and Bonotto, 2016; Hosono et al., 2011a).

Unlike nitrate, there is no maximum permissible concentration limitation for sulfate in water since no diseases relevant to human health have been associated. Nevertheless, the WHO (WHO, 2017) issued a recommendation to have concentrations below 500 mg/L in water for human consumption to avoid children's gastrointestinal diseases.

1.2   Research questions

Isotope hydrology is considered the most promising modern hydrological tool for water resource managers. Environmental isotope applications in the hydrological issues are based on the tracer concept used to understand hydrological processes. In groundwater, the main application of these techniques includes the age dating of groundwater, the identification of aquifer recharge and discharge processes, or the description of sources, fate, and contaminants' processes.

Nowadays, globally, aquifers' non-point anthropogenic contamination is one of the significant challenging water management issues. Hence, environmental isotopes such as combining $\delta^{15}N$, $\delta^{34}S$, or $\delta^{18}O$ are increasingly applied to describe the contaminant pathways and help plan suitable aquifer protection strategies. Therefore, this proposal is focused on

try to use different isotope techniques and chemical analyses to answer the questions in semi desertic aquifers in many perspectives, trying to answer the following questions:

- What processes are involved or control the groundwater chemistry?
- Which hydrochemical factors affect the variations in the concentration of nitrate and sulfate in groundwater?
- Which of the different pollution sources is mainly affecting the amount of nitrate and sulfate in groundwater?
- How much nitrate or sulfate in groundwater is derived from each pollution source?

1.3 Research objectives

1.3.1   Overall objective

Following the previously described problem, the main objectives of this research aim to evaluate the processes that control the chemistry of groundwater and identify and quantify the contribution of different sources of nitrate and sulfate in different aquifer systems. This methodology will be applied in three semi-desert areas under hydric stress with continuous economic growth in the north of Mexico.

1.3.2   Specific objectives

The main specific aims of the research are:

i)   To characterize the hydrochemical factors that affect the nitrate and sulfate concentration in groundwater, determine the influence of local and regional groundwater mixing over NO_3^- and SO_4^{2-} pollution evolution.

ii)   To determine and evaluate the different natural attenuation processes that occur employing the different isotopic compositions (H-O-N-S) and the other ions (SO_4^{2-}, NO_3^-, HCO_3^-, Cl^-) involved in the chemical reactions that control these processes.

iii)   To develop a Bayesian isotope mixing model that apportions NO_3^- and SO_4^{2-} in groundwater to sources and implement this model across different semi-arid regions of Mexico.

1.4 Dissertation organization

The structure of the Ph.D. document is intended as a series of chapters modified from journal articles published (chapters 2, 3) or under review (chapter 4), as follows:

- **Chapter 1** embodies a general introduction of nitrate and sulfate pollution, research questions, objectives, and thesis outline.
- **Chapter 2** is adapted from the published article "*Tracking nitrate and sulfate sources in groundwater of an urbanized valley using a multi-tracer approach combined with a Bayesian isotope mixing model*." It is based on an analysis of the different pollution sources affecting the levels of nitrate and sulfate in groundwater in a highly industrial and urbanized area, showing the advantage of using the Bayesian isotope mixing model (BIMM). This chapter will incorporate the use of hierarchical cluster analysis and, for the first time, the use of sulfate isotopes in BIMM.
- **Chapter 3** is adapted from the published article *"Estimation of nitrate pollution sources and transformations in groundwater of an intensive livestock-agricultural area (Comarca Lagunera), combining major ions, stable isotopes and MixSIAR model."* This chapter comprises a Bayesian isotope mixing model, including the pollution sources generated by agricultural areas, adopting a compositional data transformation to improve the hierarchical cluster analysis results and uncertainty analysis of BIMM's results.
- **Chapter 4** is based on the under review article *"Determining nitrate and sulfate pollution sources and transformations in a coastal aquifer impacted by seawater intrusion—A multi-isotopic approach combined with Self-organizing maps and a Bayesian mixing model."* This chapter is based on analyzing the different pollution sources affecting the nitrate and sulfate levels in groundwater in a coastal agricultural area, employing a multi-isotopic approach (^{15}N, ^{34}S, ^{18}O, ^{2}H). Different from chapters 2 and 3, it incorporates an artificial neural network approach (Self-organizing map) combined with a K-means cluster analysis. Furthermore, it includes, for the first time, a sulfate BIMM, which includes the effect of seawater intrusion, as well as an uncertainty analysis for sulfate models.
- **Chapter 5** summarizes the main findings drawn from the three presented research papers. It also aims to highlight how this knowledge could inform additional research

in the future. It also provides recommendations for future research on the understanding of nitrate and sulfate pollution in groundwater.

- **Appendix.** It includes three sections, which contain extra information related to chapters 2, 3, and 4.
- **References**

Chapter 2: Monterrey Metropolitan Area Case

This chapter is adapted from the published article

2.1 Introduction

Nitrate and sulfate comprise a major portion of ionic charge in most natural waters. Both ions are included in international regulations and recommendations due to their adverse effects on humans at high concentrations. The World Health Organization (WHO) guideline value for nitrate in drinking water is 50 mg/L (as nitrate ion), based on the absence of adverse health effects at concentrations below this value in epidemiological studies (WHO, 2017). Meanwhile, no adverse human health effects have been identified for sulfate. However, too much of this anion in drinking water may cause taste impairment and laxative effects. Therefore, the maximum concentration of sulfate recommended by the WHO in drinking water is 250 mg/L (WHO, 2017).

Groundwater pollution from nitrate is one of the most prevalent environmental problems (Burow et al., 2010; Meghdadi and Javar, 2018b; Popescu et al., 2015; Yang et al., 2016). Over the past decades, groundwater quality has deteriorated worldwide due to the intensive use of fertilizers in agriculture, the release of untreated urban sewage and industrial wastewater, and natural sources (natural fertilization, bacterial production, atmospheric deposition) (Ducci et al., 2019; Harter et al., 2012; Serhal et al., 2009). Besides adverse human effects, such as methemoglobinemia, thyroid effects, congenital disabilities, and cancer of the digestive tract, excess nitrate in surface waters can also contribute to acidification, eutrophication and be toxic to aquatic ecosystems (Camargo and Alonso, 2006; Leslie and Lyons, 2018; Ward et al., 2018). The treatment of contaminated water and remediation of polluted sites for water supply leads to elevated costs and other undesired side effects, such as brines' disposal. Nontreatment strategies to address impacted water sources can sometimes provide less costly solutions through wellhead protection, land use management, well abandonment, source modification, development of alternative sources, including consolidation or connection to a nearby system, or blending (Jensen et al., 2014; Ruiz-Beviá and Fernández-Torres, 2019).

Sulfate is a typical anion in water and traditionally neglected as pollution in the groundwater (Wang and Zhang, 2019). It is discharged into the water as part of domestic wastewaters, industrial wastes, and wastewaters (e.g., mining, smelting, steel manufacturing, kraft pulp, paper mills, and flue gas desulphurization circuits), through geothermal processes, seawater intrusion, and atmospheric deposition. However, the highest levels in groundwater usually are from natural sources such as sulfate minerals (e.g., gypsum), oxidation of sulfide minerals (e.g., pyrite), rainfall, and volcanic activity (Fernando et al., 2018; Galhardi and Bonotto, 2016; Hosono et al., 2011a; Li et al., 2015). Besides several diseases after excessive uptakes, such as diarrhea, dehydration, and gastrointestinal disorders (Backer, 2000; Leslie and Lyons, 2018), sulfate may be transformed in the aquatic systems into toxic substances under certain conditions, resulting in the death of particular fauna and flora and place some constraints on industrial, municipal and residential water systems such as clogging, leading to increased pumping energy, reduced heat transfer efficiency, and clogging of equipment. Further, the reduction of sulfate by bacteria produces H_2S gas, corrosive to metals and concrete (Man et al., 2014; Soucek and Kennedy, 2005; Zuo et al., 2018).

According to past trends, it is expected that constant increases in urbanization and seasonally intensified fertilizer applications enhance nitrate loads in groundwater. Similarly, it is supposed that sulfate loads in groundwater increase due to not only anthropogenic sources but also due to increasing extraction of groundwater resources from deeper geological formations in water-scarce areas and mining activities (Archana et al., 2018; Horst et al., 2011; Kinnunen et al., 2018). Therefore, developing cost-effective methods to prevent, remove, or reduce nitrate and sulfate from water are of considerable significance to meet the regulatory limits. The concentrations of these anions are measured routinely in groundwater monitoring programs and studies. However, this may not be sufficient to assess existing or potential groundwater remediation options (e.g., pump-and-treat, phytoremediation, in-situ bioremediation, in-situ denitrification) because these anions originate each from multiple sources and undergo various biogeochemical processes (Biddau et al., 2019; King et al., 2012).

Tools based on environmental tracers have been developed since the 1970s to identify contamination sources and monitor their fate and natural attenuation processes for better management of water resources (Clark and Fritz, 1997; Kendall, 1998). The first attempts of using nitrate isotopes used $\delta^{15}N_{NO3}$ as a single tracer (Flipse Jr. and Bonner, 1985; Kreitler, 1979; Mariotti et al., 1988; Mariotti and Létolle, 1977). Nevertheless, the use of a single isotope is not a conclusive tool for the identification of nitrate sources, given that there is interference caused by processes of volatilization, nitrification, denitrification, or oxidation generating overlaps between the ranges of identification of the different pollution sources (Clark and Fritz, 1997; Kaown et al., 2009). Similarly, the use of a single isotope is not sufficient for the identification of sulfate sources.

Thus, a dual-isotope approach of $\delta^{15}N_{NO3}$ combined with $\delta^{18}O_{NO3}$, and $\delta^{34}S_{SO4}$ combined with $\delta^{18}O_{SO4}$, respectively, improved the capability to identify sources and track transformation processes of nitrogen and sulfate in aquatic systems (Aravena et al., 1993; Bottrell et al., 2008; Fukada et al., 2004, 2003; Kaown et al., 2009; Mattern et al., 2011; Mingzhu et al., 2014; Murgulet and Tick, 2013; Robinson and Al Ruwaih, 1985; Samborska et al., 2013; Spalding et al., 2019; Strebel et al., 1990; Umezawa et al., 2008). Other studies developed a multi-isotopic assessment (H–O–C–N–S) (Aravena and Robertson, 1998; Einsiedl et al., 2009; Hosono et al., 2011b, 2009; Peters et al., 2015; Pittalis et al., 2018; Xie et al., 2013)

and probability mixing models (Jin et al., 2018; K.-H. Kim et al., 2015; Li et al., 2019; Matiatos, 2016; Meghdadi and Javar, 2018a; Ransom et al., 2016; Xue et al., 2012; M. Zhang et al., 2018; Y. Zhang et al., 2018a) to estimate the provenance and apportionment of nitrates in groundwater. This investigation aims to identify and quantify nitrate and sulfate sources in groundwater within an area with multiple potential sources using a multi-tracer approach combined with a Bayesian isotope mixing model. To our knowledge, this is the first study to apply a Bayesian isotope mixing model for tracing the sources and contribution of sulfate in groundwater of a contaminated aquifer.

The selected area is semi-arid Monterrey Valley, located in northeastern Mexico. This urbanized area has a record of elevated nitrate and sulfate concentrations in groundwater (IANL, 2007; Ledesma-Ruiz et al., 2015; Pastén-Zapata et al., 2014). A preliminary investigation assessing major and trace hydrochemistry suggests that along the groundwater flow path, there is an increasing gradient of sulfate and nitrate concentration exceeding 10% and 35% of the samples the threshold for drinking water, respectively. The increasing nitrate concentrations could potentially be infiltration of polluted water from the land surface or leakage from buried urban sewage pipes. In contrast, industrial activities on the land surface or rock weathering processes may account for the rising sulfate concentrations along a flow path (Mora et al., 2017). Previous works refer to the use of major ions and trace elements for determining the main hydrochemical characteristics, thus inferring some natural and anthropogenic pollution sources. However, these approaches were not conclusive for identifying anthropogenic sources. Therefore, this chapter aims to identify and quantify nitrate and sulfate's relative contributions from different groundwater sources and processes within the Monterrey area. This will be achieved by: (1) characterizing the hydrochemical factors that affect the nitrate and sulfate concentration in groundwater and identifying the main contributors by using multivariate statistical techniques and dual isotopic composition; and (2) using an isotopic mixing model to quantify the groundwater nitrate and sulfate sources. The results are useful for decision-makers or water managers to better understand groundwater nitrate and sulfate pollution at the scale across which nitrate and sulfate is added to and accumulates within a watershed and its underlying aquifer system and integrate this knowledge into the development of groundwater management plans.

2.2 Materials and methods

2.2.1 Study area description

Monterrey (~4.7 million inhabitants) is among the three largest metropolitan areas of Mexico in terms of population and also has among the top three economic growths of metropolitan areas (CONAPO, 2015). It is an important industrial and business center covering 6,680 km^2 and hosting many national and international companies. Located north-northeast of the foothills of Sierra Madre Oriental (SMO) mountain range, this area is a hilly region with mountains rising in the west (Las Mitras) and southeast (La Silla) of the city and elevations varying from 260 to 3000 m above sea level (m.a.s.l.) (**Fig. 2.1**). The climate is semi-arid with annual mean precipitation and temperature of 622 mm and 22.3 °C, respectively, with spatiotemporal variations for monthly average precipitation between 14.1 and 150.6 mm, and monthly average temperature ranging from 14.5 to 28.4 °C (**Fig. A1.1 of Appendix 1**) (Aguilar-Barajas et al., 2019, 2015; Ortega-Gaucin, 2012; Sisto et al., 2016).
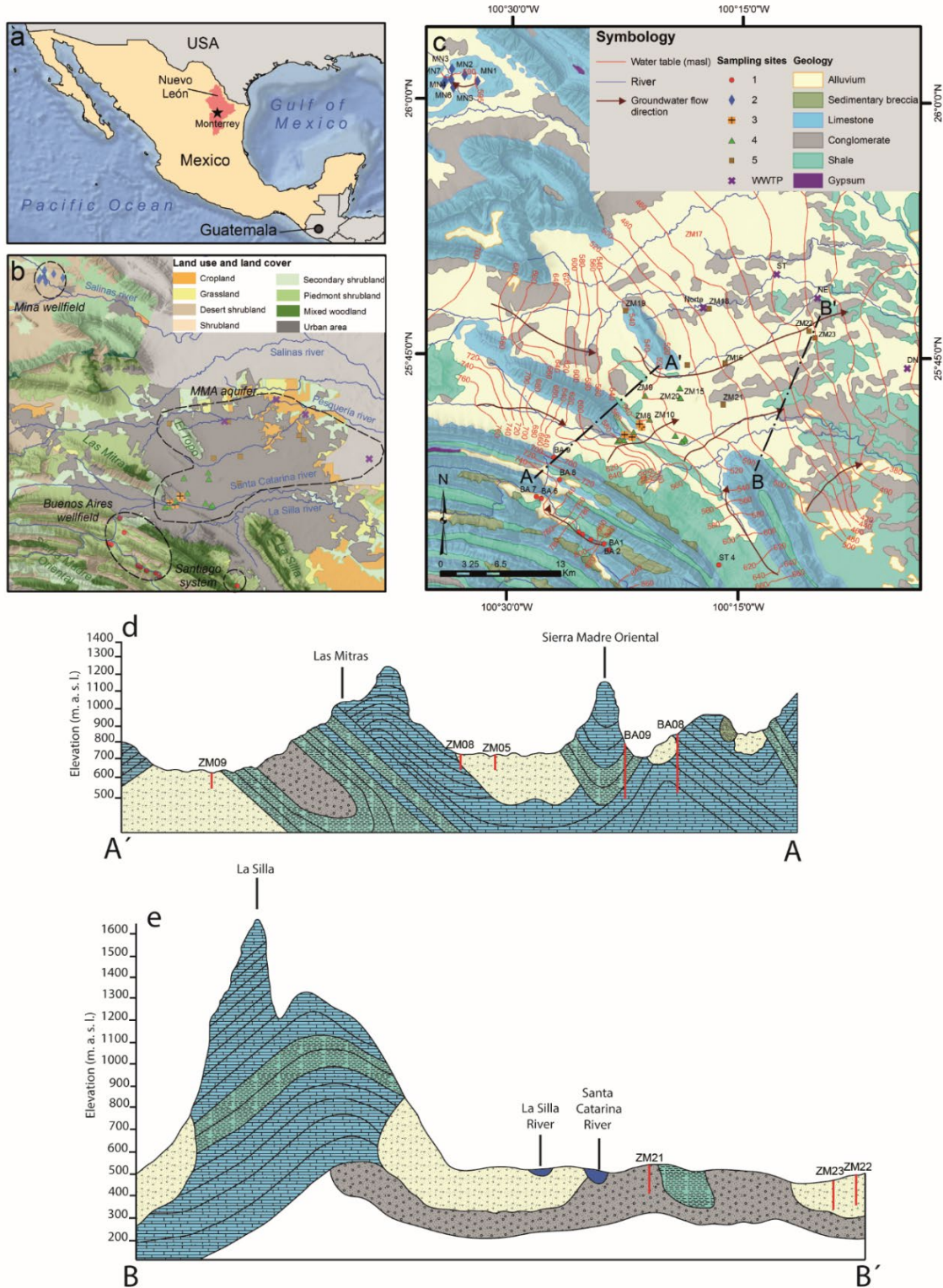
Fig. 2.1 (a) Location of the Monterrey Metropolitan Area (MMA) and the State of Nuevo Leon within Mexico, (b) land use and land cover, (c) surficial geology, and (d, e) hydrogeological cross-sections. Panels b and c include the locations of wells sampled for chemical and isotopic analysis.

Groundwater provides approximately 40% of the urban water supply and is extracted mainly from three different aquifers or wellfields. These will be referred to herein as the Buenos Aires wellfield, Mina wellfield, and Monterrey Metropolitan Area (MMA) aquifer. The Buenos Aires wellfield supplies approximately half of Monterrey's total municipal water, covering the southwestern part of the city (Oesterreich and Medina Aleman, 2002). This wellfield consists of 42 deep production wells (usually >700 m deep, and water level oscillating between 12 and 120 m below ground level) delivering high-quality drinking water (twenty-six of these wells (62%) are used for drinking water supply), mainly from confined, Early Cretaceous limestone formations (Cupido, Aurora, Cuesta del Cura) from the Buenos Aires valley. The valley lies at a higher elevation than the city, so the cost of conveying the water is low (CONAGUA, 2015a; DOF, 2011). Horizontal infiltration galleries (Santiago system) also tap into this aquifer system (**Fig. 2.1c**).

The Mina wellfield lies northeast of Monterrey. It consists of 83 production wells, which are much shallower than those in the Buenos Aires wellfield (usually <100 m deep, and an average depth of water table level below the surface of 30 m). Twenty-six of these wells (31%) are used for drinking water supply. The wells pump groundwater from mostly confined Early Cretaceous limestone formations (Cupido, Aurora) (CONAGUA, 2015b; DOF, 2011; González Sánchez et al., 2007; Ramírez Gutiérrez, 2011; Sanchez et al., 2018).

Lastly, the MMA aquifer consists of approximately 1148 shallow production wells (usually <100 m deep, and an average groundwater level of 20 m below ground level) dispersed throughout the Monterrey urban and peri-urban area. Of these, only 264 (23%) are used for potable water supply. The groundwater of this wellfield is extracted from an unconfined aquifer mainly comprised of altered lutites (Mendoza formation), conglomerates (Reynosa formation), gravels, clays, and sands from Tertiary (CONAGUA, 2015c; Dávila Pórcel, 2011; DOF, 2011; Salinas Jasso, 2014).

Significantly, the land above the MMA aquifer is primarily urban, whereas the land overlying the Buenos Aires and Mina wellfields is piedmont and desert shrubland, and mixed woodland (**Fig. 2.1b**).

2.2.2 Sampling and laboratory analysis

Thirty-nine groundwater production wells, one spring, and the influent of 4 principal wastewater treatment plants (WWTP) were sampled (**Fig. 2.1b and c**). Sites were selected using criteria such as their geographic distribution and representation of different well fields and aquifers, and relevance for the Monterrey water supply system. Previous sampling campaigns were conducted in November of 2006 and April of 2012. The sampling for this research was performed in mid-summer (July 2017), representing the end of the dry season (monthly average precipitation and temperature of 43 mm and 28.4 °C, respectively). Temperature, pH, electrical conductivity (EC), dissolved oxygen (OD), salinity, total dissolved solids (TDS), and oxidation-reduction potential (ORP) were determined in-situ using a pre-calibrated multi-meter (Hydrolab HL4, OTT Hydromet, USA). Carbonate species (HCO_3) were determined in filtered water samples onsite using the acid titration method (H_2SO_4 0.02N) until the endpoint of pH 4.3. Each water sample was filtered using a 0.45 μm acetate cellulose membrane and then transferred into a pre-washed and pre-rinsed low-density polyethylene (LDPE) bottle of 250 mL and stored at 4 °C during a week prior to laboratory analysis. The samples taken for $\delta^{15}N_{NO3}$ and $\delta^{18}O_{NO3}$ analysis were frozen. Cation samples were preserved with 1 mL of ultrapure HNO_3 to a pH < 2 avoiding major element precipitation/adsorption during storage.

Concentrations of major cations (Na^+, K^+, Ca^{2+}, Mg^{2+}) were measured using a Perkin Elmer Optima 2100DV inductively coupled plasma optical emission spectrometry (ICP-OES), while concentrations of anions (Cl^-, SO_4^-, F^-, NO_3^-, Br^-, and I^-) were analyzed using a Dionex DX-120 ion chromatograph (IC). Measurement uncertainties for all parameters were evaluated in the laboratory using duplicate samples and verifying the instruments' precision and accuracy with regular comparisons to known standards. The QA/QC procedure followed indicated that analytical error was within±5%.

The stable water isotopes ($\delta^{18}O_{H2O}$ and δ^2H_{H2O}) were analyzed using a Liquid Water Isotope Analyzer (LWIA) (Los Gatos Research (LGR), Mountain View, CA, USA, model T-LWIA-45-EP). Analyses were carried following the methodology described by Lis et al. (2008). A suite of water standards calibrated to the international reference materials VSMOW (Vienna Standard Mean Ocean Water) and VSLAP (Vienna Standard Light Antarctic Precipitation)

were used for quality control. The analytical precision for $\delta^{18}O_{H2O}$ and δ^2H_{H2O} were ±0.2‰, and ±0.8‰, respectively.

The stable isotope analyses of nitrate and sulfate were performed at the Environmental Isotope Laboratory at the University of Waterloo. The nitrate isotopes ($\delta^{15}N_{NO3}$ and $\delta^{18}O_{NO3}$) were measured based on the chemical reduction method (Granger et al., 2006; McIlvin and Altabet, 2005; Ryabenko et al., 2009; Ti et al., 2018), reducing NO_3 to NO_2 by a cadmium catalyst, subsequently chemically converting to N_2O, and finally analyzing in a Trace Gas-GVI IsoPrime-IRMS (TG-IRMS). For quality control purposes, three calibrated standards, USGS 34, USGS 35, and in-house EGC 17, were used for normalization. The analytical precision was ±0.3‰ for $\delta^{15}N_{NO3}$ and ±0.8‰ for $\delta^{18}O_{NO3}$.

The isotopic composition of sulfate ($\delta^{34}S_{SO4}$ and $\delta^{18}O_{SO4}$) was determined through acidification to pH = 3, boiling, and precipitating of $BaSO_4$ by the addition of $BaCl_2$. The $BaSO_4$ was recovered by washing and oven-drying to 80 °C. After that, the dried $BaSO_4$ was thermally decomposed in an elemental analyzer to SO_2 and a pyrolysis reactor to CO for subsequent sulfur and oxygen isotope ratio measurements, respectively, that were normalized with IAEA SO-6 and NBS-127 standards. The analytical precision for $\delta^{34}S_{SO4}$ and $\delta^{18}O_{SO4}$ was ±0.3‰ and ±0.5‰, respectively.

The stable isotope ratios relative to Air ($\delta^{15}N_{NO3}$), to the Vienna Standard Mean Ocean Water (VSMOW) ($\delta^{18}O_{NO3}$, $\delta^{18}O_{H2O}$, δ^2H_{H2O}, $\delta^{18}O_{SO4}$), and the Vienna Cañon Diablo Troilite (VCDT) ($\delta^{34}S_{SO4}$) are expressed using the standard definition of the δ value of the heavier isotope (h) of a given chemical element (E),

$$\delta\ ^hE = \frac{R_{sample} - R_{std}}{R_{std}} \qquad \text{(Eq. 2.1)}$$

where R represents $^{15}N/^{14}N$ for $\delta^{15}N$, $^{18}O/^{16}O$ for $\delta^{18}O$, $^2H/^1H$ for δ^2H, $^{34}S/^{32}S$ for $\delta^{34}S$ in samples (R_{sample}) and standards (R_{std}) (Kendall et al., 2008).

2.2.3 Interpretation techniques

Statistical analyses were performed with the software SPSS 25.0 (IBM, 2017). Historical chemical data from the BA, MMA, and ST were obtained for 2006 and 2012 (Mora et al., 2017). Fifteen sampling points from different campaigns (2006, 2012, 2017) were compared using a Kruskal-Wallis test to elucidate the different parameters' trends.

A hierarchical cluster analysis (HCA) was applied to identify groups that demonstrate similar water chemistry and isotopic ratios. The HCA was performed using 24 variables (temperature, pH, electrical conductivity, oxidation-reduction potential, total dissolved solids, dissolved oxygen, Ca^{2+}, Mg^{2+}, Na^+, K^+, HCO_3^-, SO_4^{2-}, Cl^-, NO_3^-, F^-, B^-, Br^-, I^-, $\delta^{18}O_{NO3}$, $\delta^{18}O_{H2O}$, δ^2H_{H2O}, $\delta^{18}O_{SO4}$, $\delta^{15}N_{NO3}$, $\delta^{34}S_{SO4}$) employing the average linkage rule of Ward's method. Once the groups were identified, the nonparametric Kruskal-Wallis test was used to establish significant differences between chemical and isotopic datasets among the different groups generated by the HCA. A principal component analysis (PCA) was implemented after the HCA to explain the possible contributors to the total chemical variance controlled by different processes defined by one or more natural/anthropogenic factors. The varimax normalized rotation method was implemented as factor rotation to significantly distribute weights with geochemical data (Charizopoulos et al., 2018; Das et al., 2018; Tiwari et al., 2019). The Kaiser-Meyer-Olkin (KMO) and Bartletts' tests were used to verify the PCA's adequacy, with KMO values of more than 0.7 and Bartlett's significance values lowers than 0.05 (IBM, 2017; Meghdadi and Javar, 2018a).

Halides (Br^-, Cl^-, and I^-) were used to identify potential pollution sources in the solutes. These elements have a conservative nature, resulting in the minimum amount of interactions with the groundwater flow and subsoil (Panno et al., 2006; Pastén-Zapata et al., 2014). These techniques have been adapted from several previous studies which used the relations Cl^-/Br^- vs. Cl^- (Alcalá and Custodio, 2008; Katz et al., 2011; Khazaei and Milne-Home, 2017; McArthur et al., 2012; Panno et al., 2006; Whaley-Martin et al., 2017), I^-/Na^+ vs. Br^- (Panno et al., 2006; Pastén-Zapata et al., 2014), B^-/Cl^- vs. Br^-/Cl^- (Awaleh et al., 2017; Vengosh, 2014), and NO_3^-/Cl^- vs. Cl^- (Lu et al., 2015; Yue et al., 2017; Zeng and Wu, 2014) in combination with diverse end-members to differentiate pollution sources besides mixing and transformation processes.

To estimate the relative contribution of different nitrate and sulfate sources in water samples, the Bayesian isotope mixing model MixSIAR (Stock and Semmens, 2016) was employed. MixSIAR is a combination of models integrated by IsoSource (Phillips and Gregg, 2003), MixSir (Moore and Semmens, 2008), SIAR (Parnell et al., 2010), IsotopeR (Hopkins and Ferguson, 2012), FRUITS (Fernandes et al., 2014) and others. It has been used to assess the contributions of pollution sources such as NO_3^- (Griffiths et al., 2016; M. Zhang et al., 2018), heavy metals (Kong et al., 2018; Longman et al., 2018), and sediments (Blake et al., 2018; Dang et al., 2018; Dutton et al., 2019; Liu et al., 2017; Smith et al., 2018; Upadhayay et al., 2018). The authors are not aware of a previous study that assesses the contribution of sources of SO_4 using these techniques. The mixing model for a set of N mixture measurements with j isotopes and k sources is described by the following equations (Parnell et al., 2010):

$$X_{ij} = \sum_{k=1}^{k} p_k \left(S_{jk} + C_{jk} \right) + \varepsilon_{ij} \qquad \text{(Eq. 2.2)}$$

$$S_{jk} \sim N(\mu_{jk}, \omega_{jk}^2) \qquad \text{(Eq. 2.3)}$$

$$C_{jk} \sim N(\lambda_{jk}, \tau_{jk}^2) \qquad \text{(Eq. 2.4)}$$

$$\varepsilon_{ij} \sim N(0, \sigma_j^2) \qquad \text{(Eq. 2.5)}$$

Where X_{ij} represents the isotope value j of the mixture i, in which $i = 1, 2, 3, …, N$ and $j = 1, 2, 3, …, J$; S_{jk} indicate the source value k of isotope j ($k = 1, 2, 3, …, K$), which is normally distributed with mean μjk and standard deviation ωjk; pk is the proportional contribution of source k, which is estimated by the MixSiar model; Cjk describes the isotope fractionation factor of isotope j on source k, which follow a normal distribution with mean λjk and standard deviation τjk; and εij is the residual error representing the additional unquantified variation between individual mixtures, which follows a normal distribution with mean zero and standard deviation σj. More detailed information on the MixSiar model can be found in Stock et al. (2018). In this study, the mean values (μjk) and standard deviations (ωjk) of nitrate, sulfate, and oxygen isotopes associated with different end-members were obtained from previous studies.

2.3 Results

2.3.1 Spatial and temporal trends of groundwater chemistry

To evaluate groundwater chemistry changes over time, the Kruskal-Wallis test (K–W) was applied in three different zones: MMA aquifer, Buenos Aires wellfield, and Santiago system. The test evaluated if there are significant differences (p-value < 0.05) between the years 2006, 2012, and 2017 (**Table 2.1**).

The results show no significant differences in temperature, pH, Ca^{2+}, Mg^{2+}, Na^+, K^+, NO_3^-, and HCO_3^- for the Buenos Aires wellfield; nevertheless, Cl and SO_4 concentrations increase two-fold between 2012 and 2017. For the MMA aquifer, there are no significant differences in any of the parameters over time, except for reduced K^- concentrations in 2017. The Santiago System shows no significant differences in any parameter. The values of physicochemical and isotopic parameters of 2017 are shown in **Table A1.1** of **Appendix 1**. According to their statistical similarities and geographic correspondence, samples were classified into five groups to understand local geochemical trends (**Fig. 2.2**). The obtained clusters were spatially defined as follow: Group 1 comprises samples collected from the Buenos Aires wellfield and La Estanzuela spring; Group 2 represents wells located in Mina wellfield; Group 3, 4, and 5 are all located in the MMA aquifer and represent samples in the recharge area, transition zone and discharge area of this aquifer, respectively. **Table 2.2** shows the statistical summary of physicochemical parameters and isotopic ratios of each group.

Across all five groups, the average temperature varies substantially between 22.9 and 30.4°C, whereas the average pH ranges over a narrow interval of near-neutral values from 7.0 to 7.4. Across all groups, anion concentrations decreased in the order: HCO_3^- > SO_4^{2-} > Cl^- > NO_3^-. In contrast, cation concentrations decreased in the order: Ca^{2+} > Mg^{2+} > Na^+ > K^+ for groups 1 and 3; and Ca^{2+} > Na^+ > Mg^{2+} > K^+ for groups 2, 4 and 5. The synthetic parameters (HCO_3^--(SO_4^{2-}+Cl^-)) and ((Ca^{2+}+Mg^{2+})-(Na^++K^+)) were plotted against each other as a scatter plot (Chadha, 1999) to evaluate the hydrogeochemical processes that control groundwater chemistry (**Fig. 2.3a**).

Table 2.1. Temporal comparison of physicochemical parameters of groundwater samples in different areas of the Monterrey valley. Mina wellfield is not included because this zone was not considered in the 2006 and 2012 sampling campaign. Note: K–W indicates the significance level (p) of the Kruskal-Wallis test with the gray shaded areas indicating a significant difference across the three sampling years; BA = Buenos Aires, MMA = Monterrey Metropolitan Aquifer, ST = Santiago System.

Zone	Year	n	T (°C)	K-W	pH	K-W	Ca (mg/L)	K-W	Mg (mg/L)	K-W	Na (mg/L)	K-W
	2006	5	22.20±1.26	0.98	7.46±0.06	0.93	71.74±1.29	0.93	13.08±3.49	0.85	3.67±1.51	0.91
BA	2012	4	21.78±0.45	0.32	7.49±0.18	0.053	71.15±1.60	0.11	11.08±0.61	0.44	3.00±0.69	0.40
	2017	9	22.99±1.39		7.26±0.11		74.76±3.78		9.97±2.06		2.33±0.85	
	2006	9	26.11±2.79	0.97	7.23±0.31	0.70	136.10±52.10	0.61	21.75±13.77	0.66	56.10±66.80	0.57
MMA	2012	7	26.44±2.80	0.82	7.38±0.32	0.19	159.90±64.10	0.47	27.90±15.67	0.13	73.80±72.50	0.20
	2017	23	26.38±2.28		7.13±0.18		129.58±41.32		16.50±5.90		37.75±35.73	
	2006	8	19.13±2.54	0.66	7.31±0.49	0.26	120.70±40.90	0.97	5.56±1.82	0.50	6.52±4.59	0.95
ST	2012	6	20.64±1.31	0.98	7.68±0.22	0.98	101.10±41.00	0.44	7.60±3.72	0.81	4.06±1.63	0.11
	2017	4	20.89±0.64		7.57±0.44		82.79±14.52		6.09±2.57		2.58±0.39	

Zone	Year	n	K (mg/L)	K-W	Cl (mg/L)	K-W	SO$_4$ (mg/L)	K-W	HCO$_3$ (mg/L)	K-W	NO$_3$ (mg/L)	K-W
	2006	5	0.86±0.16	0.68	-	-	-	-	241.80±51.40	0.34	-	0.09
BA	2012	4	0.71±0.07	0.08	2.05±0.51	0.01	22.85±8.22	0.045	214.80±32.70	0.44	1.10±0.22	-
	2017	9	0.47±0.09		3.91±1.24		42.37±19.56		244.51±6.04		1.27±0.33	
	2006	9	2.00±1.37	0.67	58.80±59.00	0.48	130.40±117.50	0.67	352.60±76.50	0.21	6.57±4.40	0.80
MMA	2012	7	2.11±0.68	0.01	97.00±85.40	0.85	200.60±168.90	0.99	302.60±88.00	0.97	8.41±6.60	0.96
	2017	23	0.87±0.48		70.60±62.20		165.00±127.70		306.50±46.22		11.65±6.35	
	2006	8	0.72±0.33	0.93	6.18±5.03	0.41	78.70±67.2	0.98	358.30±113.70	0.14	0.41±0.15	0.75
ST	2012	6	0.62±0.16	0.12	2.31±1.02	0.96	75.20±63.60	0.86	215.50±43.30	0.90	0.51±0.17	0.58
	2017	4	0.38±0.05		1.94±0.13		62.50±52.00		223.00±20.20		0.48±0.18	

This plot suggests that Groups 1, 3, and 4 are recharge waters of the Ca–Mg–HCO3 type, and groups 2 and 5 are more chemically evolved and controlled by reverse ion exchange processes, which lowered the Na concentrations in pore waters even more to produce waters of the Ca–Mg–Cl type. Na in the solution is exchanged for Ca on the clay surfaces in the cases of reverse ion exchange. Inverse ion exchange is typical where solutes with high Na^+ concentrations mix with freshwater, such as in coastal areas with saline intrusion (Mahlknecht et al., 2017; Tamez-Meléndez et al., 2016). In such settings, seawater Na^+ replaces continental Ca^{2+} (and Sr^{2+}) in the aquifer clay surfaces. In this study, Na^+ concentration increments are possibly due to sewage infiltration since group 5 represents waters in the urbanized discharge area, possibly promoting inverse exchange processes (Thivya et al., 2014). Samples from group 2 exhibit an increased Na content from the weathering of silicate minerals in the Mina wellfield.
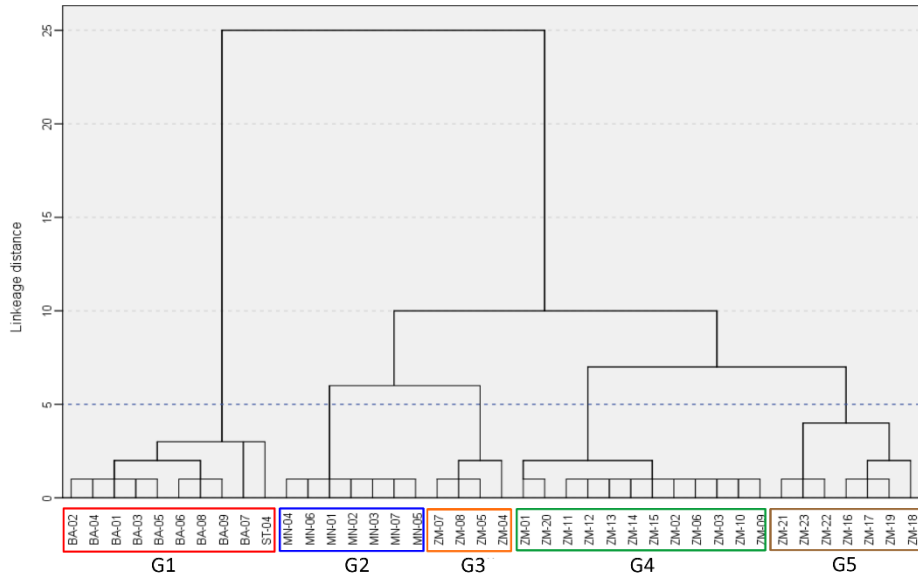
Fig. 2.2. Dendrogram derived with HCA using the log-transformed and standardized (z-score) water chemistry and isotopic ratios dataset for the 2017 sampling campaign. A dashed horizontal line (phenon line) is used to define five groups of water samples.

The positive correlation between TDS and $(NO_3^-+Cl^-)/HCO_3^-$ (**Fig. 2.3b**) confirms that water chemistry is heavily influenced by anthropogenic activities (Jalali, 2009; Xiao et al., 2017). Geothermal waters can carry high Cl^- concentrations; however, there is no evidence of geothermal waters in the study area. Using this reasoning, group 5 is the most impacted by excess Cl^- and NO_3^-, likely coming from vertical infiltration through the urban landscape.

Table 2.2. Statistical summary of physicochemical parameters and isotopic ratios according to groups. For the values of individual samples, see **Table A1.1** of **Appendix 1**. Note: n denotes the number of samples, and SD denotes standard deviation.

Parameter	Unit	Group 1 (n=10)		Group 2 (n=7)		Group 3 (n=4)		Group 4 (n=12)		Group 5 (n=7)	
		Mean	SD	Mean	SD	Mean	SD	Mean	SD	Mean	SD
Temp	°C	22.87	1.43	30.37	0.38	30.02	1.61	24.90	0.74	26.84	1.80
pH	-	7.35	0.31	7.20	0.10	7.37	0.09	7.14	0.10	6.98	0.17
EC	µS/cm	445.49	39.75	955.54	73.67	560.20	8.71	779.46	139.48	1650.86	369.73
ORP	mV	362.42	8.14	373.00	13.89	328.25	17.56	368.33	33.18	343.14	30.79
TDS	mg/L	285.39	25.41	623.16	77.72	357.80	5.69	520.53	41.57	1056.64	236.61
DO	mg/L	7.17	0.54	3.72	0.28	5.58	0.73	6.76	0.48	5.86	1.17
Ca	mg/L	74.47	3.66	110.04	7.76	93.53	1.01	111.10	9.11	181.89	36.95
Mg	mg/L	9.20	3.11	12.66	1.13	9.72	0.09	15.89	3.07	21.40	7.13
Na	mg/L	2.31	0.80	59.27	6.52	6.91	0.81	23.11	3.17	80.49	38.32
K	mg/L	0.46	0.10	1.17	0.25	0.41	0.27	1.08	0.42	0.77	0.49
HCO_3	mg/L	239.46	16.93	257.64	3.63	253.17	3.72	299.03	28.02	349.78	46.83
SO_4	mg/L	41.49	18.65	156.33	25.61	70.83	4.76	101.62	16.37	327.39	120.75
Cl	mg/L	3.73	1.30	119.57	19.45	18.33	1.47	40.62	5.75	151.74	52.96
NO_3	mg/L	1.18	0.43	1.46	0.36	3.58	0.42	11.22	2.69	17.02	7.57
F	mg/L	0.28	0.12	0.57	0.05	0.60	0.03	0.27	0.06	0.43	0.14
B	µg/L	14.60	5.76	62.43	23.34	21.00	4.69	75.67	28.29	115.57	146.28
Br	µg/L	23.10	5.86	85.00	25.07	21.25	3.10	110.83	33.46	217.57	280.77
I	µg/L	2.27	0.45	2.93	1.08	2.05	0.42	4.97	1.78	13.79	25.14
$\delta^{18}O\text{-}H_2O$	‰ VSMOW	-9.21	0.22	-7.54	0.16	-7.15	0.19	-7.56	0.80	-6.91	1.28
$\delta^2H\text{-}H_2O$	‰ VSMOW	-61.63	1.84	-48.58	1.14	-44.07	0.89	-50.08	5.57	-44.55	8.97
$\delta^{18}O\text{-}NO_3$	‰ VSMOW	1.68	1.14	5.20	0.68	4.04	2.89	2.39	0.79	5.58	2.60
$\delta^{15}N\text{-}NO_3$	‰ Air	3.77	0.70	6.82	0.83	3.88	0.38	9.64	0.60	12.55	2.02
$\delta^{18}O\text{-}SO_4$	‰ VSMOW	8.53	0.84	11.07	0.71	8.13	0.64	7.44	1.02	9.38	0.37
$\delta^{34}S\text{-}SO_4$	‰ VCDT	4.89	2.58	9.56	1.97	6.65	1.05	6.65	0.79	7.67	1.32
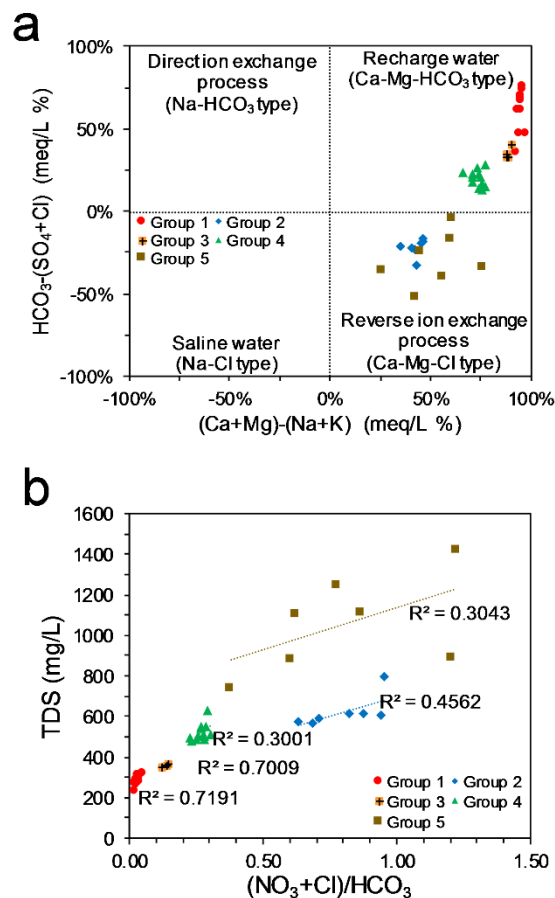
Fig. 2.3. (a) Plot showing the relationship between HCO_3^--$(SO_4^{2-}+Cl^-)$ and $(Ca^{2+}+Mg^{2+})$-(Na^++K^+) to evaluate potential hydrochemical processes; (b) Plot showing the relationship between TDS and $(NO_3^-+Cl^-)/HCO_3^-$ to evaluate anthropogenic influences, meq/L were used to calculate the synthetic parameter.

2.3.2   Correlation between hydrochemical parameters and pollution sources

As indicated by the Shapiro-Wilks test, a logarithmic transformation was applied to normalize all variables except Mg^{2+}, $\delta^{18}O_{H2O}$, $\delta^{18}O_{NO3}$, and $\delta^{18}O_{SO4}$. Five principal components were identified using PCA, in which the first three explain 65.8% of the total variance. The loadings of the varimax rotated components are shown in **Table 2.3**. The KMO and Bartlett's sphericity test value was 0.79, and the Chi-square value resulted in 1395.43 (p-value < 0.05), demonstrating an accurate reduction of the hydrochemical data in terms of dimension.

Table 2.3. Loadings for each parameter on each new principal component (PC) resulting from the varimax rotation with Kaiser Normalization. The total variance explained by each PC is stated. Bold values indicate parameters that are highly correlated to a given PC (>0.6).

	PC1	PC2	PC3	PC4	PC5
pH	**-0.814**	0.103	-0.114	-0.099	-0.152
EC	**0.783**	0.317	0.376	0.193	-0.040
ORP	-0.209	-0.049	0.004	0.254	**0.779**
DO	-0.108	-0.202	**-0.848**	0.029	-0.212
TDS	**0.808**	0.347	0.356	0.221	-0.007
Ca	**0.802**	0.408	0.228	0.146	-0.102
Mg	**0.860**	-0.034	0.071	0.155	0.131
Na	**0.655**	0.536	0.400	0.247	0.110
K	0.330	0.068	0.069	0.020	**0.801**
F	0.107	-0.058	**0.823**	0.220	-0.274
Cl	**0.665**	0.442	0.480	0.276	0.071
NO_3	**0.772**	0.245	-0.314	0.394	-0.150
SO_4	**0.736**	0.368	0.450	0.240	-0.044
HCO_3	**0.933**	0.121	-0.126	0.089	-0.096
B	0.296	0.257	0.098	**0.872**	0.178
Br	0.312	0.248	0.045	**0.866**	0.181
I	0.206	0.105	-0.105	**0.897**	0.011
$^{18}O\text{-}H_2O$	0.273	**0.868**	0.122	0.242	-0.055
$^{2}H\text{-}H_2O$	0.221	**0.905**	0.104	0.166	-0.061
$^{15}N\text{-}NO_3$	**0.887**	0.257	-0.014	0.256	0.136
$^{18}O\text{-}NO_3$	0.456	0.219	**0.647**	-0.091	-0.073
$^{18}O\text{-}SO_4$	-0.086	0.257	**0.776**	-0.185	0.184
$^{34}S\text{-}SO_4$	0.081	**0.832**	0.245	0.115	0.133
Total	7.727	3.726	3.576	3.136	1.618
% of variance	33.59	16.20	15.55	13.64	7.03
Cumulative %	33.59	49.79	65.34	78.98	86.01

The first component (PC1) explains 33.59% of the total variance and broadly describes water-rock interaction processes, namely the dissolution of carbonates and evaporites being responsible for most of the salinity in groundwater of the study area. Nitrate and sulfate concentrations, as well as nitrate isotope ratios, are also correlated with this component. A similar trend was observed in a neighbor aquifer (Pastén-Zapata et al., 2014; Ledesma et al. 2015), where nitrate was found to be originated mostly from sewage leakage and application of manure. However, in this study area, the application of manure is not a common practice. The second component (PC2) explains 16.20% of the variance and relates water isotopes with $\delta^{34}S_{SO4}$ isotope. It is remarkable that Ca^{2+}, Na^+, and Cl^- are also positive but less significantly related to this component. Thus, this component could indicate the different origins of groundwater at different altitudes providing distinct signatures. The third component (PC3) represents 15.55% of the variance and describes the long-term water-rock interaction process, evidenced by a strong relationship between F^- and temperature (Chae et al., 2007; Morales-Arredondo et al., 2018; Singaraja et al., 2018), as

well as a significant inverse relationship between $\delta^{18}O_{NO3}/\delta^{18}O_{SO4}$ and dissolved oxygen, suggesting denitrification processes and sulfate reduction (Li et al., 2019). This component appears to be related to processes that mitigate nitrate and sulfate contamination. The fourth component (PC4) contributes 13.64% to the variance and is related mainly to the mobility of B^-, Br^-, and I^- in groundwater. These elements are positively correlated with NO_3^- concentration, which likely indicates anthropogenic contamination from industrialized and urban areas. The fifth component (PC5) depicts a minor proportion of variance (7.03%) and relates the alkali metal K^- with redox condition (ORP). This component is possibly related to mobilization of K through grass degradation and leaching processes, since other sources such as the dissolution of K-silicate minerals or evaporites would not have a relevant influence in the redox potential. Unfortunately, commonly measured redox-sensitive elements beyond DO, NO_3^-, and SO_4^{2-}, which could provide further insight into this component (e.g., NH_4^-, Fe(II)/Fe(III), Mn(II), H_2S) were not measured (McMahon and Chapelle, 2008).

An examination of the PCA confirms that most groundwater processes can be ascribed to carbonates and evaporites' dissolution. This is evidenced by the strong correlation between Ca^{2+}, Mg^{2+}, HCO_3^-, SO_4^{2-}, Cl^-, and salinity (TDS). These water-rock interactions are accompanied by nitrate pollution derived from urbanization. Nitrate concentrations in the study area are likely generated from organic processes in soils, leakage of sewage lines and wastewater treatment plants, drainage from barnyards, septic tanks, and cesspools, leaching from the use of inorganic and organic fertilizers, and landfills. Regarding sulfate concentrations, there is strong evidence that marine evaporites generate part of the pollution; however, other human-made sources can be inferred due to its high correlation with nitrate. Remarkably, denitrification and sulfate reduction processes are suggested by PCA.

2.3.3 Isotopic composition of water

The values of $\delta^{18}O_{H2O}$ and δ^2H_{H2O} for groundwater in the study area ranged from −9.5 to −5.4‰ and from −63.9 to −36.0‰, respectively (**Fig. 2.4a**). The samples plot between the global meteoric water line (GMWL; Rozanski et al., 1993) and the local meteoric water line for the Sierra Madre Oriental (LMWL; Aguilar-Ramírez et al., 2017), which indicates a

meteoric origin of groundwater. As expected, the most depleted (most negative) δ²H and δ¹⁸O values occur in the Buenos Aires wellfield, which is at a higher altitude compared to the other two wellfields. Samples from Mina wellfield cluster narrowly in the central part of the graph. In contrast, samples from MMA aquifer have a considerable variation and are the most enriched (least negative). In particular, samples from group 5 wells in northeastern Monterrey's valley floor represent the most enriched samples reflecting the lowest topographic elevation in the study area. Except for groups 2 and 3, a slight evaporation trend is observed.
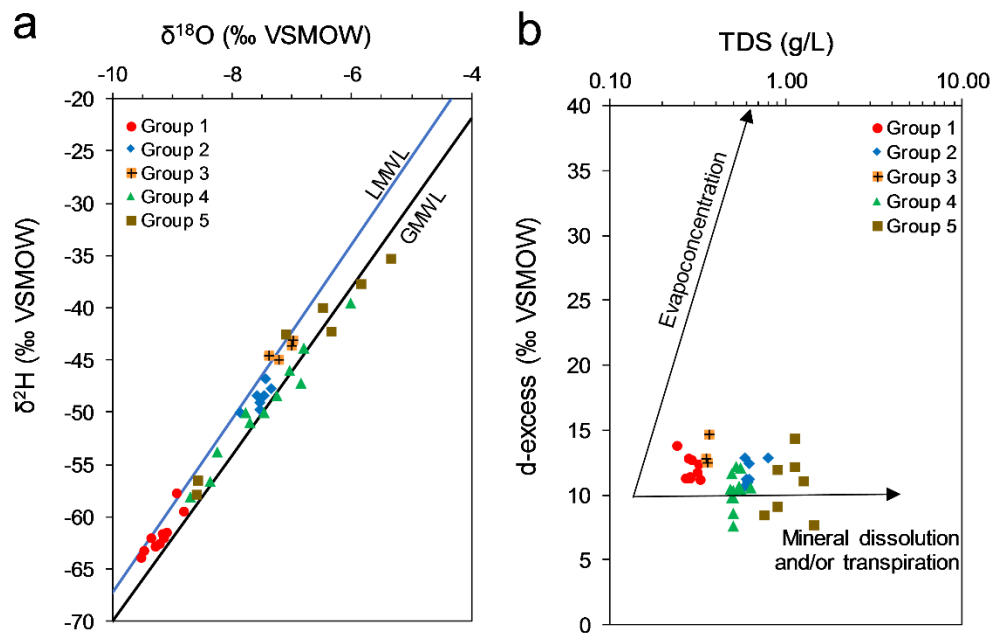
Fig. 2.4. (a) Dual isotope plot of δ2H–H2O and δ18O–H2O of water samples. Note: GMWL is the Global Meteoric Water Line (Rozanski et al., 1993), and LMWL is the Local Meteoric Water Line (Aguilar-Ramírez et al., 2017). (b) Relationship between TDS and d-excess (Huang and Pang, 2012).

The deuterium excess (d-excess) may help identify the contributions of evaporation and/or mineral dissolution to groundwater mineralization. The d-excess is estimated as d = ²H–8∗¹⁸O, assuming for precipitation an average of 10‰ ((Dansgaard, 1964). The relationship between d-excess and EC (Huang and Pang, 2012) shown in **Fig. 2.4b** shows that almost all samples are higher than 10‰ and consistent with a mineral dissolution trend. This validates that evaporation is present; however, the influence of evapoconcentration is relatively insignificant.

2.4 Discussion

2.4.1 Identification of possible pollution sources via halides

Halides (Br^-, Cl^-, and I^-) are conservative with minimum interactions with the subsoil; thus, these elements are useful for identifying potential pollution sources (Panno et al., 2006; Pastén-Zapata et al., 2014). Results of this study indicate that Group 1 could be considered as recently infiltrated water derived from rainfall (e.g., dissolution of gaseous CO_2) with minimal impacts from water-rock interactions (**Fig. 2.5a and b**). Likewise, Group 3 is considered recharge water in pristine conditions with specific trends of water-rock interactions (evaporite dissolution such as halite) and mineralization of soil organic matter with nitrate as an end product. Group 2 appears to be affected by sewage from untreated wastewater and/or septic tanks and landfills in Mina municipality. It is notable that the NO_3^- to Cl^- is relatively low (**Fig. 2.5c**). Group 4 and 5 falls close to or in the range of water affected by human sewage and leaching of landfills and dumps, which agrees with their location in the metropolitan area (**Fig. 2.5**).
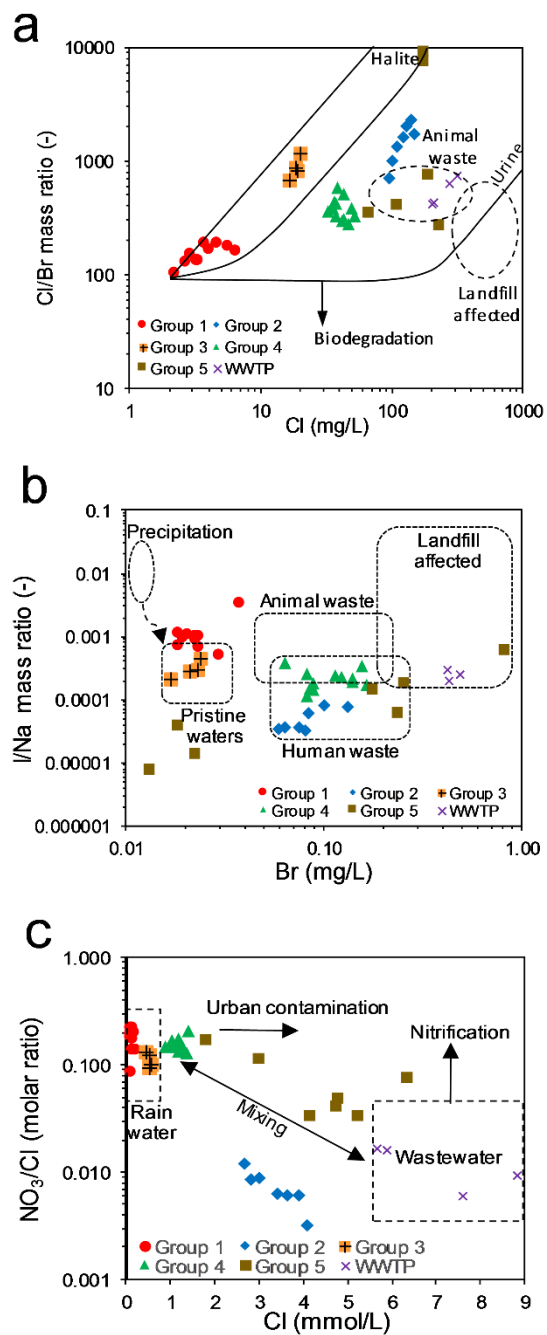
Fig. 2.5. (a) Relationship between Cl⁻/Br⁻ mass ratio and Cl⁻ for identifying sources (adapted from Pastén-Zapata et al., 2014); (b) Relationship between I⁻/Na⁺ mass ratio and Br⁻; (c) Relationship between NO_3^-/Cl⁻ molar ratio and Cl⁻.

2.4.2 Nitrate sources and attenuation processes

Typical nitrogen transformations (nitrification or denitrification) occur primarily in shallow aquifers. Nitrification is the oxidation of NH_4^- to NO_3^- and is mediated by bacteria that derive metabolic energy (Kendall, 1998). Denitrification reduces NO_3^- to N_2, N_2O, or NO, which generally occurs under anaerobic environments (Brandes and Devol, 1997; Koba et al., 1997). In this study, $\delta^{15}N_{NO3}$ and $\delta^{18}O_{NO3}$ values varied from +2.0 to +14.8‰ and from −0.3 to +9.9‰, respectively. Different nitrate sources were identified for the water samples of the study area using the dual isotopic approach (**Fig. 2.6a**). The isotopic signatures of $\delta^{15}N_{NO3}$ and $\delta^{18}O_{NO3}$ of sampled water, combined with the different potential NO_3^- sources, illustrate that soil organic N and manure/sewage sources were the two primary nitrate sources. Samples from groups 1, 2, and 3 were within the compositional field of soil organic N. The origin of NO_3^- for these samples could be related to natural soil sources, which is congruent with their location in recharge areas with limited anthropogenic impact (shrubland, dispersed housings). Samples from Group 2 (Mina well field) exhibit a denitrification process identified by a ratio trend between the range from 1:1.3 to 1:2.1 (Aravena and Robertson, 1998; Minet et al., 2012), resulting in an enrichment of the isotopic composition of $\delta^{15}N_{NO3}$ and $\delta^{18}O_{NO3}$. This may explain the reduced NO_3^- vs. Cl^- ratio for Group 2 in **Fig. 2.5c**.

On the other hand, samples from Groups 4 and 5 fell into the compositional field of manure/sewage, consistent with the land use of their location (mostly urbanized and partly agricultural land use towards northeast). These two groups also evidence a denitrification process.

The Eh values of the sample waters range from 279 to 443 mV, while dissolved oxygen content varies from 3.2 to 8.1 mg/L. This suggests oxic conditions for most of the studied wells, which would favor nitrification processes. The $\delta^{18}O_{NO3}$ produced during the nitrification of NH_4^- is described as two-thirds of oxygen from soil water and one-third from atmospheric oxygen (Andersson and Hooper, 1983), as expressed in the following:
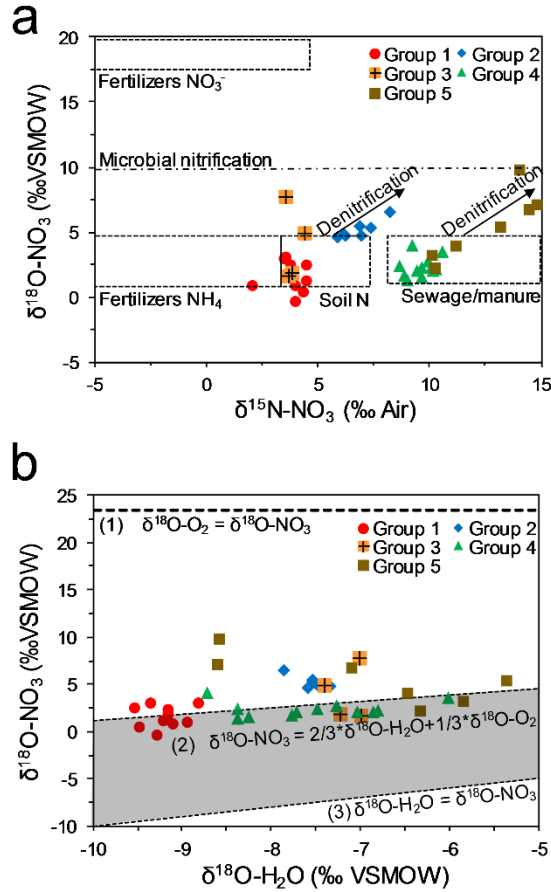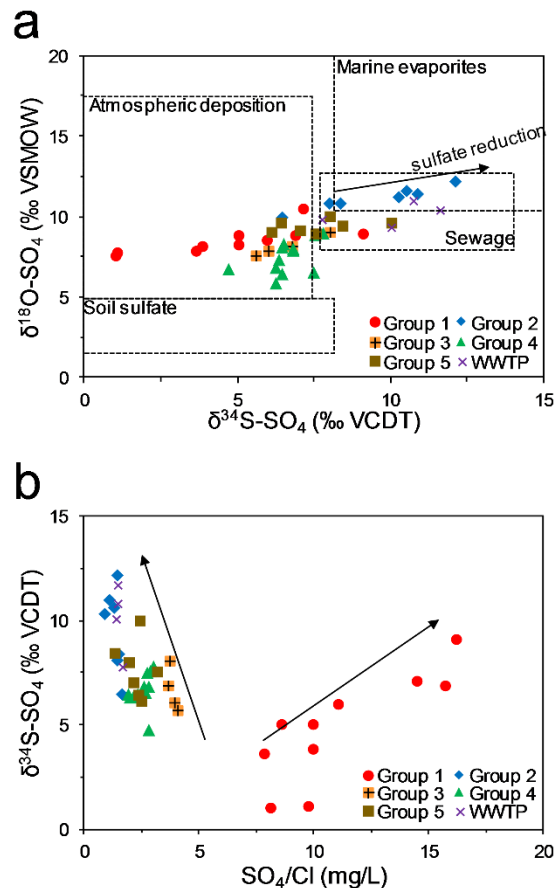
Fig. 6. (a) Dual isotope plot of $\delta^{15}N_{NO3}$ and $\delta^{18}O_{NO3}$ of dissolved NO_3 in water samples collected in the study area. The isotopic composition of the primary NO_3 sources considered are ammonium fertilizers, nitrate fertilizers, soil N, and manure or sewage (Kendall et al., 2008; Puig et al., 2017; Vitòria et al., 2004; Xue et al., 2009); (b) $\delta^{18}O_{H2O}$ vs. $\delta^{18}O_{NO3}$ with predicted theoretical trends under different conditions: (1) exchange with O_2, (2) nitrification, and (3) exchange with H_2O.

$$\delta^{18}O_{NO3} = 2/3 \cdot \delta^{18}O_{H2O} + 1/3 \cdot \delta^{18}O_{O2} \qquad (Eq.\ 2.6)$$

Where $\delta^{18}O_{H2O}$ represents the range of observed ratios (−9.5 to −5.4‰) and $\delta^{18}O_{O2}$ the theoretical atmospheric O_2 (+23.5‰) (Xue et al., 2009), the solid gray area in **Fig. 2.6b** represents theoretical values of $\delta^{18}O_{NO3}$ formed from microbial nitrification, confirming this process in most samples, except for Group 2, where all of the isotopic signatures of $\delta^{15}N_{NO3}$ and $\delta^{18}O_{NO3}$ were larger than theoretically expected, confirming nitrate attenuation processes (denitrification) (Rivett et al., 2008).

2.4.3 Pollution sources and attenuation processes of sulfate

The $\delta^{34}S_{SO4}$ and $\delta^{18}O_{SO4}$ signatures of samples from the study area show compositional ranges from +1.03 to +12.16‰, and from +5.79 to +12.12‰, respectively. Four sources can be related to SO_4^{2-}, according to **Fig. 2.7a**: atmospheric deposition from SO_2 emissions, the influence of soil-derived SO_4, sewage, and marine evaporites.

Fig. 2.7. (a) Dual-isotope plot of $\delta^{34}S_{SO4}$ and $\delta^{18}O_{SO4}$ in water samples collected in the study area. The isotopic composition of the primary SO_4 sources is represented by atmospheric deposition, soil sulfate, sewage and marine evaporites (Pittalis et al., 2018; Puig et al., 2017; Vitòria et al., 2004); (b) $\delta^{34}S_{SO4}$ vs. SO_4/Cl ratio in water samples collected in the study area.

Samples from Groups 1, 3 and 4 plot almost all within the atmospheric deposition range, while samples from Group 5 lie between atmospheric deposition and sewage. For most samples of Group 2, it was not possible to identify the source of sulfate due to an overlapping of source fields (i.e., marine deposits, sewage) and sulfate reduction processes identified by

the typical ratio trends between 1:4 and 1:2.5 (Mizutani and Rafter, 1973) (**Fig. 2.7a**). The following equation describes this process:

$$SO_4^{2-} + 2CH_2O \rightarrow H_2S + 2HCO_3^- \qquad (Eq.\ 2.7)$$
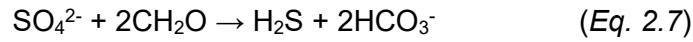
Furthermore, in all samples $\delta^{34}S_{SO4}$ decreases with increasing SO_4/Cl ratio, except for Group 1 (**Fig. 2.7b**), suggesting that isotopically light SO_4^{2-} was removed and the residual SO_4 became enriched in ^{34}S and ^{18}O during sulfate reduction in Groups 2, 3, 4, and 5 (Pittalis et al., 2018). For Group 1, an inverse trend is observed with smaller initial sulfate isotope values and larger SO_4^{2-}/Cl^- ratios than the rest. This can be related to an initial SO_4^{2-} pool, which agrees with the limestone-gypsum geology of the Buenos Aires wellfield and a subsequent mixture with sulfate from atmospheric deposition (Guo et al., 2015; Mora et al., 2017).

The dual-isotope diagram of $\delta^{15}N_{NO3}$ vs. $\delta^{34}S_{SO4}$ further constrains the variety of sources are responsible for each of these contaminants even within the same aquifer (**Fig. 2.8**). It confirms that the primary sources of pollution in the sites close to recharge areas (Groups 1, 2, and 3) are atmospheric deposition and mineralization of soil organic matter. In contrast, an additional source, the infiltration of sewage leaks, was identified for samples located in the urban area (Group 4 and 5). This is generally congruent with the findings for nitrate in the previous section.
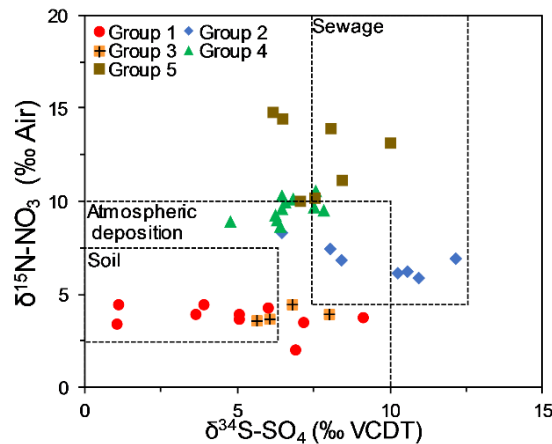
Fig. 2.8. Dual isotope plot of $\delta^{34}S_{SO4}$ and $\delta^{15}N_{NO3}$ in water samples collected in the study area. The isotopic composition of the primary pollution sources is represented by atmospheric deposition, soil, sewage, and manure (Otero et al., 2009; Puig et al., 2017).

2.4.4 Apportionment of nitrate and sulfate using a Bayesian isotope mixing model

A Bayesian mixing model (MixSIAR) was developed to estimate the proportional contributions of nitrate from the three identified potential sources: atmospheric deposition (AD), soil organic nitrogen (SON), and manure and sewage (M&S). Similarly, a mixing model was developed to estimate the contributions of sulfate from the four identified potential sources: atmospheric deposition (AD), soil sulfate (SS), manure and sewage (M&S), and marine evaporites (ME)). The mean and standard deviation of the isotopic composition used in the MixSIAR for the different pollution sources was estimated from a local end-member and literature (**Table A1.2 of Appendix 1**) and is shown in **Table 2.4**.

Table 2.4. Summary of $\delta^{15}N_{NO3}$, $\delta^{18}O_{NO3}$, $\delta^{34}S_{SO4}$, and $\delta^{18}O_{SO4}$ values, from various probable end-members used in MixSIAR model (extended results in **Table A1.2 of Appendix 1**).

Source	$\delta^{15}N$-NO_3 Mean ± SD	$\delta^{18}O$-NO_3 Mean ± SD	$\delta^{34}S$-SO_4 Mean ± SD	$\delta^{18}O$-SO_4 Mean ± SD
Atmospheric deposition	0.89±2.12	57.59±12.47	5.47±1.39	11.65±1.54
Soil organic nitrogen	3.98±1.95	2.51±1.41	-	-
Soil sulfate	-	-	2.74±1.44	3.66±2.78
Marine evaporites	-	-	16.02±3.14	13.32±4.27
Sewage/Manure	13.25±3.24	4.87±1.87	5.98±1.98	6.86±1.60

The results reveal that the nitrate source contribution in the study area generally followed SON > M&S > AD, with mean and standard deviation values of 60.6 ± 12.4%, 37.8 ± 12.5%, and 1.6 ± 1.2%, respectively, as illustrated in **Fig. 2.9a,c**. Specifically, groups 1, 2, and 3 showed similar patterns, with the highest shares derived from SON with 96.8 ± 4.2%, 68.4 ± 15.9%, and 78.4 ± 11.3%, respectively. In contrast, for groups 4 and 5, the dominant nitrate source was M&S (54.5 ± 18.6%, and 84.5 ± 12.5%, respectively). Atmospheric deposition contributed little nitrate to the groundwater. This agrees with studies performed in other areas (Li et al., 2019; Matiatos, 2016; Xue et al., 2012; Yue et al., 2017). These results are generally consistent with the qualitative analysis of the dual isotopic approach (**Fig. 2.6a**).
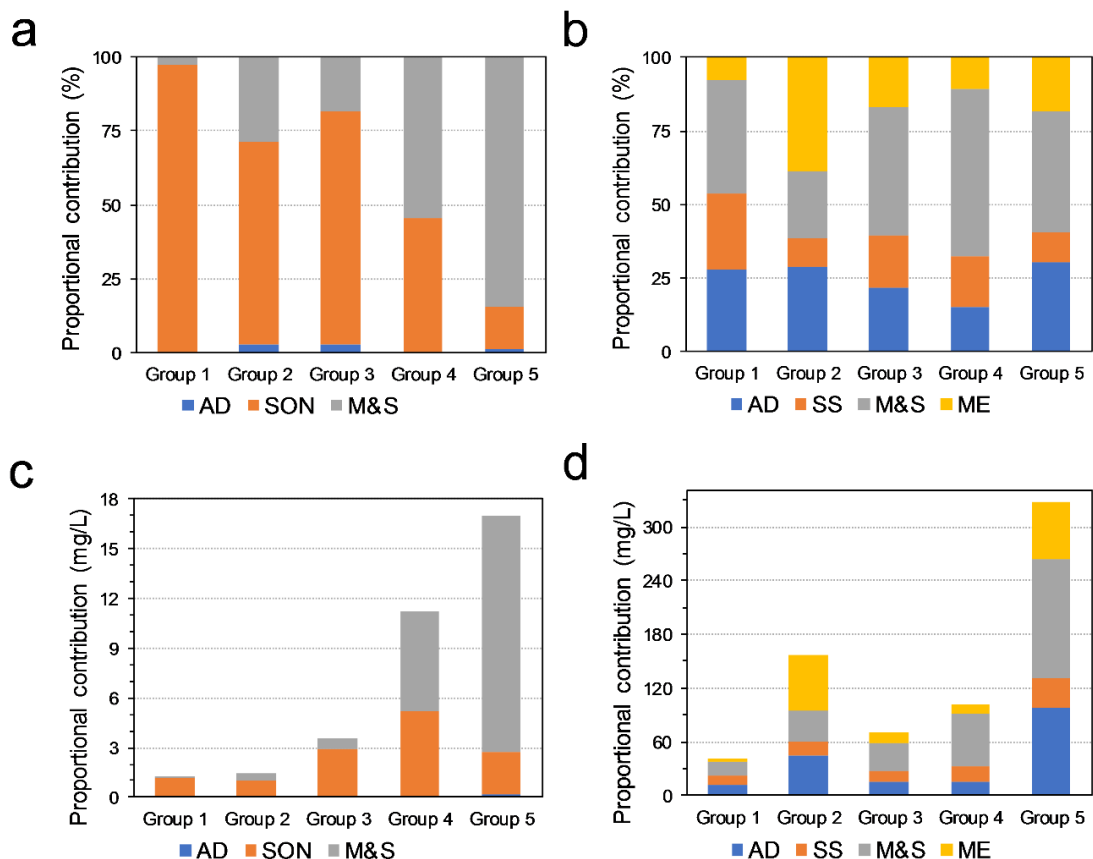
Fig. 2.9. (a) Average proportional contributions of three potential nitrate sources estimated by MixSIAR model for the different groups as a percentage; (b) average proportional contributions of four potential sulfate sources as percentage estimated by MixSIAR model for the different groups as a percentage; (c) average contribution of potential nitrate sources as concentration (mg/L); (d) average contribution of sulfate sources as concentration (mg/L).

Sulfate source contribution generally followed M&S > AD > ME > SS with mean and standard deviation values of 40.6 ± 18%, 24.9 ± 10%, 18.4 ± 5.5%, and 16.1 ± 11.9%, respectively. The main sulfate source was M&S for group 1 (38.9 ± 29.8%), group 3 (43.4 ± 22.6%), group 4 (57.0 ± 22.7%), and 5 (41.1 ± 21.6%), while for group 2 it was marine evaporites (38.7 ± 11.7%) (**Fig. 2.9b and c**). This mixing model exercise helped to discern the contribution of distinct sulfate sources whose isotopic compositional ranges show overlaps in **Fig. 2.7a**.

The summary of the results employing this multi-tracer approach combined with the Bayesian isotope mixing model is shown in **Table A1.3** of **Appendix 1**. In general, the isotope mixing model results using the Bayesian approach were consistent with interpretations based on the hydrochemical and isotopic data. However, one limitation of this approach is that the isotopic ranges of sources were derived from literature. Further

investigations to constrain local end-members' isotopic and chemical composition are necessary to reduce the results' variance and uncertainty.

2.4.5 Recommendations for reducing nitrate and sulfate pollution and future research

Based on the results of this study, soil organic nitrogen and sewage were the most critical nitrate and sulfate sources in groundwater. While there exist natural denitrification processes in the study area, these are locally limited. Monterrey's rapid economic and industrial growth during the last 100 years resulted in reduced or lost ecological processes of the urban mosaic. Specifically, the urban Santa Catarina river and its tributaries have been degraded and extremely "flashy" today, exhibiting a rapid increase in flow following storms. The increase in imperviousness, changes to the hydrological flow path, and the increase of nitrate sources in the urban landscape have all contributed to a decrease in water quality. The biogeochemical implications of the engineered changes are that riparian zones with their expected high levels of denitrification due to their vegetation composition, microbial populations, soil conditions, and hydrological regimes are faulty because they are altered and disconnected from urban streams, followed by a transition from anaerobic to aerobic conditions reducing the potential of denitrification.

Designs that re-establish ecological processes (restauration) can create hotspots of denitrification where the stream–riparian interface has been modified to facilitate the interaction of stream water with the riparian zone. Infrastructure can be added, which serves as nitrate sink, as in detention basins, or removed from daylighting buried urban streams, or modified as in bioretention ponds and level spreaders to mimic natural structures and ecological processes better. The introduction of green roofs or permeable surfaces to enhance water infiltration farther upslope in the hydrological flow paths are other strategies that increase the capacity of mitigation of nitrate.

Monterrey has a special status in Latin America regarding access to drinking water and sanitation. The population enjoys universal access to water distribution and sewerage. This means that practically all generated water and wastewater is treated in treatment facilities. The sewage system has been built starting in the early 1900s and expanded over time. It operates as a combined system, simultaneously collecting surface runoff and sewage water

in a shared system. Hence, the existence of reaches of old pipes and tunnels combined with limited preventive maintenance over prolonged periods and overflows during the rainy seasons have contributed to groundwater pollution (Olds et al., 2018; Selvakumar et al., 2004), especially considering that the groundwater table of MMA is located only about 7–20 m below ground level.

In this sense, it is recommended that the water and sanitation utility pays special attention to the oldest parts of the city/sewage system, which coincide geographically with shallow unconfined aquifer conditions (sample groups 3 and 4). In these areas, exfiltration of the sewage from damaged reaches is a common problem and needs rehabilitation measures. These rehabilitation projects will take many years to complete.

On the other hand, the discharge zone of MMA is strongly industrialized (group 5). According to Mexican law, industries are forced to comply with environmental standards when discharging the generated wastewater into water bodies. Thus, it is imminent to monitor industrial discharges in terms of water quality and avoid illegal dumping to the environment.

Furthermore, a revision of the sanitation plan is required, including promoting decentralized approaches in peri-urban and rural areas. For example, Mina (group 2) and Buenos Aires (group 1) are appropriate candidates for this kind of solution. They may maintain low nitrate and sulfate concentrations by reducing the infiltration of untreated wastewater from septic tanks and cesspools to the shallow aquifer and preserve the actual situation of water quality (Clemens et al., 2020; Oakley et al., 2010).

Finally, it is essential to create a long-term groundwater monitoring network of nitrate and sulfate in the entire aquifer system to control the evolution of the contamination in time and space. Future research efforts should be developed towards evaluating seasonal changes of pollution and the use of microorganisms and micropollutants as co-tracers for a more robust conceptualization of contamination paths and evaluation of mitigation measures in a complex groundwater system.

2.5 Conclusion

A multi-tracer study using chemical and isotopic fingerprints combined with a probability mixing model was conducted to understand the origin and source contribution of nitrate and sulfate pollution in groundwater of the urbanized valley of Monterrey. Nitrate pollution was mainly derived from sewage leaks in the urban area (37.8%). In contrast, soil organic nitrogen was responsible for nitrate concentration in the recharge areas (81.2%). Similarly, sulfate pollution in the city was caused by sewage infiltration (45.1%) in the groundwater and atmospheric deposition (24.9%) due to anthropogenic emissions. In recharge areas, sulfates result from the interaction between water and marine evaporites (38.7%).

The hydrochemical data suggests that groundwater of the study area is dominated by a Ca–Mg–HCO_3 water type in the topographically elevated, non-urbanized areas (Buenos Aires) and a Ca–Mg–Cl water type in transition and discharge areas of the Monterrey metropolitan area and Mina (northwest of Monterrey). The latter chemistry type and locations suggest mixing between recharge waters and sewage leaks and possibly inverse cation exchange processes.

Stable water isotopes suggest that water in the study area has a meteoric origin with some evaporation effects in the transition areas. However, evapoconcentration is insignificant compared to mineral dissolution. The multivariate analysis confirms that carbonate and evaporite dissolution drives groundwater mineralization.

The halide concentrations evaluation revealed that samples close to recharge areas in Buenos Aires indicate recently recharged meteoric water un-impacted by anthropogenic contaminants. These waters represent recent infiltrated water that has experienced water-rock interactions, such as carbonate and halite dissolution, and mineralization of soil organic matter with nitrate as an end product. Along the flow path, these groundwaters mix with sewage leakages and leach from landfills. These processes are likely operating within the Mina wellfield and the transition and discharge zone of MMA aquifer.

The dual-isotope approach confirms that natural contamination by mineralization of soil organic nitrogen and anthropogenic contamination by sewage leakages and leaching from

landfills is the primary nitrate source. Also, it suggests the presence of denitrification processes in the Mina area and the discharge zone of MMA aquifer northeast of the Monterrey area. On the other hand, sulfate contamination originated naturally by the dissolution of marine evaporites such as gypsum, especially in the Buenos Aires area, and from anthropogenically-contaminated from atmospheric deposition from emissions and leakages from sewage in the urbanized area.

Probability mixing models using the Bayesian method confirm that leakage derived from sewage is not the only important pollution source of NO_3 and SO_4, proving that natural sources (nitrogen and sulfate derived from the soil) play also impact groundwater chemistry. Moreover, mixing with different pollution sources could be identified for the urbanized area. However, future investigations should perform a detailed characterization of the isotopic composition ranges of the different local sources to reduce the uncertainty of the probability mixing results.

Monterrey's rapid economic and industrial growth resulted in reduced and lost ecological processes in the urban mosaic and limited sewage system maintenance. Restauration efforts can create natural structures and infrastructure which serve as nitrate and sulfate sink. The continuous rehabilitation of the sewage system in the older urban landscape may reduce exfiltrations to the underlying close groundwater table. Decentralized on-site treatment systems may be promoted in periurban and rural areas as cost-effective solutions to prevent pollution in distant areas. A long-term monitoring network serves to control the pollution and to evaluate mitigation measures.

This methodology is a useful tool that can be successfully applied in catchments for a qualitative and quantitative evaluation of the contribution of different pollution sources in groundwater, providing essential information for water managers.

Chapter 3: Comarca Lagunera Region Case

This chapter is adapted from the published article

3.1 Introduction

Nitrate (NO_3^-) is a ubiquitous environmental pollutant that occurs naturally and is released by human activities. These activities include the production and use of fertilizers, the combustion of fossil fuels (resulting in atmospheric deposition, hereafter AD), the leakage and discharge of both industrial and domestic sewage systems, and the alteration of natural vegetation with nitrogen (N)-fixing crops (Gutiérrez et al., 2018; Ward et al., 2018). Population growth has led to an increased food demand, which has resulted in the production and disposal of considerable amounts of N in the form of natural (manure) and synthetic fertilizers, especially in places where intensive-farming practices are performed (Tilman et al., 2002). The application of large quantities of fertilizers to meet the N demand of crops, combined with the return flow associated with irrigation, has increased the NO_3^- concentrations in the surface water bodies and groundwater of agricultural in particular (Merchán et al., 2020). Therefore, N-fertilizers' indiscriminate use raises significant human and ecological issues due to the resultant excessive NO_3^- concentrations in water. This may lead to the degradation of surface waters, groundwater, and coastal or marine ecosystems (Gutiérrez et al., 2018; Mekonnen and Hoekstra, 2015; Nikolenko et al., 2018).

Although it is difficult to distinguish the sources of NO_3^- in complex systems, source identification is of primary importance for proposing appropriate management plans in NO_3^- vulnerable zones. This relates to potential adverse health effects (Blaisdell et al., 2019) and biota (Camargo et al., 2005) associated with NO_3^- pollution. The stable isotopes of NO_3^- (i.e., $\delta^{15}N$ and $\delta^{18}O$) have been widely used to differentiate the sources that can account for the total NO_3^- concentration in surface water and groundwater. Unfortunately, the use of dual-isotope fingerprints to trace NO_3^- sources have not been entirely successful to date due to the possibility of overlapping areas of two or more NO_3^- sources, which hampers the distinction among origins (Minet et al., 2017; Xue et al., 2012; Zhu et al., 2019). In addition, the transformation of N in the environment and the use of regional agricultural methods can also preclude the identification of NO_3^- sources when the dual-isotope method is used. Both nitrification and denitrification processes lead to a shift in the NO_3^- isotopic composition due to the fractionation of stable N and oxygen isotopes (Aravena and Robertson, 1998; Snider et al., 2010). Moreover, the potential sources of NO_3^- can display different isotopic values

from one region to another, depending on people's lifestyles and farming practices (Y. Zhang et al., 2018a).

Accordingly, recent studies have mainly focused on identifying the sources of NO_3^- by combining dual-isotope NO_3^- analysis with other chemicals, biological and/or statistical approaches; for example, halide ratios (Katz et al., 2011; Pastén-Zapata et al., 2014), boron and strontium isotopes (Meghdadi and Javar, 2018b), multivariate statistical methods (Matiatos, 2016; Meghdadi and Javar, 2018a), groundwater bacteria (Meghdadi and Javar, 2018a) and multi-stable isotope approaches (Biddau et al., 2019). Furthermore, some methods have been implemented to develop a reliable way of providing quantitative estimates of the contributions of natural and anthropogenic NO_3^- sources to the total NO_3^- pool in specific environments. These methods include the use of chemical and mathematical tools such as mass balance calculations (Degnan et al., 2016), end-member mixing analysis (Grimmeisen et al., 2017; Ogrinc et al., 2019), and statistical models including multi-linear regression analysis (Meghdadi and Javar, 2018a) and the Bayesian mixing models (Liu et al., 2018; Matiatos, 2016; Meghdadi and Javar, 2018a; Xue et al., 2012; Y. Zhang et al., 2018a; Zhao et al., 2019).

The Comarca Lagunera Region (CLR) is an economically significant irrigation district in northern Mexico, where livestock and agricultural activities make a significant contribution to the national gross domestic product. The water supplied the CLR originates from both groundwater and surface water sources, although the latter only includes Francisco Zarco Reservoir, which is used for irrigation purposes. Rapid population growth, arid conditions, and prolonged droughts in CLR mean that groundwater has become a crucial resource for public supply, livestock, agricultural, and mining activities. Groundwater is the principal drinking water source for the approximately 1.6 million inhabitants of the CLR, who mainly live in three cities. Hence, the regional water table has dropped rapidly over recent decades, resulting in the over-exploitation of the aquifer system and water quality deterioration, including an increased arsenic (As) concentration in groundwater (Ortega-Guerrero, 2017).

Although some research on the water quality has been undertaken regarding water quality and pollution in the CLR, these have focused mainly on assessing the behavior of As in groundwater (Del Razo et al., 1990; Mejía-González et al., 2014; Ortega-Guerrero, 2017).

Despite CLR being an important area for livestock and agricultural production, there are no known studies that have evaluated the dynamics of NO_3^- in groundwater or the effect of groundwater over-exploitation on the NO_3^- concentration. Thus, the objectives of this chapter are: 1) to assess the NO_3^- concentration in the groundwater of the CLR, 2) to identify the sources and transformation processes of NO_3^- in groundwater by using stable isotopes, and 3) to quantify the apportionment of different potential NO_3^- pollution sources through the use of a Bayesian isotope mixing model. This chapter will help improve the knowledge about NO_3^- source apportionment in complex groundwater environments with multiple diffuse sources.

3.2 Materials and methods

3.2.1 Description of the study area

The CLR (31000 km^2) is located in the central region of northern Mexico (24°22' to 26°45' N, 102°14' to 104°48' W) in an inter-mountain basin enclosed by the physiographical sub-provinces of Laguna de Mayrán and Bolsón de Mapimí. The regional topography ranges from the highest peaks that reach 3700 m above sea level (a.s.l.) to the valley plains at about ~1050 m a.s.l. The underlying geology of these sub-provinces includes limestone, dolomite, and conglomerates. The basin floor comprises alluvial deposits (depth of 50-500 m), including sand, gravel and conglomerate, lacustrine sediments, and gypsum. The basin is located at the Nazas and Aguanaval rivers' confluence, which are the main surface waterways of the area. However, their main channels run dry as they only receive water during intense rainfall events due to the Lázaro Cárdenas and Francisco Zarco reservoirs, which were built for drinking and irrigation purposes.

The climate in this zone is arid to semi-arid, with a mean annual temperature of 21.3 °C. Temperatures range from 0 to 8 °C during the autumn and winter (November-February), whereas a maximum of 45 °C can occur during the summer (July-August). The average annual rainfall is 250 mm, most of which occurs between June and September. Due to the scarce rainfall and high temperatures during the summer, the surface water availability is low. Thus, the entire region depends on groundwater resources obtained from six administrative aquifer units that comprise the interconnected basin's groundwater system,

namely Principal-Lagunera Region, Vicente Suárez, Villa Juárez, Oriente-Aguanaval, Pedriceña-Velardreña, and Nazas (**Fig. 3.1**).
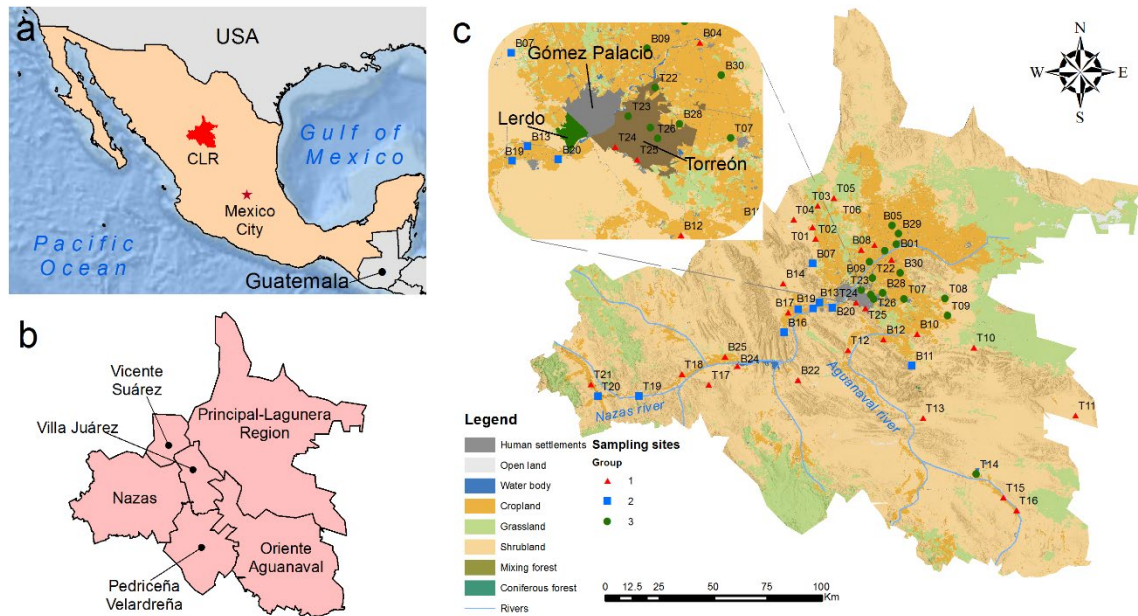
Fig. 3.1. (a) Location of the Comarca Lagunera Region (CLR) in northern Mexico; (b) the administrative delimitation of aquifers; (c) land use/land cover, the locations of the sampled wells, and the main metropolitan area in the CLR, which includes Torreón, Gomez Palacio and Lerdo.

The study area is characterized by intensive agricultural and livestock areas covering 11.6% of the CLR's total area. The principal crops of the region are alfalfa (3.4 million ton/year), corn (2.5 million ton/year), sorghum (745 000 ton/year), wheat (674 000 ton/year), and melon (160 000 ton/year); livestock breeding includes mainly cattle (>400 000 heads of cattle raised for milk production, and > 350 000 for meat production) and poultry   (SIAP, 2018a, 2018b). As mentioned, the CLR has a total population of ca. 1.6 million, which is mostly represented by the Laguna metropolitan area, which comprises Torreón, Gómez Palacio, and Lerdo cities (**Fig. 3.1c**), covering ~0.9% of the total area of the CLR. The remaining area of the CLR includes grassland (18.5%), shrubland (68.5%), and mixed forests (0.5%).

Several studies have shown that groundwater in the study area can be strongly affected by salinization as the total dissolved solids concentration has been found to range from 140 to 5100 mg/L (Azpilcueta Pérez et al., 2017; Brouste et al., 1997; Saldarriaga-Noreña et al., 2014). High salinization is mainly due to: (1) the drying up of ancient lakes, which led to the

development of evaporite rocks as a result of climatic factors, (2) the construction of the Lázaro Cárdenas and Francisco Zarco dams on the Nazas River, which blocked water inputs to the river, and (3) the groundwater return flow from irrigation. Moreover, several studies have pointed out that the groundwater flow in the area has reversed from the ancient lakes towards urbanized and agricultural zones due to the continuous abstraction of groundwater for public purposes and irrigation/livestock activities (Brouste et al., 1997; Ortega-Guerrero, 2003; Saldarriaga-Noreña et al., 2014). Overall, we focused our research on the sources and sinks of NO_3^- in four of the six aquifer units of the CLR: Principal-Lagunera Region, Villa Juárez, Oriente-Aguanaval, and Nazas. These aquifers are located in urbanized areas or areas where intensive livestock and agriculture activities are performed (**Fig. 3.1**). The hydrogeological characteristics of these aquifers are summarized in **Appendix 2**.

3.2.2 Sample collection

By considering the different land-use patterns, the potential pollution sources, and the previous hydrochemical data from the Mexican National Water Agency (Comisión Nacional del Agua - CONAGUA), 53 sampling sites, covering most of the study area, were selected. All samples were taken from production wells that are mainly used for irrigation and municipal water supply. These wells are primarily located in alluvium or limestone at depths typically ranging from 50 to 500 m. In the basin's upper region, the production wells near the Nazas and Aguanaval rivers' paths have construction depths ranging from 75 to 150 m (DOF, 2015). In the intermediate zone that includes the region limited by the metropolitan area, 60 deep wells are ranging from 125 to 500 m deep (García-Salazar and Mora-Flores, 2008), and finally, in the lower part of the basin, the depth of the wells varies from 150 to 300 m (Rivas Sada, 2011). For wells used for municipal drinking water supply, it is mandatory to include a 6 m (minimum) stainless steel casing from the top of the well, whereas there are no restrictions for irrigation wells (CONAGUA, 2019; SEMARNAP, 1997). Consequently, most of the CLR production wells are fully screened to the bottom below the casing.

Samples were collected during November 2018, when there were no rain events. To avoid the collection of stagnated water, boreholes were purged until measurements of pH and electrical conductivity (EC) were stabilized before collecting the groundwater samples. Field

parameters (pH, temperature, oxygen reduction potential (ORP), salinity, and EC) were subsequently determined directly in situ using a pre-calibrated YSI Professional Plus multiparameter meter. After collection, all water samples were filtered through 0.45-µm pore-size acetate cellulose membranes by frontal filtration. Bicarbonate was measured in the filtered water samples in situ by the acid titration method using H_2SO_4 (0.02N) until a pH of 4.3. Samples for analyses of anions, cations, and stable nitrate isotopes were collected in triple-rinsed HDPE bottles. Samples for cation analysis were acidified with ultrapure HCl to pH < 2 to prevent major element precipitation or adsorption during storage. Samples for cation and anion analyses were stored at 4 °C until processing. Samples for $\delta^{15}N_{NO3}$ and $\delta^{18}O_{NO3}$ analyses were frozen at -20°C to avoid variations caused by biological processes. Stable nitrate isotope analysis was carried out a month after the sampling campaign.

3.2.3   Analytical procedures

Chemical analyses were performed by Activation Laboratories Ltd. (Canada). Anions were analyzed using ion chromatography (Dionex DX-120), while cations were analyzed using inductively coupled plasma optical emission spectrometry (ICP-OES; Agilent Axial). The charge balance was verified in all samples by considering those with error values of < 10 % as acceptable.

Isotopic analyses were performed at the Environmental Isotope Laboratory (EIL) of the University of Waterloo in Canada. The δ^2H_{H2O} and $\delta^{18}O_{H2O}$ analyses followed the methodology described by Berman et al. (2013) using an off-axis integrated cavity output spectroscopy (OA-ICOS) water isotope analyzer (LWIA, Los Gatos Research Inc.). The $\delta^{15}N_{NO3}$ and $\delta^{18}O_{NO3}$ values were determined following the chemical reduction method (Ti et al., 2018) by first reducing NO_3^- to NO_2^- via a cadmium catalyst chemically converting to N_2O, before using a trace-gas isotope-ratio mass spectrometer (TG-IRMS; GVI IsoPrime). For quality control purposes, a normalization using two international calibrated standards (USGS 34 and USGS 35) and one internal laboratory standard (EGC 17) were applied. The analytical accuracy was ± 0.3‰ for $\delta^{15}N_{NO3}$ and ± 0.8‰ for $\delta^{18}O_{NO3}$.

All stable isotope results were expressed as delta values by representing the deviations in per mil (‰) from the respective reference standard following **Eq. 3.1**:

$$\delta(‰) = 1000 \times (R_{sample}/R_{standard}) - 1 \qquad \text{(Eq. 3.1)}$$

where, R_{sample} and $R_{standard}$ are the measured isotopic ratios ($^2H/^1H$, $^{15}N/^{14}N$, or $^{18}O/^{16}O$) for the sample and standard, respectively. The $^{15}N/^{14}N$ ratio in nitrates is reported as $\delta^{15}N_{NO3}$ with respect to atmospheric N_2, whereas $^2H/^1H$ and $^{18}O/^{16}O$ ratios are reported with respect to the Vienna Standard Mean Ocean Water (VSMOW).

3.2.4 Data analyses

Multivariate statistical analysis is a common approach used for groundwater classification and provides insights into the relationships among different hydrochemical parameters for a given set of groundwater samples. In this research, two multivariate statistical methods were performed using R software (R Core Team, 2019): a hierarchical cluster analysis (HCA) and a principal component analysis (PCA) in Q and R modes.

The HCA and PCA were applied to the entire dataset, including field parameters (temperature, ORP, pH, dissolved oxygen (DO), TDS and EC), major constituents (Ca^{2+}, Mg^{2+}, Na^+, K^+, HCO_3^-, Cl^-, F^-, NO_3^-, SO_4^{2-}, and Si), and minor constituents (Br^- and I^-). For the statistical analyses and graphical results, values below the detection limit (DL) were replaced by 0.5 of the DL value. Typically, most chemical parameters distribution does not follow a normal distribution; thus, to avoid spurious correlations, a compositional data technique, namely centered log-ratio (clr) transformation, was applied. This transformation involves dividing each component (x) by the geometric mean (g(X)) of all variables according to the equation **Eq. 3.2**:

$$clr(x_i) = ln\frac{x_i}{g(X)} \qquad \text{(Eq. 3.2)}$$

Once the data were transformed, an HCA was performed to determine significant groups of water samples via Ward's method. The normality of each resulting group was analyzed using the Shapiro-Wilk test, and the difference of the variables among the groups was compared using an analysis of variance (ANOVA) test at a significance level of $p < 0.05$. The non-parametric Kruskal-Wallis test was applied if the normality assumption was not met across

the groups. After conducting the HCA, a PCA was applied to extract variables and infer the main natural or anthropogenic factors controlling each groundwater group (nitrate content).

3.2.5   Estimation of contributions from different nitrate pollution sources

The proportional contributions of the different NO_3^- pollution sources were assessed using the Bayesian stable isotope mixing model MixSIAR (version 3.0.2) developed in the R environment. A detailed description of the MixSIAR model is described in Stock et al. (2018). Dual-isotopic nitrate values of the groundwater samples and six potential sources (atmospheric deposition (AD), synthetic fertilizers (NH_4^+ (NHF) and NO_3^- (NOF) based fertilizers), soil organic nitrogen (SON), and sewage (S) and manure (M) were included in the model to quantify the fractional contribution of NO_3^-. The different end-member isotopic compositions were defined based on previous literature (Fenech et al., 2012; Gutiérrez et al., 2018; Nikolenko et al., 2018; Xue et al., 2009) as follows: AD ($\delta^{15}N_{NO3}$: 0.11 ± 1.69‰, $\delta^{18}O_{NO3}$: 54.97 ± 7.63‰); NHF ($\delta^{15}N_{NO3}$: 1.24 ± 1.44‰, $\delta^{18}O_{NO3}$: 3.44 ± 2.47‰), NOF ($\delta^{15}N_{NO3}$: -0.07 ± 2.85, $\delta^{18}O_{NO3}$: 24.12 ± 3.17‰), SON ($\delta^{15}N_{NO3}$: 3.26 ± 1.99‰, $\delta^{18}O_{NO3}$: 3.34 ± 2.04‰) and M&S ($\delta^{15}N_{NO3}$: 10.14 ± 4.53‰, $\delta^{18}O_{NO3}$: 5.69 ± 2.91‰).

3.3 Results

3.3.1   Water sample groupings and hydrogeochemical characterization

The mean, range, median, and standard deviation (SD) of the physicochemical variables (temperature, ORP, pH, EC) major ions (Ca^{2+}, Mg^{2+}, Na^+, K^+, HCO_3^-, F^-, Cl^-, NO_3^-, SO_4^{2-}), and stable isotopes ($\delta^{18}O_{H2O}$, δ^2H_{H2O}, $\delta^{15}N_{NO3}$, $\delta^{18}O_{NO3}$) of the groundwater samples from the CLR are summarized in **Table 3.1** and provided in full in **Table A2.1** of **Appendix 2.** The detailed results obtained from the HCA are displayed in **Fig.3.2.** According to these results, the water samples were classified into three groups defined by their statistical similarities obtained from the horizontal phenon line with a linkage distance (pairwise distances between observations) above 6.0 in order to understand local geochemical trends (**Fig.3.2.**). The clusters were spatially defined as follows: group 1, which comprises the most mineralized/NO_3^- polluted water samples that mainly corresponded to groundwater

discharge areas; group 2, which represents wells located in a transition zone; group 3, which denotes samples in the groundwater recharge areas.

There was no significant difference between the depth to the water table across the three groups, which fluctuated between 3.2 and 192.7 m below ground level; however, in terms of administrative units, water table levels from the Principal-Lagunera Region unit were significantly lower ($p<0.01$) than the rest of the units. The groundwater temperature across the groups varied substantially from 20.70 to 34.40 °C; however, within-group 3 varied from 30 to 34.4°C, which was significantly higher ($p<0.01$) than that of both groups 1 and 2. The samples from groups 1 and 2 had near-neutral pH values (6.8-7.9), whereas some of the samples in group 3 had slightly alkaline pH values (mean 7.9 ± 0.6) that were significantly higher than those of the other two groups ($p<0.001$). The redox potential varied from 114.7 to 491.5 mV in all groups and was not significantly different. The DO concentration in group 1 (mean of 4.6 mg/L) was significantly higher ($p<0.01$) than that in groups 2 and 3, which exhibited means of 2.6 and 3.9 mg/L, respectively.
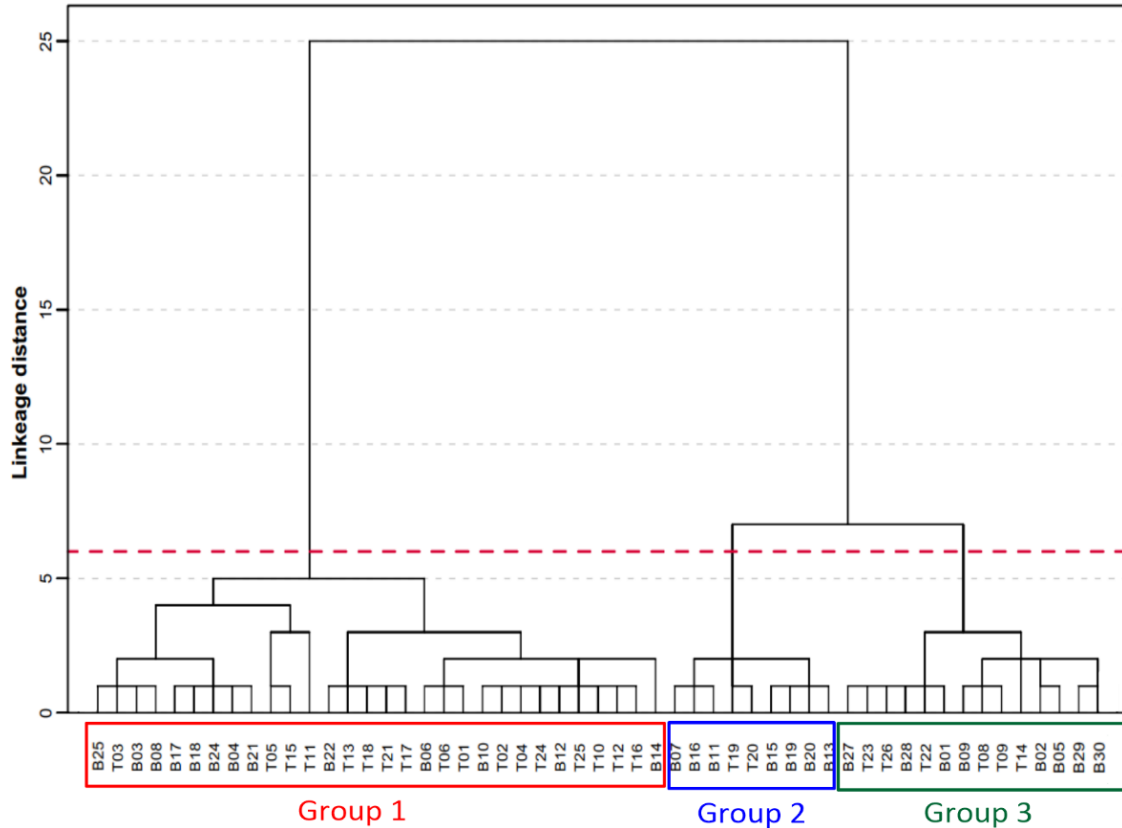
Fig. 3.2. Dendrogram derived from an HCA employing the centered log-ratio transformation of water chemistry and isotopic ratio dataset. Note: A dashed horizontal line (phenon line) is used to define the three groups of water samples. The x-axis denotes the grouping of the different sampling wells.

Mean TDS and EC values for group 1 were 1942.9 µS/cm and 1473.6 mg/L, respectively, and mean Na^+, Cl^-, SO_4^{2-}, Br^-, I^-, and Si concentrations were 203.4 mg/L, 70.1 mg/L, 671.5 mg/L, 949.6 µg/L, 149.7 µg/L, and 21.4 mg/L, respectively. Overall, these values were significantly higher ($p<0.01$) than those for groups 2 and 3. Additionally, the Mg^{2+}, K^+, and HCO_3^- concentrations for groups 1 and 2 were significantly higher than those of group 3 ($p<0.05$). The mean Ca^{2+} and NO_3^- concentrations decreased significantly ($p<0.05$) in the order of group 1 (Ca^{2+}: 205.9 mg/L; NO_3^-: 20.2 mg/L) > group 2 (Ca^{2+}: 83.8 mg/L; NO_3^-: 4.27 mg/L) > group 3 (Ca^{2+}: 33.4 mg/L; NO_3^-: 1.19 mg/L). There was a significant difference between the three groups.

Table 3.1. Statistical summary of descriptive statistics for physicochemical parameters and isotopic ratios in the CLR. Note: d: deuterium excess = $\delta^2H - 8\,\delta^{18}O$.

Group		T (°C)	ORP (mV)	pH	DO (mg/L)	EC (µS/cm)	Ca (mg/L)	Mg (mg/L)	Na (mg/L)	K (mg/L)	HCO$_3$ (mg/L)	F (mg/L)
1 (n=29)	Max.	34.40	448.60	7.94	7.31	5957.00	591.00	99.50	969.00	15.10	402.60	4.54
	Min.	20.70	114.70	6.79	1.82	904.00	73.00	3.85	55.50	3.05	113.46	0.12
	Mean	26.01	247.86	7.33	4.60	1942.93	205.94	35.25	203.40	6.84	238.04	1.08
	Median	26.10	241.30	7.32	4.53	1560.00	152.00	31.20	135.00	6.12	218.38	0.78
	SD	2.74	71.82	0.30	1.55	1130.31	137.19	20.60	196.37	3.10	90.92	0.98
2 (n=9)	Max.	33.60	305.30	7.39	5.43	1019.00	109.00	33.40	101.00	5.10	394.06	1.08
	Min.	22.70	226.00	6.99	1.01	532.00	59.60	4.92	22.00	2.54	218.38	0.25
	Mean	26.27	255.54	7.16	2.59	755.11	83.81	21.06	52.12	4.12	296.73	0.59
	Median	25.30	247.20	7.15	2.14	730.00	82.00	23.70	45.90	3.91	312.32	0.47
	SD	3.53	30.10	0.13	1.32	132.28	17.63	8.78	26.48	0.78	57.49	0.33
3 (n=15)	Max.	33.40	491.50	8.64	6.80	1029.00	54.80	6.88	164.00	3.34	287.92	3.09
	Min.	26.20	144.60	6.00	1.29	332.10	3.76	0.09	35.10	0.85	104.92	0.31
	Mean	29.54	260.97	7.88	3.88	596.96	33.35	2.10	83.93	2.08	159.22	1.01
	Median	29.30	262.20	7.97	3.92	556.00	37.70	1.27	70.70	1.81	154.94	0.64
	SD	2.47	79.19	0.62	1.99	190.82	15.41	2.31	40.45	0.95	44.48	0.82

Group		Cl (mg/L)	NO$_3$ (mg/L)	SO$_4$ (mg/L)	Br (µg/L)	I (µg/L)	Si (mg/L)	$\delta^{18}O_{H2O}$	δ^2H_{H2O}	d	$\delta^{15}N_{NO3}$	$\delta^{18}O_{NO3}$
1 (n=29)	Max.	180.00	109.00	2850.00	2430.00	1210.00	34.30	-6.84	-52.42	13.3	39.67	14.89
	Min.	10.30	1.55	145.00	143.00	20.60	12.50	-12.51	-86.72	-0.6	9.22	-0.93
	Mean	70.08	20.16	671.45	949.55	149.70	21.37	-8.10	-60.97	3.8	13.74	6.67
	Median	51.40	12.30	435.00	788.00	60.70	20.00	-8.02	-60.86	3.1	12.14	6.88
	SD	45.69	23.46	673.58	585.64	273.48	5.68	1.08	6.43	2.9	6.01	3.60
2 (n=9)	Max.	23.40	6.90	178.00	248.00	41.02	21.10	-6.32	-50.82	11.7	15.34	10.25
	Min.	5.46	0.14	32.00	88.00	9.80	10.90	-9.97	-71.54	-0.4	8.86	-0.02
	Mean	13.65	4.27	111.54	182.89	22.52	16.59	-8.11	-60.06	4.8	10.61	5.35
	Median	14.10	5.67	119.00	205.00	20.80	18.30	-8.11	-59.32	4.4	9.74	4.66
	SD	6.37	2.76	56.98	63.10	10.77	4.14	1.39	7.41	4.0	2.29	3.64
3 (n=15)	Max.	42.70	2.59	342.00	556.00	275.00	26.00	-7.50	-58.00	6.2	24.82	12.06
	Min.	3.51	0.01	32.10	50.00	10.20	14.70	-9.40	-69.03	0.9	10.21	-0.21
	Mean	16.17	1.19	106.82	185.33	64.37	19.17	-8.07	-61.62	2.9	14.74	3.96
	Median	12.60	0.97	75.20	158.00	37.0	19.20	-7.97	-60.68	2.9	12.41	0.86
	SD	12.15	1.01	80.65	135.87	73.32	3.09	0.47	3.18	1.1	5.77	5.57

To further identify the factors contributing to NO$_3^-$ contamination of groundwater in the study area, a PCA based on 18 parameters (temperature, ORP, pH, DO, EC, TDS, Ca^{2+}, Mg^{2+}, Na$^+$, K$^+$, HCO$_3^-$, F$^-$, Cl$^-$, NO$_3^-$, SO$_4^{2-}$, Br$^-$, I$^-$, and Si^{4-}) was performed. The Kaiser-Meyer-Olkin (KMO) and Bartlett's tests were used to prove the competence of the PCA. The KMO value was 0.70 ($p<0.05$), and Bartlett's sphericity test was significantly different from the identity correlation matrix ($p<0.05$); hence, the results from the PCA were validated and provide

significant reductions in dimensionality. The first two eigenvectors (PC1 and PC2) from the PCA are depicted in **Fig.3.3**, which includes the scores of each sampling site on both principal components (the complete dataset is provided in **Table A.2.1 in Appendix 2**), which together explained 78.3% of the total variance in the dataset.
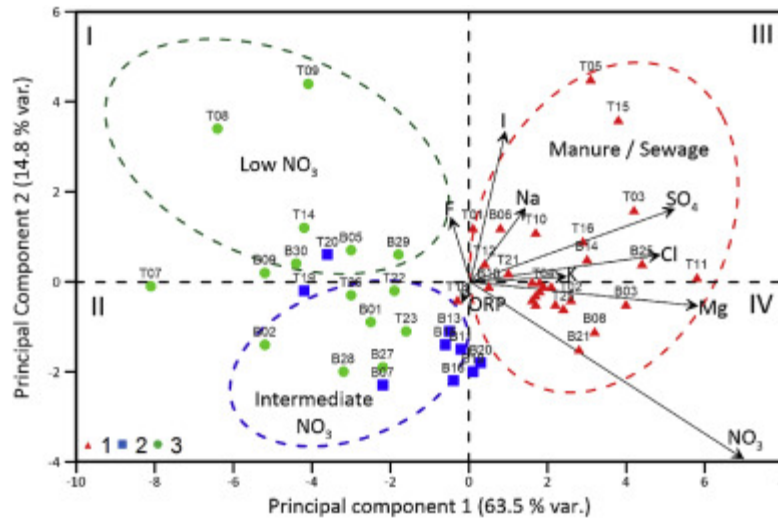

Fig. 3.3. Compositional clr-biplot showing the relationship between major and minor components with NO_3^- sources (the PCA was carried out using the data from **Table A.2.1**)

The first quadrant in **Fig. 3.3** is located in the opposite direction of the NO_3^- ray, indicating that this area (green ellipse) comprises the most NO_3^--depleted samples (group 3). The second quadrant (II) in **Fig.3.3** is in the direction of the NO_3^- ray on the PC2 axis, which indicates an increase in the NO_3^- concentration (groups 2 and 3, blue ellipse). Quadrants III and IV depict the positive scores of PC1, which correspond to the most NO_3^--rich samples (group 1, red ellipse). Both quadrants were associated with M&S sources because contamination of groundwater derived from domestic sewage typically presents significant enrichments of Na^+, Cl^-, SO_4^{2-} (Held et al., 2007; Vystavna et al., 2019; Wang et al., 2019), as well as natural fertilizers (manure as organic-N), which agrees with the land use/land cover.

3.3.2 Isotopic composition of water

The $\delta^{18}O_{H2O}$ and δ^2H_{H2O} values of groundwater samples from CLR ranged from -12.51‰ to -6.31‰, and -86.72‰ to -50.82‰, respectively, with no significant differences among the three groups. **Fig. 3.4a** displays the $\delta^{18}O_{H2O}$ versus δ^2H_{H2O} values, which fell below the global meteoric water line (GMWL; Rozanski et al., 1993) and the local meteoric water line (LMWL; Aguilar-Ramírez et al., 2017). The linear evaporation trend in the dataset (δ^2H_{H2O} = $5.6\delta^{18}O_{H2O}$ -15.37) reflects the groundwater recharge's evaporation process. As a slope of > 5 is atypical for a semi-arid climate, the observed trend suggests the mixing of evaporated soil water with infiltrated rainwater/recirculated agricultural water (Clark and Fritz, 1997; Mahlknecht et al., 2008). Deuterium excess varied mostly between 0‰ and 10‰ (**Fig. 3.4b**), which infers that a post-condensation evaporative effect was associated with the groundwater samples (Clark and Fritz, 1997; Mahlknecht et al., 2008). Although the TDS concentration of the samples ranged widely (257- 4874 mg/L), the $\delta^{18}O_{H2O}$ value was relatively stable at around -9‰ (**Fig. 3.4c**). This suggests that direct evaporation enriched stable isotopes, but it was not the leading cause of the increased TDS concentration (Jia et al., 2017). From these observations, it can be concluded that there are at least two recharge processes in the CLR: (1) recharge from mountainous areas (groups 2 and 3); and (2) vertical aquifer recharge from rainfall or anthropogenic activities (group 1, **Fig. 3.4c**), as evidenced by the evolution trend of the Cl⁻ concentration (i.e., irrigation return flow or sewage leakages).
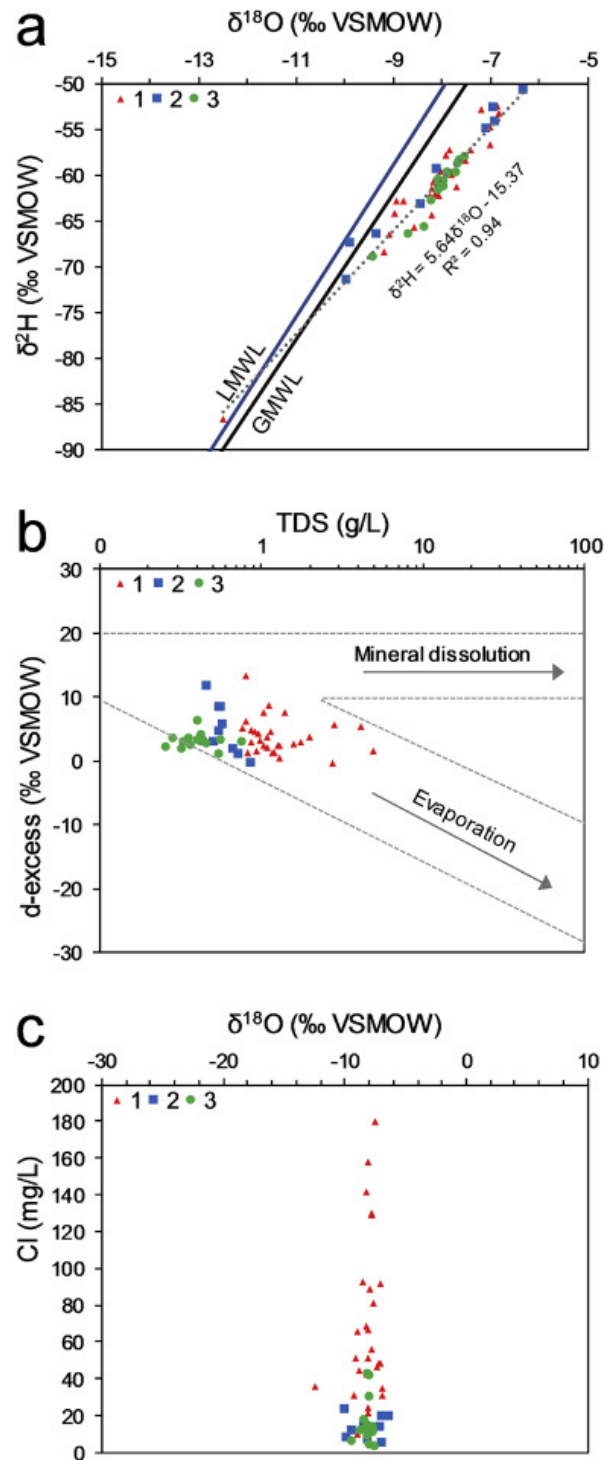
Fig. 3.4. a) Plot showing the mean values of δ18OH2O and δ2HH2O in groundwater of the CLR; GMWL is the global meteoric water line (Rozanski et al., 1993) and LMWL is the local meteoric water line proposed by Aguilar-Ramírez et al. (2017) for northeastern Mexico. b) TDS concentration compared to d-excess. c) $\delta^{18}O_{H2O}$ vs. Cl⁻ concentration. Note: the three groups determined by the HCA are shown in different colors: red triangles (group 1), blue squares (group 2), and green circles (group 3).

3.3.3 Isotopic composition of nitrate

The $\delta^{15}N_{NO3}$ and $\delta^{18}O_{NO3}$ value of the groundwater samples in the study area ranged from 8.86‰ to 39.67‰ and -0.93‰ to 14.89‰, respectively (**Table 3.1**). In the absence of previous nitrate isotope studies for the CLR, the results were compared to typical end-members' values reported in the literature reviews (Section 3.2.5). Based on these reviews, the $\delta^{15}N_{NO3}$ values in the samples were higher than those reported in the literature for synthetic fertilizers (from -6‰ to 6‰). All 53 samples fell between the overlapped range reported for NO_3^- originating from SON (from +3‰ to +8‰), sewage (+4‰ to +19‰), and manure (+5‰ to +35‰). The $\delta^{18}O_{NO3}$ values in the samples from the CLR were lower than those reported for AD (+25‰ to +75‰) and synthetic fertilizers (+17‰ to +25‰). However, the $\delta^{18}O_{NO3}$ values of 16 samples were within the range reported for M&S (+0.5‰ to +5‰), and the $\delta^{18}O_{NO3}$ values of 18 samples were between those of M&S and the theoretical value of NO_3^- derived from nitrification (+10‰). Eight samples were above the microbially-produced NO_3^-, although these $\delta^{18}O_{NO3}$ values could have also been associated with the same origin if $\delta^{18}O_{H2O}$ was enriched due to the evaporative process (Xue et al., 2009). Although the $\delta^{15}N_{NO3}$ and $\delta^{18}O_{NO3}$ values were of different ranges and exhibited diverse N sources, there were no significant statistical differences (*p>0.05*) among the three groups of samples.

3.4 Discussion

3.4.1 Nitrate sources and attenuation interpreted by chemical indicators

The NO_3^- (as N) concentrations ranged from 0.01 to 109 mg/L, with 58% of the samples (mostly belonging to groups 1 and 2) exceeding the threshold value (3 mg/L) for anthropogenic influence (Ogrinc et al., 2019), thus highlighting the severity of NO_3^- contamination problem in the study area. The findings suggest that NO_3^- contamination during the study period was due to leakages from the sewage systems, manure, and/or agricultural inputs. Likewise, 32% of the samples contained a NO_3^- concentration that exceeded the maximum permissible limit (10 mg/L as N) for safe drinking water established by the World Health Organization (WHO, 2017). The lowest NO_3^- concentrations were found at sites T07, T08, and T09 (mean groundwater depth of 113 m), which can be attributed to

the absence of human impact, coupled with their proximity to local groundwater recharge areas. Elevated NO_3^- concentrations were found at sites T11 (109 mg/L), B14 (74.8 mg/L), or B03 (45 mg/L), where the water table depth was 134, 158, and 90 m below ground level, respectively, and which are areas associated with the long-term application of fertilizers or manure.

Chloride is usually considered an essential conservative tracer because it is generally inert to biological or chemical transformations in hydrologic systems (Clark and Fritz, 1997). As a tracer, Cl^- is useful for identifying anthropogenic pollution sources such as sewage leakage, fertilizers, manure, and natural sources (e.g., rainfall or the dissolution of Cl-bearing minerals) that can increase the Cl^- concentrations. A significant positive correlation ($r_s = 0.61, p < 0.001$) was found between NO_3^- and Cl^- in the sampled groundwater of CLR; hence, it can be assumed that manure and sewage are potential sources of NO_3^- (Kohn et al., 2015; Rao, 2006) (**Fig. 3.5b**). In this study, the NO_3^-/Cl^- ratios were used to distinguish whether NO_3^- was derived from agricultural inputs, SON inputs, or sewage inputs (**Fig. 3.5a**). The elevated Cl^- concentration and low NO_3^-/Cl^- ratios (**Fig. 3.5a**) in groundwater samples in group 1 indicate that NO_3^- was derived from M& S (Widory et al., 2005). Group 3 was associated with the lowest Cl^- concentrations and lowest NO_3^-/Cl^- ratios, thus indicating the extent of NO_3^- derived from soil inputs (Guo et al., 2020). Group 2 did not fit in the range of any specific potential NO_3^- input, which suggests that NO_3^- was derived from mixing between soil, sewage, and agricultural sources. Samples with a NO_3^-/Cl^- ratio equal to 1 could be associated with a mixture of agricultural inputs.
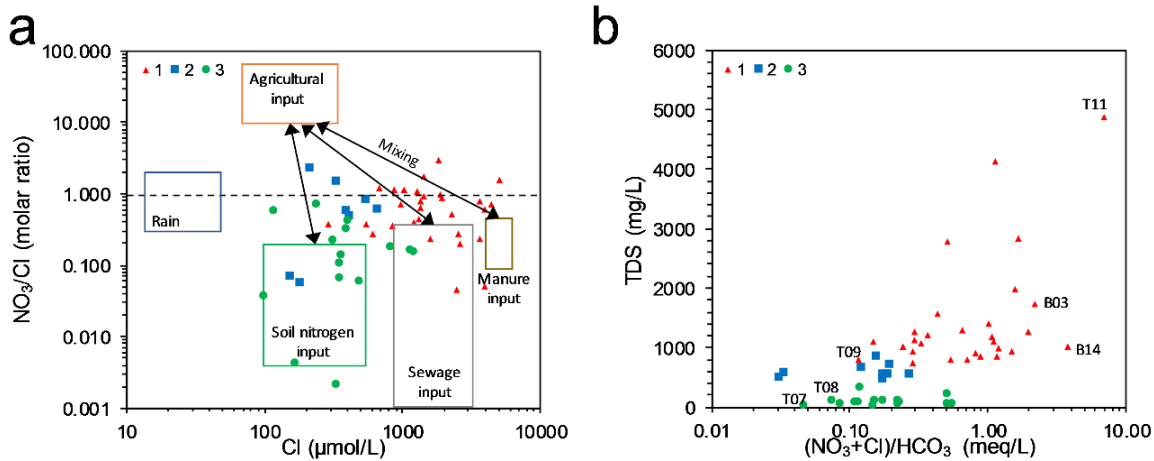
Fig. 3.5. a) Variation of Cl-molar concentrations contrasted with NO3-/Cl-molar ratios of groundwater samples collected in the CLR (adapted from Guo et al., 2020; Widory et al., 2005); b) Scatterplot of TDS vs. $(NO_3^- + Cl^-)/HCO_3^-$

Furthermore, according to **Fig. 3.5b**, the samples within groups 2 and 3 contained a TDS concentration of < 1000 mg/L, whereas group 1 exhibited a TDS concentration of up to ~5 000 mg/L. A $(NO_3^-+Cl^-)/HCO_3^-$ ratio of < 1 for groups 2 and 3, as some samples of group 1 were observed. The samples with a relatively high HCO_3^- concentration could be attributed to the anoxic biodegradation of organic matter (**Eq. 3.3**, Jørgensen et al., 2004).

$$5CH_2O + 4NO_3^- \rightarrow 2N_2 + 4HCO_3^- + CO_2 + 3H_2O \qquad \text{(Eq. 3.3)}$$
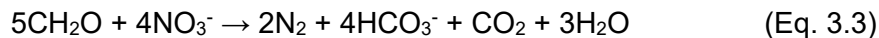
On the other hand, most of the samples in group 1 had a $(NO_3^- + Cl^-)/HCO_3^-$ ratio of > 1, which exhibited a weak positive correlation with the TDS concentration ($r^2=0.37$). This suggests that urea employed in the study area at the time of sampling had suffered hydration (**Eq. 3.4**), which generated an enrichment of HCO_3^- and promoted the nitrification of ammonium (NH_4^+) (**Eqs. 3.5, 3.6**). Moreover, urban and rural sewage contains a large amount of NH_4^+ (Galloway, 2003), which may have contributed to the relatively high NO_3^- concentrations in the water samples.

$$CO(NH_2)_2 + H^+ + H_2O \rightarrow 2NH_4 + HCO_3^- \qquad \text{(Eq. 3.4)}$$

$$2NH_4^+ + 3O_2 \rightarrow 2NO_2^- + 2H_2O + 4H^+ \qquad \text{(Eq. 3.5)}$$

$$2NO_2^- + O_2 \rightarrow 2NO_3^- \hspace{4cm} \text{(Eq. 3.6)}$$
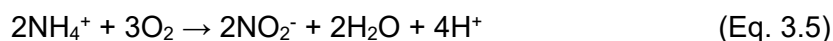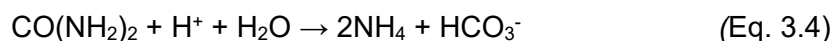
3.4.2 Nitrate sources and biogeochemical processes in the studied groundwater

Nitrogen transformations such as nitrification, denitrification, and volatilization are biogeochemical processes inherent to shallow aquifers. We found no clear correlations between NO_3^- and $\delta^{15}N_{NO3}$ or $\delta^{18}O_{NO3}$ ($r_s = $ *-0.01* and $r_s = $ *0.34*, respectively) in the groundwater samples from the CLR, thus indicating that multiple mixing and biogeochemical processes were responsible for the measured NO_3^- concentrations. **Fig. 3.6a** plots $\delta^{15}N_{NO3}$ vs. $\delta^{18}O_{NO3}$ and includes the isotopic composition of the primary NO_3^- sources and possible biogeochemical processes (Vitòria et al., 2004; Xue et al., 2009).

Local $\delta^{18}O_{NO3}$ values can be used to estimate the contribution of NO_3^- derived from the nitrification of NH_4^-. This contribution can be described by the experimental equation (Andersson and Hooper, 1983), which suggests that it is necessary to incorporate two molecules of oxygen from water and one molecule from dissolved oxygen from atmospheric oxygen for the nitrification process (**Eq. 3.7**).

$$\delta^{18}O_{NO3} = 2/3 \, \delta^{18}O_{H2O} + 1/3 \, \delta^{18}O_{O2} \hspace{2cm} \text{(Eq. 3.7)}$$

where $\delta^{18}O_{H2O}$ represents the measured values in the groundwater samples, and $\delta^{18}O_{O2}$ represents the value for atmospheric oxygen (taken to be +23.5‰) (Aravena and Mayer, 2010). The results revealed that the observed $\delta^{18}O_{H2O}$ values in the study area ranged from -12.5‰ to -6.3‰ (**Fig. 3.6b**). The expected values of $^{18}O_{NO3}$ derived from the nitrification of NH_4^- contained in precipitation, fertilizers, or soil should fall between -0.5‰ and 3.6‰ (identified by the grey area shown in **Fig. 3.6a**).
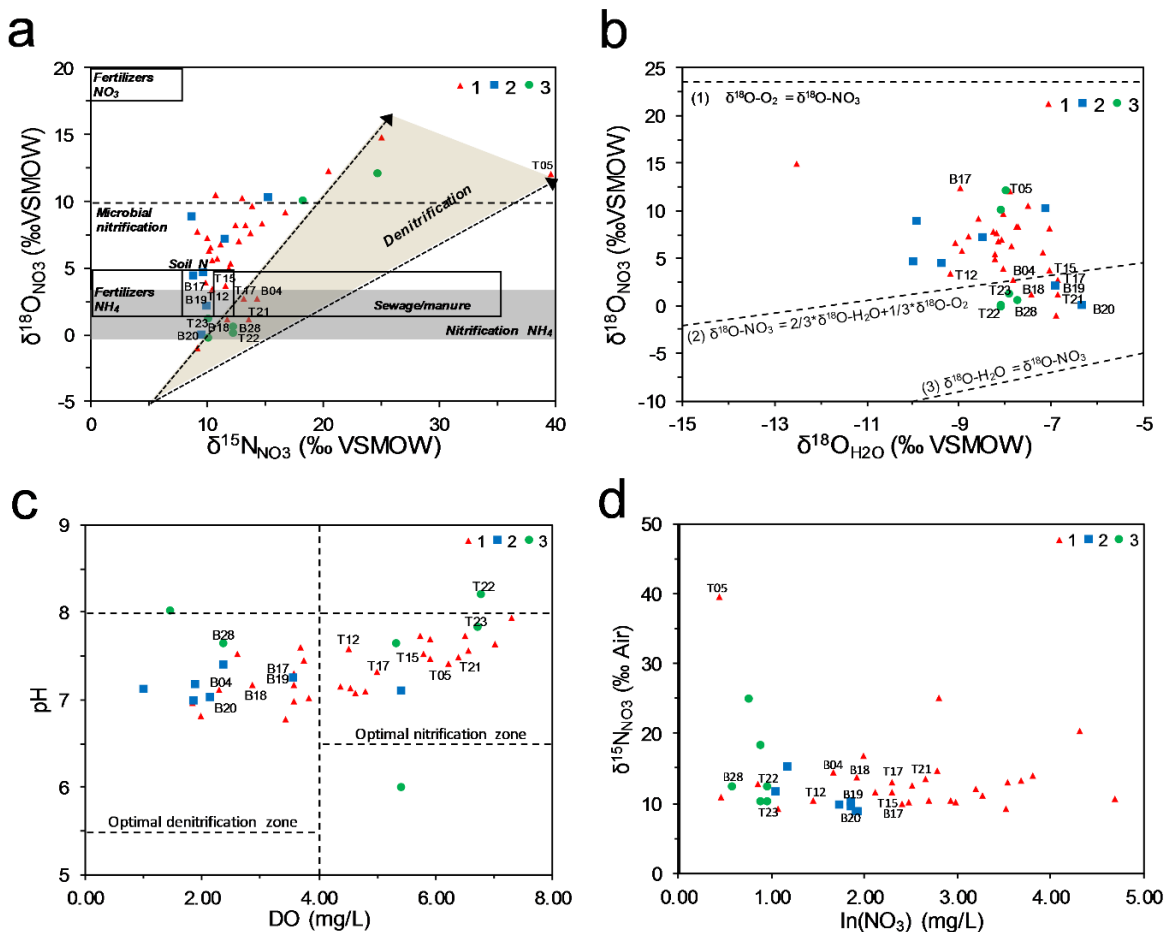
Fig. 3.6. a) Bi-plot of δ15NNO3 versus δ18ONO3. The range of end-members values for the potential sources in the study area was adapted from literature (Kendall, 1998; Xue et al., 2009). b) Plot of δ18O$_{H2O}$ versus δ18O$_{NO3}$, where the line (1) represents the limit of exchange with O$_2$, line (2) represents the limit of the nitrification process, and line (3) shows the limit of exchange with H$_2$O. c) Scatterplot contrasting pH with DO, where the dashed line divides the trends for nitrification (right side) and denitrification (left side) processes. d) Plot showing the δ15N$_{NO3}$ and ln(NO$_3^-$) values in the CLR. Note: the samples belonging to the three different statistical groups are shown in different colors.

Fig. 3.6a confirms the existence of one or more biogeochemical processes that masked the nitrate isotopic composition derived from the original sources in the CLR. Hence, by taking into account the nitrification factors of DO with values > 4mg/L and a pH range of between 6.5 and 8 (Nikolenko et al., 2018) (**Fig. 3.6c**), it can be inferred from **Fig. 3.6a** that the NO$_3^-$ in groundwater samples T23, T22, B28, and B26 (group 3); B19 and B20 (group 2); and T21 and T17 (group 1) were entirely from nitrification. On the other hand, samples T12, B17, and T15 (group 1) were associated with a mixing process, whereby partial nitrification contributed an estimated 49%, 63%, and 84% of the NO$_3^-$, respectively.

Another process is denitrification, which involves the natural attenuation producing a reduction of NO_3^- concentration and a release of HCO_3^-, CO_2, or SO_4^{2-}. If denitrification occurs, the $\delta^{15}N_{NO3}$ or $\delta^{18}O_{NO3}$ values become elevated and follow a positive linear relationship in the residual NO_3^-, with a $\delta^{18}O_{NO3}/\delta^{15}N_{NO3}$ ratio in the range of 1:1.13 to 1:2.1 (Böttcher et al., 1990; Fukada et al., 2003). Some samples (B04, B18, T05, T12, B17, and T15) fell into the ideal zone for denitrification in **Figs. 3.6a-c**, as revealed by an increase of the $\delta^{15}N_{NO3}$ values and a decrease of NO_3^- along the groundwater flow path. Denitrification resulting from the oxidation of organic matter should lead to a decrease in the NO_3^- concentration and a simultaneous increase of HCO_3^- concentration.

Similarly, the relationship between $\delta^{15}N_{NO3}$ and the logarithmic concentration of NO_3^- ($\ln(NO_3^-)$) was employed to understand better the processes occurring in the groundwater system. **Fig. 3.6d** shows that all of the samples followed a negative slope. Groups 1 and 3 negative slopes with low correlations ($r^2=0.040$ and 0.045, respectively) suggest a mixing process, whereas group 2 exhibited a moderate correlation ($r^2=0.64$), which suggests that a denitrification process could have been responsible for the shifting values of $\delta^{15}N_{NO3}$ and $\delta^{18}O_{NO3}$.

The isotopic enrichment of certain samples (e.g., B1, B3, B08, B12, B13, B14) could be explained by an NH_4^+ volatilization process, which can occur within the pH range of these samples (**Eq. 3.8**, Kendall, 1998). In the CLR, manure is produced as dry matter at 1 000 000 t/year, typically used as a natural fertilizer without pretreatment (Acevedo Peralta et al., 2017; Figueroa Viramontes et al., 2015). Thus, NH_4^+ volatilization is favored during storage (before use) and after spreading (Nikolenko et al., 2018; Shalev et al., 2015; Vitòria et al., 2008).

$$CO(NH_2)_2 \rightarrow NH_3 \boxed{\leftrightarrow} NH_4^+ \rightarrow NO_3^- \quad \text{(Eq. 3.8)}$$

3.4.3   Apportionment of NO_3^- sources based on the MixSIAR model

A Bayesian mixing model was used to estimate the probability distribution of the proportional contributions of NO_3^- in combination with land-use/land-cover information for the study area, from which six potential sources were obtained (**Table A.3.1 of Appendix 3**). The MixSIAR

model outputs showed a similar pattern across the different groups, with a low contribution (~10%) of four potential sources: AD, SON, NOF, and NHF (**Fig. 3.7 a-c**); meanwhile, M&S had the highest contribution for all the groups. To simplify the model, manure is referred to as the leaks derived from the storage in confined feeding operations (CAFOs) in the study area, and the manure spread used as a natural fertilizer.
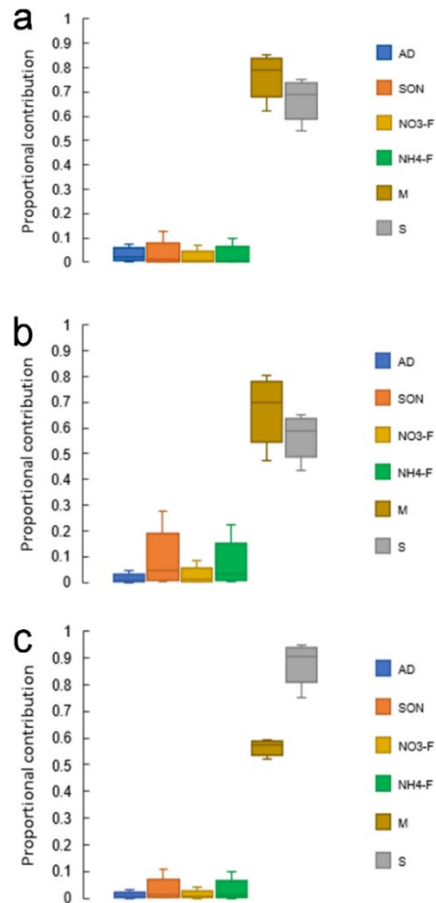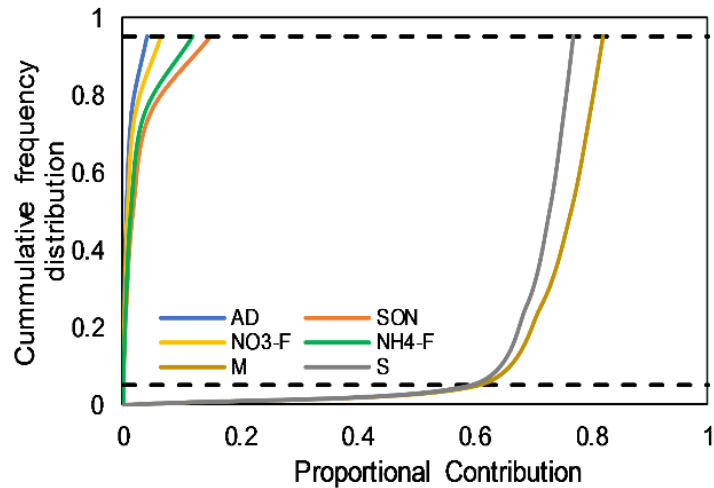

Fig. 3.7. Proportional contributions of the primary potential NO_3^- sources estimated by the MixSIAR model. Boxplots illustrate the 25th, 50th, and 75th percentiles; the whiskers indicate 5th and 95th percentiles. Note: the order a, b, c corresponds to groups 1, 2, and 3. The different NO_3^- sources are shown in different colors.

For the entire study area, the percentage contribution of NO_3^- sources was ranked as: M > S > SON > NHF > NOF > AD. Thus, that of AD was the lowest at 1.2 ± 1.5% of all of the samples. This agrees with findings from other temperate to dry areas (Li et al., 2019; Matiatos, 2016; Torres-Martínez et al., 2020a; Xue et al., 2012) and is in accordance with the low annual rainfall in the study area. The percentage contribution of SON was similar for groups 1 and 3 (3.0 ± 4.8% and 2.8 ± 4.1%, respectively), which were lower than that of

group 2 (7.9 ± 9.2%). This agrees with the lower NO_3^-/Cl^- ratios and lower Cl^- concentrations in **Fig. 3.5a**. Further, NOF and NHF contributed means of 1.7 ± 2.4% and 3.0 ± 4.5%. However, the most significant source of NO_3^- to groundwater in the study area was from M&S, with mean contributions of 47.7 ± 4.3% (M) and 42.6 ± 4.3% (S), which are consistent with **Figs. 3.3** and 3.5**5a**. Thus, during sampling, the CLR was mainly polluted by anthropogenic inputs from leakage of the municipal sewage system in metropolitan areas, septic tanks leakage in rural communities, and the intensive application of manure as an organic fertilizer. Even though the CLR is an important agricultural area of Mexico, our results indicate that synthetic fertilizers were not the main cause of elevated NO_3^- concentrations during our study.

The sum of the estimated proportional contributions should be equal to 1 (**Fig. 3.8**). However, each estimated contribution is a probability distribution in a particular range. Thus, an uncertainty index (UI_{90}) was calculated as the difference between the proportional contribution of 0.95 and 0.05 (considering the rapid increase segment of 90%), divided by 0.9, to characterize the uncertainty strength. Overall, AD and NOF were relatively stable, showing a UI_{90} of 0.05 and 0.07, respectively. Besides, NHF and SON exhibited similar UI_{90} values (0.13 and 0.17, respectively), whereas the highest uncertainty was associated with M (0.24) and S (0.20). The increased uncertainty in M and S sources could be attributed to isotope fractionation during the different transformation processes along the groundwater flow path that affects the isotopic fingerprint.

Fig. 3.8. Cumulative probability distributions for proportional contributions of the different potential NO_3^- sources based on MixSIAR results. Note: the different NO_3^- sources are shown in different colors.

In summary, six different potential NO_3^- sources were identified in the CLR and evaluated by combining the results of major ion chemistry, stable isotopes, and MixSIAR, a Bayesian isotope mixing model. The findings of this chapter could provide technical support for stakeholders aiming to improve water quality management in the CLR. As urban sewage and manure applications were by far the primary sources of groundwater NO_3^-, local authorities should consider rehabilitating the sewage pipelines used to collect industrial and domestic sewage in urban areas. Furthermore, there is a need to enhance the treatment, management, and disposal of manure for agricultural activities. Considering that manure is the main fertilizer used in the study area, it is necessary to minimize its overuse and establish a manure regulatory policy because there is no strict regulation in Mexico (Acevedo Peralta et al., 2017).

Although our results provide essential information for identifying, evaluating, and controlling NO_3^- concentrations in groundwater, there are some limitations. It should be noted that the MixSIAR model allows an estimation of the proportional contribution of NO_3^- sources with relatively low uncertainty values inherent to NO_3^- inputs. Another uncertainty exists because most production wells have an open casing (full-screened) regardless of the depth. Hence, the collected samples in this research are a mix of different circulation depths, which also contributed to the uncertainty in the model results. We note that, although the findings revealed the source contributions at a specific season (autumn), there was no rain during

our sampling, and temporal changes over the entire year may have been negligible due to the predominantly dry climate. Further investigations based on additional isotope tracers (e.g., $\delta^{11}B$, $\delta^{34}S$, $\delta^{87}Sr/^{86}Sr$, $\delta^{13}C$) could help to improve the understanding of the different biogeochemical processes and pollution sources that affect the N cycle in the selected study area.

3.5 Conclusion

This chapter exhibited an example of using hydrochemical compositions and isotopic fingerprints (δ^2H, $\delta^{18}O_{H2O}$, $\delta^{15}N_{NO3}$, $\delta^{18}O_{NO3}$) in combination with a Bayesian isotope mixing model to elucidate the sources, transformations, and contributions of NO_3^- pollution in the overexploited groundwater of the arid CLR in Mexico. The results showed that 58% of the groundwater samples from the CLR exceeded the threshold for anthropogenic inputs, and 32% exceeded the WHO´s safe drinking water limit of 10 mg/L. From this, a low (<3 mg/L; group 3), moderate (<10 mg/L; group 2) and high (>10 mg/L; group 1) NO_3^- concentrations zones were identified.

NO_3^- in the groundwater was derived from multiple sources, including soil organic nitrogen (SON), synthetic fertilizers (NHF and NOF), manure, urban sewage, and precipitation. Results showed that using a Bayesian isotope mixing model in combination with land-use and land-cover maps could be successfully applied to estimate proportional contributions of non-point NO_3^- sources, confirming that leakage derived from the intensive use of manure ($\sim$48%) and urban sewage or septic tanks leakages ($\sim$43%) were the primary NO_3^- pollution sources in the CLR. In comparison, synthetic fertilizers ($\sim$5%) and SON ($\sim$4%) contributed less to the enhancement of NO_3^- concentration in groundwater. Furthermore, by combining isotopic fingerprints (δ^2H, $\delta^{18}O_{H2O}$, $\delta^{15}N_{NO3}$, $\delta^{18}O_{NO3}$), a substantial nitrification process was identified as the predominant transformation in samples from recharge areas. Contrarily, samples from discharge areas were influenced by a denitrification transformation, which agrees with the low NO_3^- concentrations. Otherwise, transition-zone samples showed a combination of different biogeochemical processes: nitrification, denitrification, and volatilization.

Chapter 4: La Paz Aquifer Case

4.1 Introduction

The human population is unevenly distributed globally, and the majority of economic development has occurred along rivers and coastal areas (Erostate et al., 2020; Grimm et al., 2008; Rodrigues Braga et al., 2020). Coastal zones are attractive for multiple reasons, such as an abundance of different natural resources, access to marine trade or transport opportunities, and the provision for recreational activities. However, increasing urban sprawls also causes radical changes in coastal environments, including land-use changes and increasing environmental pollution. This creates a severe demand for natural resources, exacerbated by a lack of government planning and management (Erostate et al., 2020; Neumann et al., 2017; Sterzel et al., 2020). Arid coastal areas are mainly dependent on groundwater resources, which, together with accelerated population growth, generates water stress and often leads to groundwater contamination due to seawater intrusion into freshwater resources.

The coastal aquifer system of La Paz, Mexico, is an example of an arid urban environment with prolonged periods of drought, relying on groundwater to satisfy the needs of approximately 270,000 inhabitants, 3,800 ha of agricultural land, and more than 320,000 tourists per year (INEGI, 2017; SIAP, 2018b). A lack of proper water management policies has resulted in over-drafting of the aquifer system, promoting an inversion in the hydraulic gradient, which has triggered the seawater intrusion. Previous research on this coastal aquifer system has focused on hydrogeological characterization (CONAGUA, 1997; Cruz-Falcón, 2007; Cruz-Falcón et al., 2010), assessing seawater intrusion using groundwater flow models(CONAGUA, 2001; Escolero and Torres-Onofre, 2007; Monzalvo, 2010; Torres-Martinez et al., 2019), and evaluating groundwater quality (CONAGUA, 2010, 2001; Cruz-Falcón et al., 2017; Torres-Martínez et al., 2017). Additionally, some studies have assessed the groundwater flow (Tamez-Meléndez et al., 2016) and seawater intrusion (Mahlknecht et al., 2017) in that zone using multi-isotopic techniques. This suggests that elevated NO_3^- and SO_4^{2-} concentrations could be attributed to agricultural practices in the area, contributing to groundwater quality degradation. Nevertheless, the aforementioned studies did not use conclusive tools to support this assumption.

Almost all previous studies have focused only on water quality problems due to seawater intrusion. However, human-derived pollution is a significant reason for deteriorating water quality; such pollution results mainly from non-point sources, including agricultural practices or leaks in the sewage system, leading to NO_3^- and SO_4^{2-} groundwater pollution. Although distinguishing NO_3^- or SO_4^{2-} sources in coastal environments is a complicated task, it is vital to establish opportune management plans because both substances can damage human health (Blaisdell et al., 2019; Sharma and Kumar, 2020) and result in adverse biota effects (Gomez Isaza et al., 2020; Sharma and Kumar, 2020).

A typical method for differentiating NO_3^- and SO_4^{2-} pollution sources is the use of the dual-stable isotopic compositions of nitrate ($\delta^{15}N_{NO3}$ and $\delta^{18}O_{NO3}$) and sulfate ($\delta^{34}S_{SO4}$ and $\delta^{18}O_{SO4}$). Unfortunately, despite the ability of the dual-isotope plot to trace the origin of NO_3^- and SO_4^{2-} contamination, uncertainties remain because two or more sources may sometimes overlap, hindering the correct differentiation of the origin (Nikolenko et al., 2018; Wang and Zhang, 2019). Moreover, the biogeochemical transformations in the environment affect the isotopic fingerprint, which complicates the source's identification. To avoid overlapping-related issues in nitrate source identification, some studies have utilized a combination of different techniques, using stable nitrate isotopes in conjunction with halide ratios (Pastén-Zapata et al., 2014; Torres-Martínez et al., 2020a), boron isotopes (Kruk et al., 2020; Lasagna and De Luca, 2019), multivariate statistical methods (Guo et al., 2020; Matiatos, 2016; Torres-Martínez et al., 2020b), microbiological approaches (Romanelli et al., 2020; Zhu et al., 2019), and multi-isotopic approaches (Li et al., 2020; Pittalis et al., 2018; Zhang and Wang, 2020). Although the identification of SO_4^{2-} sources in groundwater has not been studied extensively, some studies have combined sulfate isotopes with carbon isotopes (Han et al., 2016; Hosono et al., 2014) and multi-isotopic (Hosono et al., 2011b; Puig et al., 2013) or bacterial approaches (Valiente et al., 2017) to elucidate the origins of sulfate in groundwater.

Several methods have also been used to develop a reliable technique for providing quantitative estimates of natural and anthropogenic nitrate sources' contribution to the total nitrate pool in specific groundwater environments. These methods include using analytical and mathematical tools such as mass balance calculations (Degnan et al., 2016; Janža et al., 2020), end-member mixing analysis (Grimmeisen et al., 2017; Ogrinc et al., 2019), and

77

statistical models such as multi-linear regression analysis (Meghdadi and Javar, 2018b) and the Bayesian isotope mixing model (BIMM)(Cui et al., 2020; Gibrilla et al., 2020; Kazakis et al., 2020; Torres-Martínez et al., 2020b). In contrast, to estimate the contribution of different sulfate sources, only a few methods have been developed using chemical mass balance models (Sun et al., 2021; Xu et al., 2016), end-member mixing models (Chen et al., 2020), and BIMMs (Torres-Martínez et al., 2020a; Q. Zhang et al., 2020).

To the best of our knowledge, no environmental studies have estimated the proportion of seawater-derived sulfate in coastal aquifers affected by seawater intrusion using a dual-isotope sulfate analysis combined with a BIMM. Therefore, the objectives of this chapter are 1) to assess the nitrate and sulfate concentrations in groundwater from the La Paz aquifer; 2) to identify the sources of NO_3^- and SO_4^{2-} in groundwater using multiple stable isotopes; and 3) to quantify the apportionment of different potential NO_3^- and SO_4^{2-} pollution sources (including seawater-derived sulfate) using a BIMM. This study is the first to estimate the contribution and uncertainty of seawater-derived SO_4^{2-} using $^{34}S_{SO4}$ and $^{18}O_{SO4}$ combined with the BIMM.

4.2 Materials and methods

4.2.1 Study area

The La Paz aquifer system is situated in the eastern part of the California Gulf in the northeastern region of Mexico (**Fig. 4.1**). The morphological architecture of the La Paz region is characterized by a coastal plain (valley) enclosed by plateaus and mountain ranges that reach heights of 1,266 m above sea level. The geology of the area is composed of metamorphic, volcanic, and sedimentary formations (**Fig. A3.1**). Metamorphic rocks (gneiss, shales, and metasedimentary rocks) deposited from the Jurassic (Mesozoic Era) are found in the basement. Beyond this unit in the basin's mountainous part, Cretaceous volcanic rocks (mainly gabbro, granite, and granodiorite) emerge in the eastern region of the area, constituting the Las Cruces mountain range. In the western part, Neogene sedimentary rocks (sandstones and conglomerates) and fractured volcanic rocks (rhyolitic tuff and basalt) are present. In the central lowlands of the valley, Holocene deposits consisting of

unconsolidated alluvial deposits (sands, gravels, silts, and clays) and marine sediments are found (Hirales Rochin and Urcadiz Cazares, 2019; INEGI, 1995; SGM, 2007).

The study area has a semi-desert climate, with average annual temperature and precipitation of 24 °C and 263 mm, respectively. Hence, the area exhibits an unbalanced distribution between rainfall and surface runoff because most of the precipitation occurs between July and October (hurricane season), accounting for more than 75% of the annual rainfall. Land use in the area is mainly urban and agricultural. Hence, the yearly water demand for agricultural, urban, and tourist activities is met with groundwater from the basin's aquifers. However, severe over-drafting has resulted in excessive chloride concentrations in the local groundwater due to seawater intrusion (Mahlknecht et al., 2017). On the other hand, the excessive use of N-based fertilizers has led to a considerable increase in NO_3^- concentrations in groundwater from agricultural regions, necessitating identifying the origin to establish NO_3^- management plans.
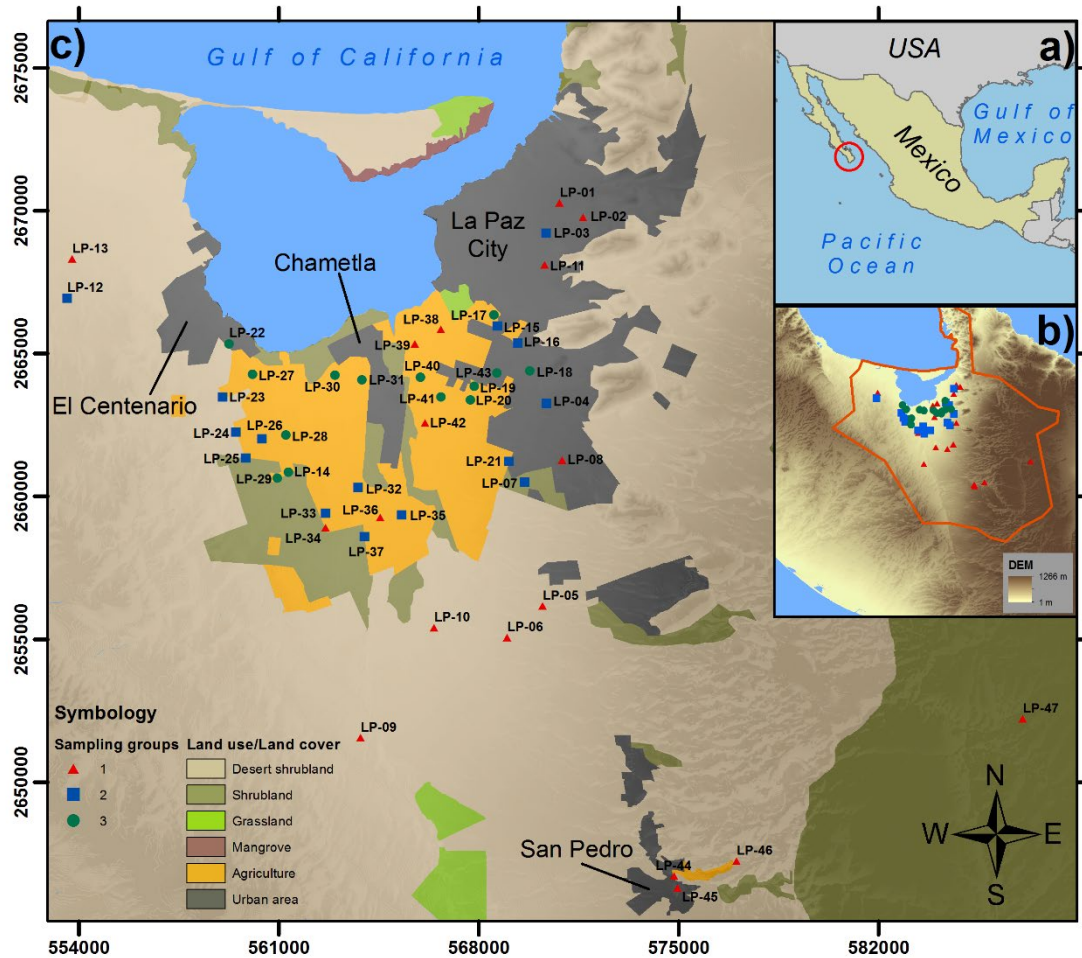
Figure 4.1. (a) Location of La Paz aquifer in northeastern Mexico; (b) delimitation of the aquifer using digital elevation model; and (c) land use/land cover, locations of the sampled sites, and main urbanized areas.

4.2.2 Sample collection and analytical methods

Considering the different land uses, potential pollution sources, and geographical coverage, water samples from 46 production wells and one spring were collected in August 2013. Groundwater samples correspond to alluvial aquifers with well depths varying from 15 to 200 m (**Table 4.2**). Before obtaining the water samples, the production wells were drained until the pH, and electrical conductivity (EC) were stabilized to prevent water stagnation and obtain a representative groundwater sample. In-situ measurements of temperature, pH, dissolved oxygen (DO), and EC were performed using a multiparameter probe (Orion Star A329, Thermo Fisher Scientific). Bicarbonate species were determined through acid-base

titration using a 0.02-N solution of H_2SO_4. The collected samples were filtered through 0.45-µm membranes and stored in triple-pre-rinsed low-density polyethylene bottles. Samples for cation analysis were acidified to pH 2 to prevent analyte losses, whereas samples for anion determination were placed in sampling kits without any preservative. All the samples for chemical analyses were maintained at 4 °C until analysis, whereas the samples for NO_3^- and SO_4^{2-} isotopes were frozen to -20 °C to minimize chemical reactions and prevent any alteration caused by biological processes.

Chemical analyses were conducted at Activation Laboratories Ltd. (Ancaster, Canada) according to the Standard Methods for the Examination of Water and Wastewater(APHA, 2012). Cations (Na^+, K^+, Ca^{2+}, Mg^{2+}) were measured using inductive-coupled plasma optical emission spectrometry (ICP-OES, Agilent Axial 730-ES), whereas anions (Cl^-, SO_4^{2-}, NO_3^-) were measured using ion chromatography (IC, Dionex DX-120). The charge-balance error (%) was calculated, considering a 10% threshold as the acceptance criterion to validate the results.

The water stable-isotope composition (δ^2H_{H2O} and $\delta^{18}O_{H2O}$) was measured at Tecnologico de Monterrey (Mexico) using off-axis integrated cavity output spectroscopy (OA-ICOS, LGR-DLT-100). The analytical procedure followed the methodology described by Berman et al. (2013), with accuracies of ±0.2‰ and ±0.8‰ for $\delta^{18}O_{H2O}$ and δ^2H_{H2O}, respectively. Nitrate isotopes ($\delta^{15}N_{NO3}$ and $\delta^{18}O_{NO3}$) and sulfate isotopes ($\delta^{34}S_{SO4}$ and $\delta^{18}O_{SO4}$) were measured at the Environmental Isotope Laboratory of the University of Waterloo (Canada). The nitrate isotopes were measured using a chemical reduction technique(Ti et al., 2018), which reduced NO_3^- to NO_2^- through a cadmium catalyst chemically converted to N_2O for analysis using a trace-gas isotope-ratio mass spectrometer (TG-IRMS, GVI-IsoPrime). The analytical accuracy was ±0.3‰ for $\delta^{15}N_{NO3}$ and ±0.8‰ for $\delta^{18}O_{NO3}$. The sulfate isotopic composition test ($\delta^{34}S_{SO4}$ and $\delta^{18}O_{SO4}$) was conducted by first acidifying the sample to a pH value of 3, followed by boiling and adding $BaCl_2$ to obtain $BaSO_4$. Then, the $BaSO_4$ was oven-dried to 80 °C, before an element analyzer (EA, Elementar PrecisION-EA) coupled to a continuous-flow isotope-ratio mass spectrometer (CF-IRMS, GVI-Isoprime) was used. The analytical precisions for $\delta^{34}S_{SO4}$ and $\delta^{18}O_{SO4}$ were ±0.3‰ and ±0.5‰, respectively.

All the stable-isotope ratios for H_2O, NO_3^-, and SO_4^{2-} were expressed in delta values (δ), representing deviations in the per mil (‰) notation following international standards (**Eq. 4.1**):

$$\delta_{sample}(‰) = \frac{R_{sample} - R_{standard}}{R_{standard}} * 1000 \qquad \text{(Eq. 4.1)}$$

where $R_{sample/standard}$ is the abundance ratios (D/H, $^{15}N/^{14}N$, $^{34}S/^{32}S$, or $^{18}O/^{16}O$) for the sample and standard, respectively; the standard for nitrogen isotope measurements pertains to atmospheric N_2. For sulfur isotopes, measurements are in accordance with the Vienna Cañon Diablo Troilite (VCDT) standard. Finally, hydrogen and oxygen are reported in accordance with the Vienna Standard Mean Ocean Water (VSMOW).

4.2.3   Interpretation techniques

4.2.3.1   Self-organizing maps

Multivariate statistics is a common approach used for processing groundwater grouping data. However, an alternative tool for determining the hydrogeochemical similarities of complex environments is the self-organizing map (SOM). The SOM is an artificial neural network technique developed by Kohonen (Kohonen, 1982) to emulate the biological processes of human brains. This technique was designed to obtain a nonlinear dimensionality reduction in which similar inputs are physically located close to each other in neurons, preserving the data structure to summarize data with unsupervised classifications (Kohonen, 2013). SOM models have been effectively used in hydrology, hydrogeochemistry, and other water-related fields (Céréghino and Park, 2009; Clark et al., 2020; Kalteh et al., 2008).

The SOM algorithm consists of an input layer and an output layer of neurons (SOM layer), typically arranged on a hexagonal lattice grid. The input layer is wholly connected to the SOM layer through a weight vector (V_i). The following procedure describes the SOM algorithm:

1. Data preprocessing. A transformation of the data is necessary before using the SOM method to ensure that all the hydrochemical parameters have the same relevance. In this study, all the variables were transformed using the compositional data technique known as centered log-ratio transformation (CLR). This transformation involves dividing each component (x) by the geometric mean (g(X)) of all variables, according to the following equation (**Eq. 4.2**):

$$clr(x_i) = ln\frac{x_i}{g(X)} \qquad \text{(Eq. 4.2)}$$

2. Determination of the SOM structure. The optimal number of nodes (neurons) was estimated using the heuristic rule $m = 5\sqrt{n}$ (Vesanto and Alhoniemi, 2000), where m is the total number of nodes, and n is the number of samples in the dataset.
3. Initialization of the weight vector (W_i) with random values.
4. Identification of the winner neuron or best-matching unit, which is the closest match to the input vector, using the Euclidian distance, D (**Eq. 4.3**):

$$D = \sqrt{\sum_{i=1}^{n}((V_i - W_i)^2} \qquad \text{(Eq. 4.3)}$$

5. Continuation of the iterative training until the integrated distance criterion is minimized.
6. Post-processing of the SOM results. Visualization maps (unified distance matrix and component planes) are generated, and each node's reference vector is projected onto the maps.

In this study, the Kohonen package developed in the R environment (Wehrens and Buydens, 2007) was used to analyze the hydrochemical data. The input layer of the SOM consisted of a matrix of 5 field parameters (temperature, pH, DO, total dissolved solids (TDS), and EC) and 11 chemical parameters (Ca^{2+}, Mg^{2+}, Na^+, K^+, HCO_3^-, Cl^-, NO_3^-, SO_4^{2-}, Si^-, Br^-, and As^-) of 47 water samples. Following the heuristic rules, a feature map with 42 (6 × 7) nodes was selected. The SOM model results were used with the k-means clustering algorithm to obtain an appropriate number of groups (Kim et al., 2020). After the groups were formed, the normality was analyzed for all groups using the Shapiro–Wilk test, and the difference in

variables between groups was evaluated using an ANOVA test ($p < 0.05$). If the assumption of normality was rejected, the non-parametric Kruskal–Wallis test was applied.

4.2.3.2 Estimation of contributions from different nitrate pollution sources

The proportional contributions of the different NO_3^- and SO_4^{2-} pollution sources in the water samples were calculated using a Bayesian stable-isotope mixing model, which employs the Markov chain Monte Carlo method with a Bayesian framework. Models were implemented using the MixSIAR package (version 3.0.2) developed in an R environment. The methodology used in the MixSIAR model has been described in detail by Stock *et al.* (2018). The different isotopic compositions of nitrate and sulfate sources used in the model were obtained through a literature review (Nikolenko et al., 2018; Torres-Martínez et al., 2020a; Wang and Zhang, 2019; Xue et al., 2009; Y. Zhang et al., 2018b) and are listed in **Table 4.1**. The model parameters were set as 500,000 iterations with a burn-in of 50,000, a sample interval of 15, and an iteration maintainer of 30,000. Furthermore, an uncertainty index (UI_{90}) defined by Ji *et al.* (2017) was applied to characterize the uncertainty based on the posterior distribution (**Eq. 4.4**) and then delineate the uncertainty associated with the apportionment of the pollution sources.

$$UI_{90} = \frac{PC_{90} - PC_{10}}{90} \qquad \text{(Eq. 4.4)}$$

where *PC_{90} and PC_{10}* denote the maximum and minimum proportional contribution values in the immediate increase segment with a 90% cumulative probability.

Table 4.1. Summary of $\delta^{15}N_{NO3}$, $\delta^{18}O_{NO3}$, $\delta^{34}S_{SO4}$, and $\delta^{18}O_{SO4}$ isotopic signatures, from some possible end-members used in the MixSIAR model

Source	$\delta^{15}N_{NO3}$ Mean ± SD	$\delta^{18}O_{NO3}$ Mean ± SD	$\delta^{34}S_{SO4}$ Mean ± SD	$\delta^{18}O_{SO4}$ Mean ± SD
Atmospheric deposition (AD)	0.1 ± 1.7	55.0 ± 7.6	5.3 ± 1.4	11.6 ± 2.1
Soil organic nitrogen (SON)	3.74 ± 2.09	2.39 ± 2.24	-	-
Soil sulfate (SS)	-	-	9.6 ± 1.4	6.0 ± 2.8
Sewage (S)	17.4 ± 3.9	5.9 ± 3.1	7.4 ± 2.0	10.5 ± 1.6
Detergents (D)	-	-	7.61 ± 8.41	14.67 ± 3.08
Synthetic fertilizer (SF)	1.24 ± 1.44	3.44 ± 2.47	3.58 ± 4.38	14.40 ± 2.55
Seawater (SW)	-	-	21.2 ± 0.5	11.1 ± 0.5

4.3 Results

4.3.1 Water sampling grouping and hydrogeochemical characterization

The field measurements, chemical parameters, and isotopic ratios measured in the groundwater samples collected from the La Paz aquifer system are summarized in **Table 4.2** (complete database is presented in **Table A.3.1 of Appendix 3**). The map size used in the SOM model was 35 (5 × 7), with minimum quantization error and topographic error values of 0.02 and 0.01, respectively; this indicates that the SOM model results were optimal. **Fig. 4.2** shows a visualization of the different component planes of each hydrochemical parameter used in the iterative trained SOM map. Each component plane matrix denotes an index value obtained after dimension reduction, which instantly recognizes dependencies among hydrochemical variables through a gradient from white to red, corresponding to low and high values, respectively. Based on contrasting of the qualitative relations of the component plane maps, Ca^{2+}, Mg^{2+}, and Cl^- have similar color change gradients (increasing to the upper right), indicating a strong correlation, which is in agreement with the results obtained by Támez-Meléndez *et al*. (2016) through a Pearson correlation analysis. Conversely, Na^+ and SO_4^{2-} exhibited an increasing trend to the lower left. The K^+, SO_4^{2-}, and NO_3^- ions did not follow patterns similar to those of the other major ions.
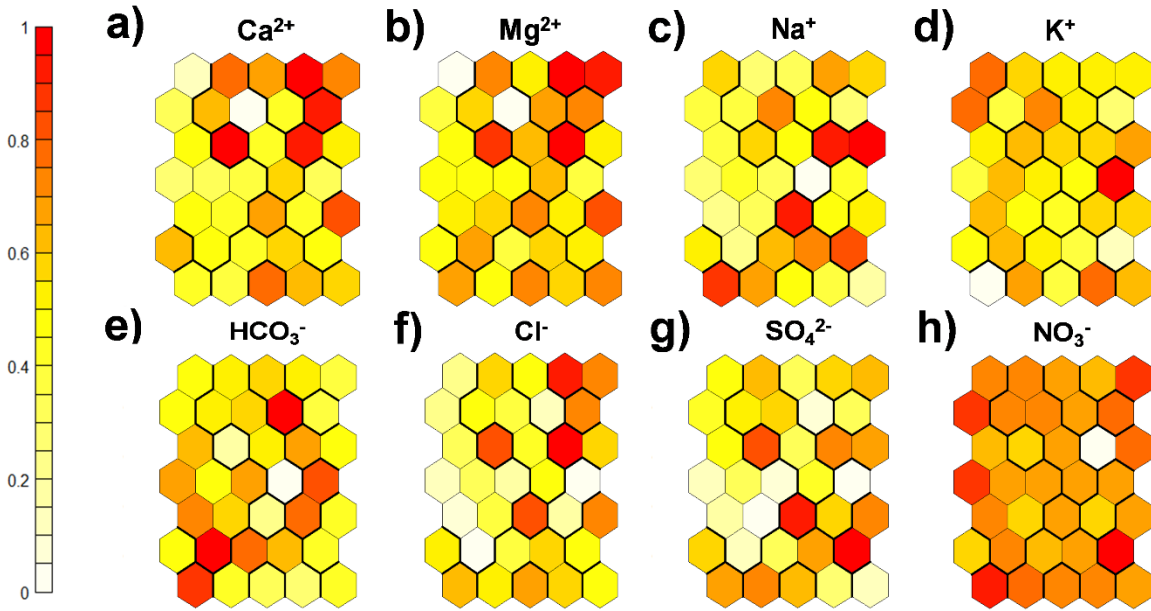
Figure 4.2. Component planes for major cations and anions: (a) Ca^{2+}, (b) Mg^{2+}, (c) Na^+, (d) K^+, (e) HCO_3^-, (f) Cl^-, (g) SO_4^{2-}, (h) NO_3^-

Considering the hydrogeochemical conditions, the results obtained using the SOM model suggested that the groundwater chemistry in the study area could be divided into three groups according to their similarities and geographical correspondence, as shown in **Fig. 4.3**. Group 1 (18 samples, red shapes) represents fresh groundwater collected from the recharge areas (southern area of the aquifer), infiltration areas with treated wastewater (LP3-38 and LP-39), and the urbanized area of La Paz city. Group 2 (14 samples, blue shapes) represents fresh to brackish water sampled near agricultural areas. Finally, Group 3 (14 samples, green shapes) represents brackish water sampled close to the coastline, irrigated land, and the El Centenario and Chametla communities.
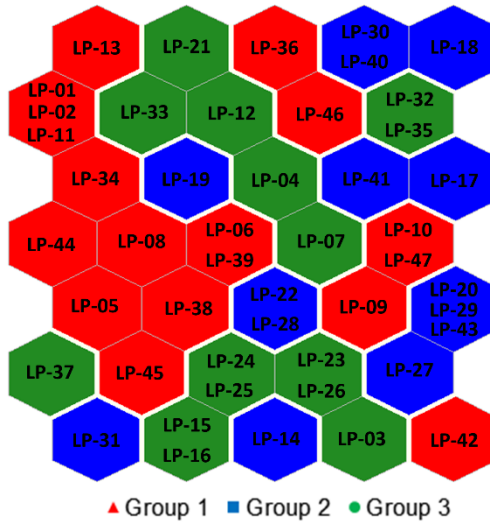
Figure 4.3. Pattern classification map of three clusters obtained by combining the SOM model and K-means algorithm. Numbers represent the Id of the water sampling points.

Table 4.2. Summary of descriptive statistics for physicochemical and isotopic parameters in La Paz aquifer

Group		Depth (m)	T (°C)	pH	DO (mg/L)	SDT (mg/L)	EC (µS/cm)	Ca (mg/L)	Mg (mg/L)	Na (mg/L)	K (mg/L)
1	Mean	92.2	29.9	7.4	7.9	562.8	844.2	48.3	18.7	68.5	3.1
(n = 18)	SD	67.4	2.0	0.3	1.8	125.8	232.6	16.1	7.2	26.5	1.1
2	Mean	84.1	30.2	7.2	7.0	1,418.6	2,101.0	139.9	45.0	196.4	4.7
(n = 14)	SD	51.0	2.0	0.1	1.3	435.3	648.0	65.7	19.8	102.7	1.8
3	Mean	43.4	29.3	7.3	6.3	3,352.0	5,087.0	338.1	141.5	499.4	8.0
(n = 14)	SD	20.5	1.06	0.1	1.2	1,129.0	1,758.0	135.4	71.1	240.0	2.9

Group		HCO$_3$ (mg/L)	Cl (mg/L)	NO$_3$ (mg/L)	SO$_4$ (mg/L)	δ^{18}O$_{H2O}$ (‰ VSMOW)	δ^{2}H$_{H2O}$ (‰ VSMOW)	δ^{15}N$_{NO3}$ (‰ Air)	δ^{18}O$_{NO3}$ (‰ VSMOW)	δ^{18}O$_{SO4}$ (‰ VSMOW)	δ^{34}S$_{SO4}$ (‰ VCDT)
1	Mean	228.1	138.7	4.0	24.2	-9.6	-68.2	8.4	0.1	7.2	12.5
(n = 18)	SD	54.7	65.7	2.9	14.5	1.0	7.5	1.6	1.5	3.4	4.9
2	Mean	378.0	519.1	6.7	91.4	-8.6	-61.9	10.1	0.9	5.5	14.0
(n = 14)	SD	128.4	196.1	3.3	49.4	0.9	6.3	4.4	2.6	1.6	3.7
3	Mean	597.7	1,462.0	15.6	243.9	-8.7	-63.2	11.6	0.6	4.6	14.5
(n = 14)	SD	251.4	648.0	14.9	111.9	0.6	4.7	2.1	1.2	1.7	1.5

The depth of the production wells across the groups varied substantially, from 15 to 201 m below the surface; however, the depths of wells from Group 3 were significantly less ($p <$ 0.05, mean 43.4 ± 20.5 m) than those of the wells from both Groups 1 and 2. There were no significant differences between groundwater temperatures and pH among the three groups, with the mean values being 29.8 ± 1.7 °C and 7.3 ± 0.3, respectively. The DO concentration

in Group 3 (6.3 ± 1.2 mg/L) was significantly lower ($p < 0.05$) than that in Groups 1 and 2, which exhibited mean values of 7.9 ± 1.8 and 7.1 ± 1.3 mg/L, respectively. The mean TDS and EC values increased significantly ($p < 0.01$) in the following order: Group 1 (TDS: 562.8 mg/L; EC: 844 µS/cm) < Group 2 (TDS: 1,418.6 mg/L; EC: 2,101 µS/cm) < Group 3 (TDS: 3,352 mg/L; EC: 5,087 µS/cm).

The average concentrations of major anions (Ca^{2+}, Mg^{2+}, Na^+, and K^+) increased significantly ($p < 0.01$) in the following order: Group 1 (Ca^{2+}: 48.3 mg/L; Mg^{2+}: 18.7 mg/L; Na^+: 68.5 mg/L; K^+: 3.1 mg/L) < Group 2 (Ca^{2+}: 139.9 mg/L; Mg^{2+}: 45.0 mg/L; Na^+: 196.4 mg/L; K^+: 4.7 mg/L) < Group 3 (Ca^{2+}: 338.1 mg/L; Mg^{2+}: 141.5 mg/L; Na^+: 499.4 mg/L; K^+: 8.0 mg/L). Major cations (HCO_3^-, Cl^-, and SO_4^{2-}) exhibited significant increments in the following order: Group 1 (HCO_3^-: 228.1 mg/L; Cl^-: 138.7 mg/L; SO_4^{2-}: 24.2 mg/L) < Group 2 (HCO_3^-: 378.0 mg/L; Cl^-: 519.1 mg/L; SO_4^{2-}: 91.4 mg/L) < Group 3 (HCO_3^-: 597.7 mg/L; Cl^-: 1,462.0 mg/L; SO_4^{2-}: 243.9 mg/L). The NO_3^- concentrations of Group 3 had a mean value of 15.6 ± 14.9 mg/L, which was significantly higher than the mean concentrations of Groups 1 and 2 (4.0 ± 2.9 and 6.7 ± 3.3 mg/L, respectively).

The resulting clusters from the SOM model were used in the isometric log-ratio (ILR)-ion plot through compositional data analysis (Shelton et al., 2018) and the hydrochemical facies evolution diagram (HFE-D) developed by Giménez-Forcada (2010) to identify seawater intrusion phases (**Fig. 4.4**). The ILR plot suggests that cations from most of the samples of Groups 1, 2, and 3 were predominantly Na^+ (bottom right in **Fig. 4.4a**), with the abundance decreasing in the order $Na^+ > Ca^{2+} > Mg^{2+} > K^+$. In contrast, anions from Groups 1, 2, and 3 were primarily Cl^- in the areas near the coastline; the order of abundance was $Cl^- > HCO_3^- > SO_4^{2-}$ (upper right in **Fig. 4.4a**). However, some samples of Group 1 from the southern part of the aquifer (recharge area) were dominated by HCO_3^-, with the order of abundance being $HCO_3^- > Cl^- > SO_4^{2-}$. Furthermore, the HFE-D (**Fig. 4.4b**) confirmed that 83% of the samples in the study area were in the seawater intrusion phase and that only 17% were in the freshening phase (recharge areas).
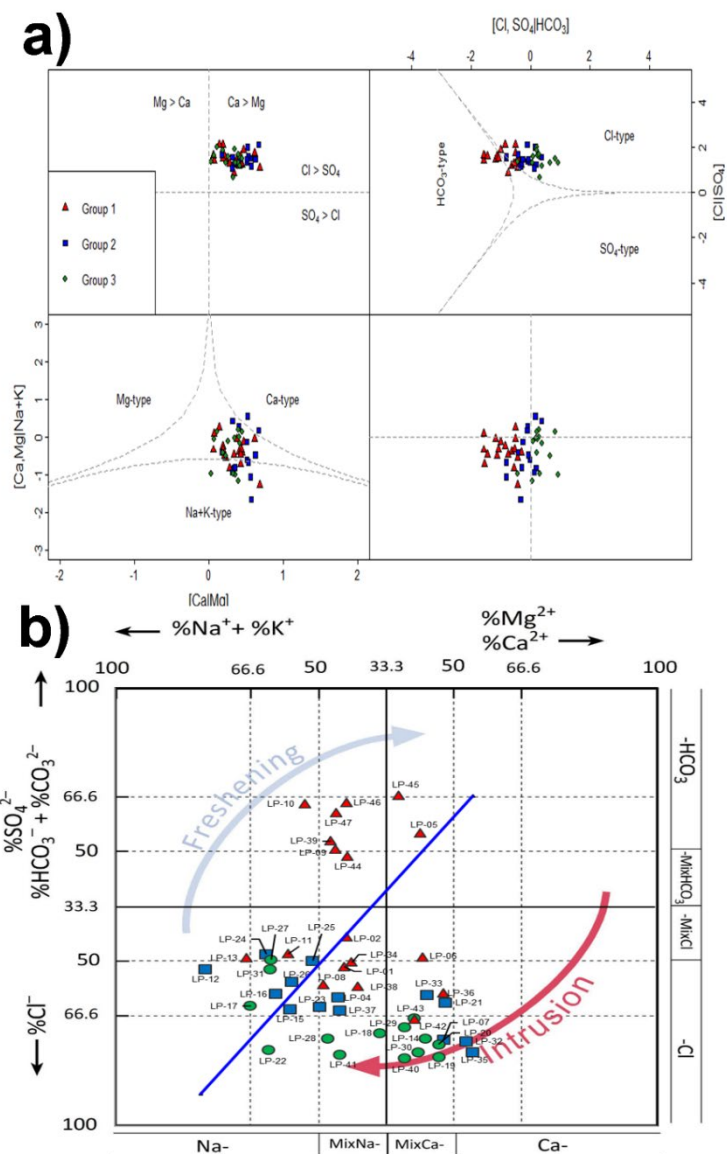
Figure 4.4. a) Isometric log-ratio (ILR)-ion plot; and b) Hydrochemical facies evolution diagram (HFE-D)

4.3.2 Stable isotopic compositions

In this study, the isotopic compositions of H_2O, NO_3^-, and SO_4^{2-} were measured to track the origin of these ions (natural and anthropogenic sources) and identify the different biogeochemical transformations involved in the groundwater system. A summary of the results is given in **Table 4.2**.

The $\delta^{15}N_{NO3}$ and $\delta^{18}O_{NO3}$ isotopic compositions of the groundwater samples in the study area ranged from 6.1‰ to 23.9‰ and from -2.2‰ to 8.6‰, respectively (**Table 4.1**). As this study represents the first multi-isotopic assessment of tracing nitrate and sulfate pollution in the La Paz aquifer, the results were compared with typical end-members reported in the literature reviews(Fenech et al., 2012; Gutiérrez et al., 2018; Nikolenko et al., 2018; Xue et al., 2009). Because NO_3^- concentrations in seawater are at trace levels, a NO_3^- seawater end-member was not considered in the dual-isotopic analysis. Contrasting the results with these reviews, the $\delta^{15}N_{NO3}$ values in most of the samples were in the overlapping zone between soil organic nitrogen (SON; from -0.5‰ to +8‰) and sewage (Se; from +9.6‰ to +25.2‰). The $\delta^{18}O_{NO3}$ values in the samples from the La Paz aquifer were significantly lower than those reported for synthetic fertilizers (SF; +17‰ to +25‰) (Nikolenko et al., 2018). Nevertheless, the $\delta^{18}O_{NO3}$ values of 17 samples were within the range reported for SON and Se (from -1.7‰ to +6.47‰ and from -0.3‰ to +12.1‰, respectively); 1 sample above the field near to the theoretical value of NO_3^- derived from nitrification (+10‰) suggesting a shifting in the isotopic composition typical from denitrification and the $\delta^{18}O_{NO3}$ values of 28 samples were below +0.5‰. The $\delta^{15}N_{NO3}$ isotopic compositions of Group 3 exhibited significantly higher values ($p < 0.05$) than Groups 1 and 2, whereas the $\delta^{18}O_{NO3}$ values were not significantly different between the three groups.

On the other hand, the $\delta^{34}S_{SO4}$ and $\delta^{18}O_{SO4}$ values in groundwater covered wide compositional ranges, from +1.5‰ to +19.3‰ and from +2.2‰ to +15.8‰, respectively (**Table 4.1**). According to literature (Torres-Martínez et al., 2020a; Wang and Zhang, 2019) and land use/land cover information on the study area, the $\delta^{34}S_{SO4}$ values are widely dispersed among different sources: atmospheric deposition (AD), soil-derived SO_4^{2-} (SS), synthetic fertilizers (SF), sewage (Se), detergents (De), and seawater (SW). Three samples fell into the overlapping area between SS, Se, and SF (-4.2‰–+12.7‰); two samples were between the boundaries of AD and SS (-4.2‰–+7.2‰); nine samples were in the SF (-4.1‰–+12.7‰) area, and the remaining samples were in a transition region between the previous sources and SW. Most of the $\delta^{18}O_{SO4}$ values in La Paz were lower than those reported for AD (+6.6‰–+12.9‰), SF (+7.8‰–+16.3‰), De (+12.0‰–+17.2‰), and SW (+8.0‰–+12.8‰), falling in the typical ranges for SS (+3.7‰–+5.6‰) and Se (+3.8‰–+10.0‰).

4.4 Discussion

4.4.1 Nitrate pollution sources and biogeochemical processes

Nitrate concentrations (as N) in the study area ranged from 0.2 to 48.8 mg/L. Among the groundwater samples, 66% had a nitrate concentration exceeding 3 mg/L—the threshold considered as a result of human influence (Ogrinc et al., 2019)—and 23% exhibited values over 10 mg/L (the maximum permissible limit for drinking water, as determined by WHO (WHO, 2017); this highlighted the critical impact of anthropogenic NO_3^- inputs on water quality. The lowest concentrations were found at sampling sites LP-09, LP-10, LP-47 (1.4, 1.5, and 1.7 mg/L, respectively), with no influence of anthropogenic activities. In contrast, elevated NO_3^- concentrations were detected at sites LP-31 (48.8 mg/L) and LP-27 (45.8 mg/L) near the rural communities of Chametla and El Centenario, respectively.

To identify the qualitative information related to the different pollution sources responsible for the increase in NO_3^- concentrations in groundwater samples from the study area, a dual-isotope biplot was drawn according to the nitrate isotopic signatures. It was contrasted with land-use/land-cover maps (**Fig. 4.5a, b**). Based on this plot, none of the groundwater nitrate isotopic fingerprints fell into the AD source area, suggesting a minimum contribution directly from precipitation. In contrast, SON and S were identified as the dominant nitrate sources in most water samples (**Fig. 4.5a**), suggesting an increase in $\delta^{15}N_{NO3}$ resulting from a mixing process. Also, the SON was the primary source in non-urban areas (**Fig. 4.5b**). None of the samples fell in the typical synthetic fertilizer range despite the agricultural activities; thus, it was assumed that the isotopic composition from fertilizers had been masked by different biogeochemical processes (Romanelli et al., 2020; Saccon et al., 2013).
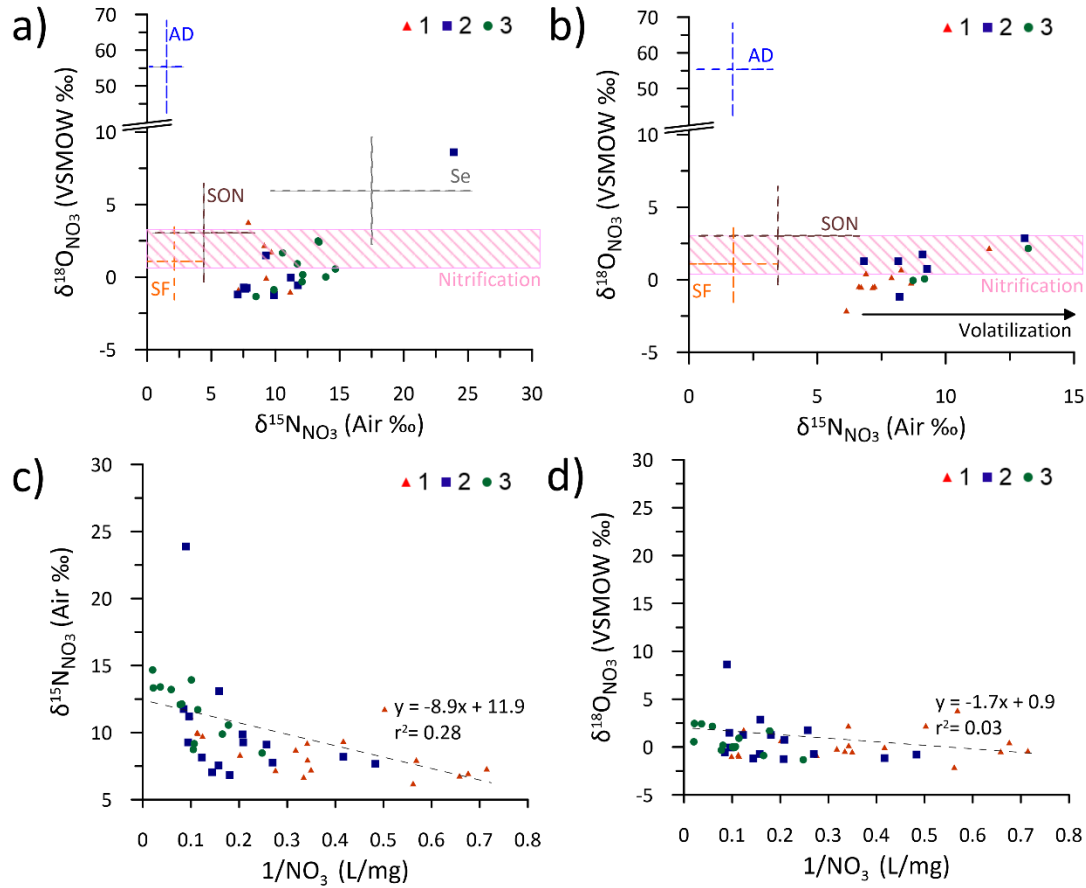
Figure 4.5. $\delta^{15}N_{NO3}$ vs. $\delta^{18}O_{NO3}$ plot according to the land-use/land-cover information in (a) urban and (b) agricultural areas; Relationship between (c) $\delta^{15}N_{NO3}$ and (d) $\delta^{18}O_{NO3}$ vs. $1/NO_3^-$ concentrations

Most nitrogen transformations depend directly on environmental conditions, such as pH, Eh, DO, and the chemical compositions of the media. Nitrification of NH_4^+ remineralized from the soil is a nitrate production process, generally involving microbes, which is favored under conditions of DO > 4 mg/L and pH values oscillating between 6.5 and 8 (Nikolenko et al., 2018; Rivett et al., 2008). The result of this process is an increase in NO_3^- concentration and a depletion in the $\delta^{18}O_{NO3}$ and $\delta^{15}N_{NO3}$ isotopic compositions (Kendall, 1998). $\delta^{18}O_{NO3}$ is a sensitive tracer for identifying the nitrification process in aquatic environments. Theoretical values of $\delta^{18}O_{NO3}$ derived from nitrification are often assumed to contribute to a 2:1 ratio of oxygen exchange with H_2O during nitrification and the relative contribution from the atmosphere ($0.66\delta^{18}O_{H2O} + 0.33\delta^{18}O_{O2}$) (Boshers et al., 2019; Snider et al., 2010). The theoretical values obtained for nitrification based on a ratio of 2:1 were estimated using the

local water isotopic composition, which ranged from -11.6 to -7.1‰ ($\delta^{18}O_{H2O}$), and assuming an $\delta^{18}O_{O2}$ value of +23.9‰ for atmospheric oxygen (Mader et al., 2017).
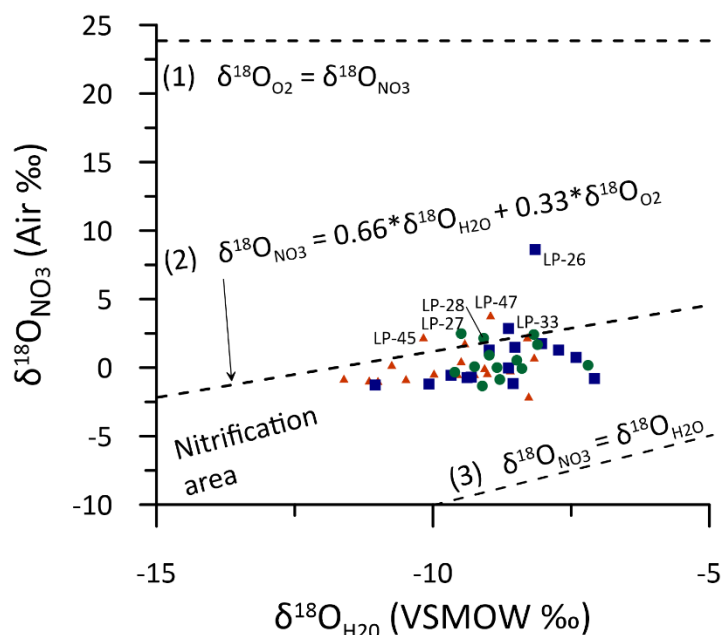
Figure 4.6. $\delta^{18}O_{H2O}$ vs. $\delta^{18}O_{NO3}$ with theoretical values of $\delta^{18}O_{NO3}$ derived from nitrification

The obtained $\delta^{18}O_{NO3}$ values of the nitrate derived from nitrification were, on average, 1.9 ± 0.7‰. Most of the values fell into the theoretical nitrification range, as shown in **Fig. 4.6**. Nevertheless, LP-26, LP-27, LP-28, LP-33, LP-45, and LP-47 exhibited values higher than the estimated values for full equilibrium with the $\delta^{18}O$ of groundwater. This could be attributed to the mineralization–immobilization–turnover process (MIT) in LP-26, LP-27, and LP-28. The MIT process results from the microbial immobilization of NO_3^- as organic N, followed by mineralization from organic N to NH_4^+ and, finally, a nitrification process (Jahangir et al., 2020; Minet et al., 2012; Puig et al., 2017). This process results in the $\delta^{18}O$ depletion of the $\delta^{18}O_{NO3}$ from the synthetic fertilizers typically employed in the region (Beltrán-Morales et al., 2019; Cardona et al., 2004; Ceseña, 2015). Although elevated DO (>4 mg/L) is not the optimal environmental condition for this process, recent research by Utom *et al*. (2020) indicated that denitrification does not always occur under strictly anaerobic conditions. Hence, samples LP-33, LP-45, and LP-47, which exhibited higher $\delta^{18}O_{NO3}$ isotopic compositions and lower NO_3^- concentrations, could be affected by a

bacterial denitrification process (Kendall et al., 2008). On the other hand, an increase in $\delta^{15}N_{NO3}$ values was observed (**Fig. 4.5b**). This isotopic fractionation could be attributed to ammonia volatilization due to the use of synthetic fertilizers combined with alkaline soil conditions (pH > 8)(López-Méndez et al., 2013) and the subsequent production of nitrified nitrate (Choi et al., 2017; Mariotti et al., 1988; Minet et al., 2012).

Additionally, to further assess the different nitrate biogeochemical processes, the $\delta^{15}N_{NO3}$ results were evaluated against nitrate concentrations. The Keeling plot (**Fig. 4.5c–d**) exhibited values of $\delta^{15}N_{NO3}$, $\delta^{18}O_{NO3,}$ and NO_3^- with negative relationships and no significant correlations (0.28 and 0.03, respectively) in all groups, confirming that the denitrification process did not influence the nitrate isotopic composition in the study area.

4.4.2   Sulfate pollution sources and biogeochemical processes

The sulfate concentration of samples collected in the study area ranged from 7.9 to 490 mg/L. Among the water samples, 10.6% had sulfate concentrations exceeding 250 mg/L, the recommended threshold for drinking water consumption (WHO, 2017). The lowest concentrations were found at sampling sites LP-06, LP-10, LP-47 (10.8, 9.8, and 7.9 mg/L, respectively), with no influence of anthropogenic activities or seawater intrusion. In contrast, elevated SO_4^{2-} concentrations were detected at sites LP-22 (490 mg/L) and LP-27 (316 mg/L) near the coastline in the Chametla community.

Upon analyzing the dual-isotope biplot approach of sulfate isotopic compositions for urban (**Fig. 4.7a**) and agricultural (**Fig. 4.7b**) areas, it was found that samples LP-08 and LP-09 were close to the SS range, which was in agreement with the results for the non-urbanized land-use area and the local reference for this pollution source. Only one sample (LP-37) fell into the AD source area, suggesting that precipitation contributes minimal SO_4^{2-} levels in groundwater. In urbanized and agricultural areas, samples exhibited a $\delta^{34}S_{SO4}$ enrichment (**Fig. 4.7a–d**) with no changes in the SO_4^{2-} concentration, suggesting the occurrence of a mixing process with an isotopically heavy end-member, which could be marine evaporites or seawater intrusion. However, according to Mahlknecht *et al*. (2017), there is no evidence of marine sulfate evaporites (gypsum) in the study area, indicating that according to the isotopic fingerprints, the dominant mixing process is between soil and seawater pollution

sources. This finding is confirmed by the vertical trend shown in **Fig. 4.7c–d** (Das et al., 2011).

Samples from Groups 2 and 3 in urbanized areas were enriched in the $\delta^{34}S_{SO4}$ isotopic fingerprint and exhibited decreasing SO_4^{2-} concentrations, suggesting a microbial sulfate reduction process (**Fig. 4.7c**) (Canfield, 2018; Tuttle et al., 2009; Yuan and Mayer, 2012). However, microbial sulfate reduction is typical in anoxic seawater and marine sediment porewater (Szynkiewicz et al., 2008). Overall, the groundwater showed aerobic conditions that do not favor microbial sulfate reduction; this indicated that reduction does not currently influence the groundwater's sulfate isotopic composition. Indeed, this process might have occurred in the past in marine-derived sulfate that had undergone sulfate reduction (Hosono et al., 2014; Szynkiewicz et al., 2008), with the $\delta^{34}S_{SO4}$-enriched sulfate now being dragged by the upconing of deeper saline groundwater in the aquifer system. The lower values of $\delta^{18}O_{SO4}$ in most samples (**Fig. 4.7e–f**) indicated that microbial processes in soils control the isotopic compositions of samples (Szynkiewicz et al., 2015).
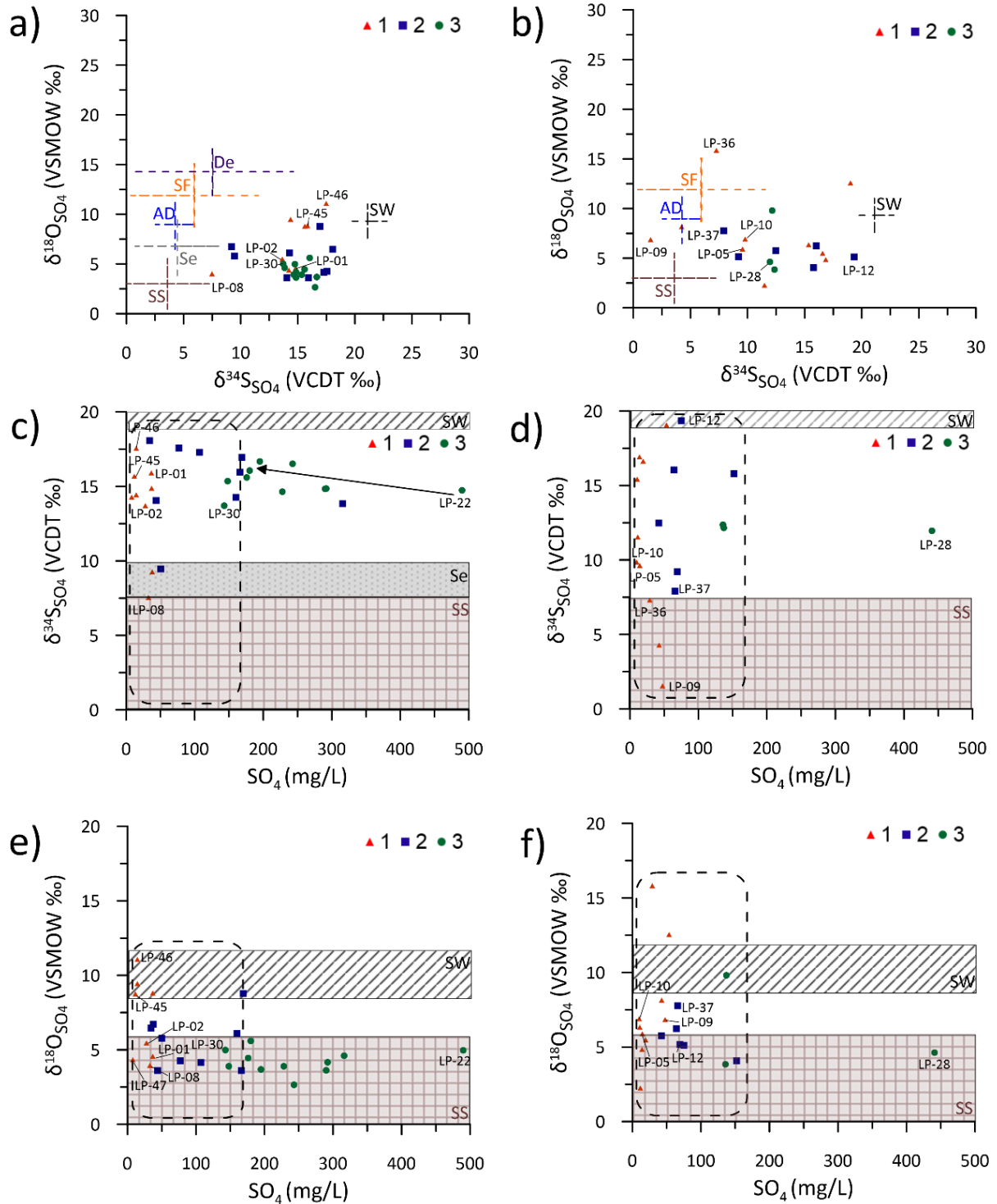
Figure 4.7. $\delta^{34}S_{SO4}$ vs. $\delta^{18}O_{SO4}$ plot according to land-use/land-cover information in (a) urban and (b) agricultural areas; Relationship between (c–d) $\delta^{34}S_{SO4}$ and (e–f) $\delta^{18}O_{SO4}$ vs. SO_4^{2-} concentrations in urban and agricultural areas.

4.4.3 Nitrate and sulfate source apportionment combined with uncertainty approach

Although the dual-isotope biplot approach provided relevant qualitative information about the different pollution sources, it is necessary to ascertain the amount NO_3^- and SO_4^{2-} derived from the previously identified sources (Section 4.4.1 and 4.4.2). Hence, a quantitative estimation of the contributions was performed using a BIMM through MixSIAR to provide decision-makers and other stakeholders relevant and precise information to improve water pollution control strategies. Based on previous analyses, no denitrification process was identified in this study, and therefore, the isotopic fractionation factor was not considered in the model.

As shown in **Fig. 4.8a–b**, results obtained from the MixSIAR model indicate that for NO_3^- pollution, SON contributed the largest amount of NO_3^- to the aquifer system (72.0 ± 10.2%, ~4.56 mg/L), followed by Se (26.3 ± 9.0%, ~3.54 mg/L), SF (1.5 ± 2.6%, ~0.16 mg/L), and AD (0.2 ± 0.4%, ~0.02 mg/L). Notably, although the output model values indicated that SON was the dominant source (71.5%), sewage leaks had a severe impact, which, at only 26.3%, has an equitable contribution to SON in terms of NO_3^- concentration. **Fig. 4.10c–d** depicts the proportional contributions of the different SO_4^{2-} pollution sources in the entire study area. Seawater (SW), with 43.0 ± 7.9%, contributes (as indicated in **Fig. 4.4b**) on average, 55.55 mg/L of sulfate, followed by soil-derived sulfate (SS), with 42.0 ± 10.7% (~46.71 mg/L). The remaining amount is contributed by detergents (5.9 ± 1.9%, ~1.33 mg/L), synthetic fertilizers (4.3 ± 3.1%, ~2.93 mg/L), precipitation (3.6 ± 3.5%, ~1.76 mg/L), and sewage (1.2 ± 1.6%, ~0.91 mg/L).
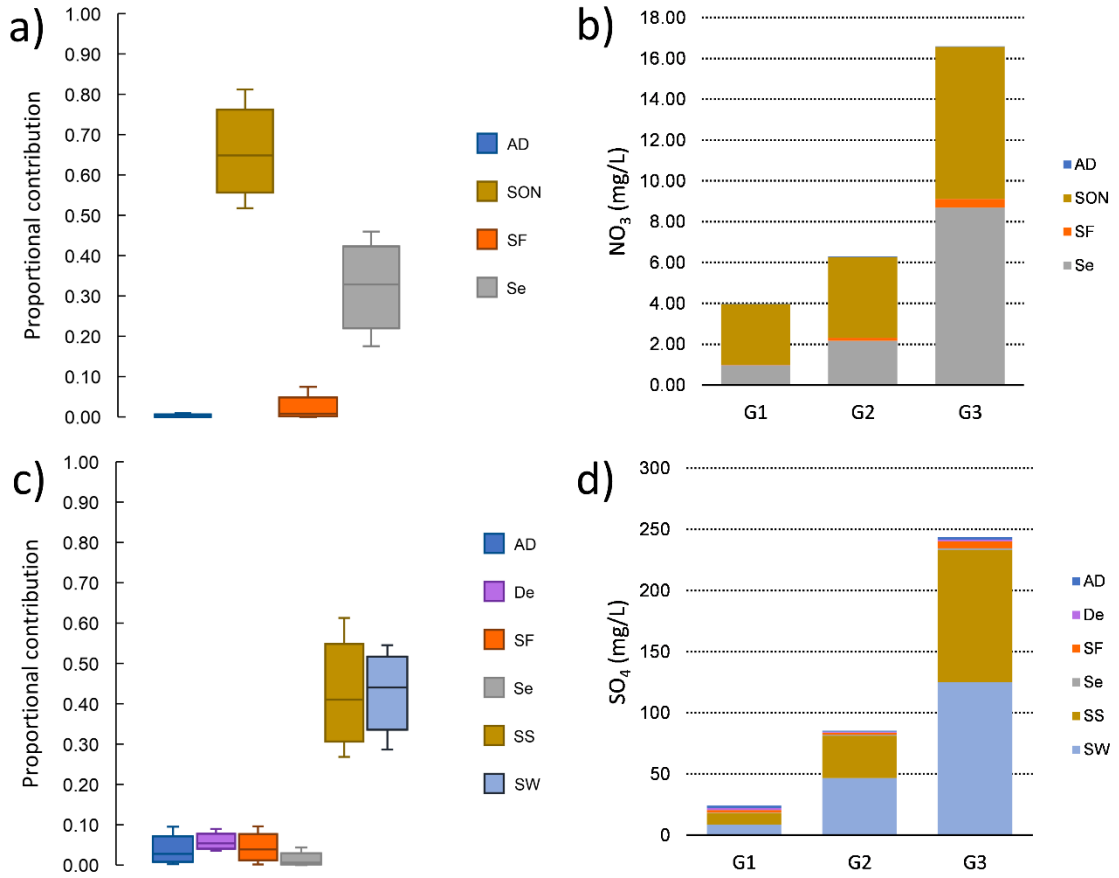
Figure 4.8. (a) Average global proportional contributions of four potential nitrate pollution sources estimated using the MixSIAR model (in percentage) and (b) NO_3^- concentration as N (mg/L); (c) Average global proportional contributions of six potential sulfate pollution sources estimated using the MixSIAR model (in percentage) and (d) SO_4^{2-} concentration (mg/L)

In recent research, it was found that small variations or overlapping in isotopic values might result in considerable changes in the source apportionment values generated by the mixing model (Torres-Martínez et al., 2020b; H. Zhang et al., 2020); this incorporates uncertainty into the estimation of the proportional contributions (**Fig. 4.9**). In the case of NO_3^- sources (**Fig. 4.9a**), AD exhibited the lowest average UI_{90} values (0.01), followed by SF (0.09), Se (0.32), and SON (0.33). In the case of SO_4^{2-} sources (**Fig. 4.9b**), Se and De exhibited the lowest average UI_{90} values (0.05 and 0.06, respectively), whereas AD and SF showed similar uncertainties (0.10). Finally, SW and SS exhibited the highest values, 0.29 and 0.38, respectively.
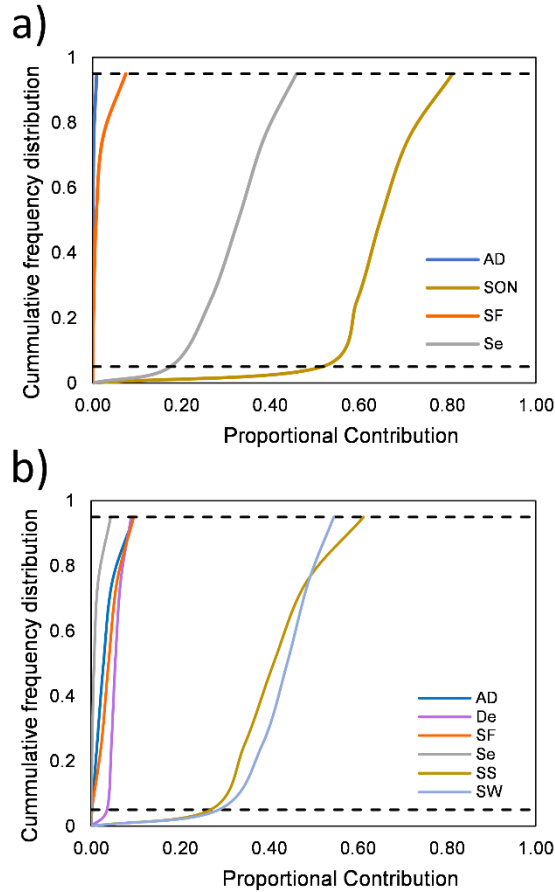
Figure 4.9. Cumulative distributions of the proportional contributions of (a) four potential nitrate sources and (b) six potential sulfate sources.

Despite the considerable uncertainty in some parameters, the UI_{90} values obtained using the NO_3^- isotope mixing model was significantly less in comparison with previous findings, which were in the range of 0.05–0.20 for AD, 0.48–0.63 for SON, 0.17–0.67 for SF, and 0.24–0.46 for Se (Ji et al., 2017; Shang et al., 2020; Torres-Martínez et al., 2020b). There is no comparison for the SO_4^{2-} isotope mixing model because this is the first uncertainty assessment performed. A significant source of uncertainty was the typical open-casing (full-screened) construction of production wells in Mexico; a mixing sample derived from different groundwater circulation depths was obtained (Knappett et al., 2020; Torres-Martínez et al., 2020b). Therefore, to reduce uncertainty in future research, it is necessary to obtain the isotopic composition from discrete depths of the aquifer to further constrain local pollution sources and provide narrow, accurate end-member ranges.

In summary, groundwater quality deterioration is currently controlled by two factors. First is aquifer mismanagement, with a lack of extraction regulations, which impacts the hydrogeological system conditions modifying the groundwater flow path. Overexploitation in the study area has led to a significant decrease in groundwater levels (Torres-Martinez et al., 2019), thereby increasing the thickness of the vadose zone. This promotes artificial conditions favored by the nitrification process (Kazakis et al., 2020; Xin et al., 2019) and promotes seawater intrusion, thereby increasing sulfate pollution. Second, there is a significant NO_3^- contribution due to the lack of maintenance of the sewage system, resulting in leaks and the absence of municipal infrastructure in rural areas (~13% of households) connected to the sewage system (CEA, 2015).

Finally, this chapter highlights that groundwater nitrate and sulfate pollution require particular attention for effective soil management under the NO_3^- and SO_4^{2-} input control strategies. It is necessary to establish a periodic sampling campaign (including increasing the number of sampling sites), which would improve the understanding of the biogeochemical transformations that affect the isotopic composition from the different pollution sources and would further aid in identifying the possible effects associated with changes in the hydrogeological flow path.

4.5 Conclusion

In this chapter, nitrate and sulfate groundwater pollution sources, their proportional contributions, and the different biogeochemical processes associated with groundwater contamination in the La Paz aquifer system were evaluated using hydrochemical and multi-isotopic datasets with a BIMM.

The multi-isotopic approach showed that groundwater nitrate mainly originated from soil organic nitrogen and its mixing with leaks from the domestic sewage system. Furthermore, nitrification was identified as the most critical biogeochemical process favored by the expansion of the vadose zone due to the overuse of the aquifer, whereas denitrification was not considered due to the aerobic conditions of the study area. Despite the use of fertilizers for agricultural activities, it was impossible to identify fertilizers' contribution using the nitrate isotopic fingerprints due to a masking ammonia volatilization process. Meanwhile, sulfate

pollution was primarily caused by the mixing of soil-derived sulfate with an intense seawater intrusion process. No significant sulfate fractionation process was identified (e.g., sulfur oxidation or reduction).

The results obtained using the Bayesian model confirmed that soil organic nitrogen and leaks from the sewage system were responsible for the elevated nitrate concentrations (~72.0% and ~26.3%, respectively), exceeding the maximum permissible limit for drinking water (10 mg/L) in 23% of the samples. In contrast, only 10% of the water samples exceeded the recommended maximum level of sulfate concentration for human consumption (250 mg/L), and sewage leaks were not a significant sulfate pollution source (~1.2%). Nevertheless, similar to nitrates' case, the soil was considered a significant sulfate pollution source (~42%), with an equal contribution from seawater intrusion (~43%), which was evaluated for the first time using this methodology employed in this study.

Chapter 5: Synthesis and outlook

5.1 Introduction

This thesis is proposed in response to the limited understanding of groundwater nitrate and sulfate pollution origin and fate in aquifers from northern Mexico. The knowledge about nitrate and sulfate source and transformation processes would help to improve groundwater pollution management. The main objective of this thesis was:

- Evaluate the processes that control groundwater chemistry and identify and quantify the contribution of different nitrate and sulfate sources in different aquifer systems.

The doctoral research outcomes are summarized in this chapter to highlight their scientific contribution evaluating the main objective in different scenarios. Following a summary of the findings, future scientific research is proposed based on the outcomes of this thesis for advancing the research in this field.

5.2 Summary of the findings

The main objective of this research was to evaluate the processes that control the chemistry of groundwater and identify and quantify the contribution of different nitrate and sulfate pollution sources in different semi-arid aquifer systems. The research executed to meet the objective is discussed in detail from Chapter 2 to Chapter 4 and is summarized below.

In **Chapter 2**, the application of a suite of chemical and isotopic tracers (δ^2H_{H2O}, $\delta^{18}O_{H2O}$, $\delta^{15}N_{NO3}$, $\delta^{18}O_{NO3}$, $\delta^{34}S_{SO4}$, $\delta^{18}O_{SO4}$) combined with a probability isotope mixing model to identify and quantify the nitrate and sulfate pollution sources in an industrialized area was discussed (Monterrey Metropolitan Area case). Results suggested that soil nitrogen and sewage were the most critical nitrate sources, while atmospheric deposition, marine evaporites, and sewage were the most prominent sulfate sources. However, the nitrate and sulfate concentrations were controlled by denitrification and sulfate reduction processes in the transition and discharge zones. The approach followed in this chapter is useful for establishing effective pollution management strategies in contaminated aquifers. In this chapter, the SO_4 pollution derived from different sources was quantified for the first time worldwide using a Bayesian mixing model.

Chapter 3 identifies nitrate (NO_3^-) sources, and biogeochemical transformations controlling diffuse pollution in groundwater were evaluated in an affected area by intensive livestock and agricultural activities (Comarca Lagunera Region case). This chapter combines chemical data, including environmental isotopes (δ^2H_{H2O}, $\delta^{18}O_{H2O}$, $\delta^{15}N_{NO3}$, $\delta^{18}O_{NO3}$), and also incorporates land use/land cover data to better understand the results of the Bayesian isotope mixing model and to reduce the uncertainty when estimating the contributions of different pollution sources. Furthermore, an uncertainty analysis for the Bayesian model was done. According to the groundwater flow path, different biogeochemical transformations were observed throughout the study area: microbial nitrification was dominant in the groundwater recharge areas with elevated NO_3- concentrations; in the transition zones, a mixing of different transformations, such as nitrification, denitrification, and/or volatilization, was identified, associated to moderate NO_3^- concentrations; whereas in the discharge the primary process affecting NO_3^- concentrations was denitrification, resulting in low NO_3^- concentrations. The MixSIAR isotope mixing model results revealed that the application of manure from concentrated animal feeding operations (~48%) and urban sewage (~43%) were the primary contributors to N pollution. In contrast, synthetic fertilizers (~5%), soil organic nitrogen (~4%), and atmospheric deposition played a less critical role. Finally, an estimation of an uncertainty index (UI90) of the isotope mixing results indicated that the uncertainties associated with atmospheric deposition and NO_3^- fertilizers were the lowest (0.05 and 0.07, respectively), while those associated with manure and sewage were the highest (0.24 and 0.20, respectively). The uncertainty analysis used in **Chapter 3** is useful for contaminated aquifers.

In **Chapter 4**, an overexploited coastal agricultural aquifer was analyzed (La Paz aquifer case). Previous studies on the study area focused mainly on seawater intrusion, resulting in limited information on nitrate and sulfate pollution. Therefore, pollution sources have not yet been identified sufficiently. In this chapter, an approach combining hydrochemical tools, multi-isotopes (δ^2H_{H2O}, $\delta^{18}O_{H2O}$, $\delta^{15}N_{NO3}$, $\delta^{18}O_{NO3}$, $\delta^{34}S_{SO4}$, $\delta^{18}O_{SO4}$), self-organizing maps, and a Bayesian isotope mixing model was used to estimate the contribution of different nitrate and sulfate sources to groundwater, evaluating for the first time SO_4 derived from seawater intrusion. Moreover, an uncertainty assessment (UI_{90}) was performed, and the potential biogeochemical transformations occurring in the coastal aquifer system were observed. Results from the MixSIAR model revealed that seawater intrusion and soil-derived

sulfates were the predominant sources of groundwater sulfate, with contributions of ~43.0% (UI_{90} = 0.29) and ~42.0% (UI_{90} = 0.38), respectively. Similarly, soil organic nitrogen (~72.0%, UI_{90} = 0.33) and urban sewage (~26.3%, UI_{90} = 0.33) were the primary contributors of nitrate pollution in groundwater. The dominant biogeochemical transformation for NO_3^- was nitrification. Denitrification and sulfate reduction were discarded due to the aerobic conditions in the aquifer system. Results of **Chapter 4** indicate that dual-isotope sulfate analysis combined with MixSIAR models is a powerful tool for estimating sulfate sources' contributions (including seawater-derived sulfate) in the groundwater of coastal aquifer systems affected by seawater intrusion.

5.3 Comparison with other study cases

From the results obtained in this doctoral research and contrasting them with other studies, it is possible to observe in **Table 5.1** that, despite the existence of differences between nitrate concentrations in the different environments represented by the study areas, in terms of contributions, atmospheric deposition oscillates between 0.2 and 2%, except for two cases Chengdu Plain and Asopos Basin with 18%. In the case of nitrate derived from organic decomposition, the results vary widely, ranging from 3 to 72%. Manure and sewage differ only in two case studies: La Comarca Lagunera Region and Chengdu Plain. Finally, fertilizers' use contributes between 1.5 and 60% to the contamination of groundwater by nitrates.

Table 5.1. Summary of nitrate contributions derived from Bayesian mixing models in different study cases

Study Area	Reference	Precipitation (mm/year)	Land Use	NO₃ (mg/L)	AD	SON	Manure	Sewage	M&S	Fertilizers
Monterrey Metropolitan Area	This study	622	Urban/ Industrial	7.3±7.0	1.6%	60.6%		37.8%		
Comarca Lagunera Region	This study	250	Agricultural/ Livestock	12.1±19.3	1.2%	3.8%	47.7%	42.6%		4.7%
Upper East Regio, Ghana	Gibrilla et al., 2020	1100	Agricultural/ Livestock	4.7±40	2%	23%			65%	10%
La Paz Aquifer	This study	260	Agricultural/ Urban	8.3±9.6	0.2%	72.0%		26.3%		1.5%
Laizhou, China	Wen et al., 2018	640.3	Agricultural/ Urban	44.5±29.8		12.0%			43.6%	41.6%
Chengdu Plain, China	H. Zhang et al., 2020	1088	Agricultural/ industrial	6.8±4.3	18%	25%	15%	10%		32%
Shandong Province, China	Yu et al, 2020	658	Agricultural/ urban	61.6±40	1.5%	14%			23.7%	60.8%

| Asopos Basin, Greece | Matiatos 2016 | 400 | Urban / Industrial / agricultural | 12.5±10.6 | 17.8% | 18.1% | | 22.2 | 42% |
| Yarmouk river basin, Jordania | Obeidat et al., 2020 | 218 | Agricultural/ urban | 17.8±15.4 | | | | 46.4 | 52.7% |

On the other hand, regarding groundwater contamination associated with sulfates (**Table 5.2**), only three studies have been developed, representing different environments. Regarding atmospheric deposition, La Paz aquifer and Laizhou present similar contributions of 3.6 and 3.3%, respectively, significantly differing from Monterrey Metropolitan Area (24.9%), despite having an annual precipitation which is similar to the Chinese case. Regarding sewage, Monterrey Metropolitan Area and Hebei Province, a contribution of 37 to 45% is reported. Sulfide oxidation was only detected in China's case, while seawater intrusion was only reported in the La Paz aquifer adjacent to the Ocean. Regarding contamination by fertilizers, with low percentages of 4.3-9.7% were identified in La Paz and the China case.

Table 5.2. Summary of sulfate contributions derived from Bayesian mixing models in different study cases

Study Area	Reference	Precipitation (mm/year)	Land Use	SO$_4$ (mg/L)	AD	SS	Evaporite	Sewage	Sulfide oxidation	Seawater	SF
Monterrey Metropolitan Area	This study	622	Urban/ Industrial	7.3±7.0	24.9%	24.9%		45.1%			
La Paz Aquifer	This study	260	Agricultural/ Urban	8.3±9.6	3.6%	42.0%		7.1%		43%	4.3%
Hebei Province, China	Zhang et al., 2020	600	Agricultural/ Urban / industial	255.5±29.8	3.3%		5.1%	37.4%	44.5%		9.7%

5.4 Future research

In general, this doctoral research results from the Bayesian isotope mixing modeling were consistent with interpretations based on previous hydrochemical and isotopic data. However, one limitation of this approach is that the isotopic ranges of sources were derived from literature. For this reason, further investigations to constrain the isotopic and chemical composition of local end-members is necessary to reduce the variance and uncertainty of the results. Moreover, it could be useful to try different isotopic or microcontaminants as

tracer combinations in the mixing models to clarify the origin of groundwater pollution in complex systems.

On the other hand, it is necessary to establish groundwater quality baselines and create long-term monitoring networks during different seasons, which would improve the understanding of the biogeochemical transformations that affect the isotopic composition from the different pollution sources and would further aid in identifying the possible effects associated with changes in the hydrogeological flow path in time and space.

Further investigations based on the combination of additional isotope tracers (e.g., $\delta^{11}B$, $\delta^{34}S$, $\delta^{87}Sr/^{86}Sr$, $\delta^{13}C$) could help to improve the understanding of the different biogeochemical processes and pollution sources. Similarly, the use of microorganisms, micropollutants, and pesticides as co-tracers would help for a more robust conceptualization of contamination paths and evaluation of mitigation measures in a complex groundwater system.

References

Acevedo Peralta, A.I., Leos Rodríguez, J.A., Figueroa Viramontes, U., Romo Lozano, J.L., 2017. Política ambiental: uso y manejo del estiércol en la Comarca Lagunera. Acta Univ. 27, 3–12.

Aeschbach-Hertig, W., Gleeson, T., 2012. Regional strategies for the accelerating global problem of groundwater depletion. Nat. Geosci. 5, 853–861.

Aguilar-Barajas, I., Sisto, N.P., Ramiréz, A., Aguilar-Barajas, I., Sisto, N.P., Ramírez Orozco, A., 2015. Agua para Monterrey - Logros, retos y oportunidades para Nuevo León y México, 1st ed. Agencia Promotora de Publicaciones, S.A. de C.V., Monterrey.

Aguilar-Barajas, I., Sisto, N.P., Ramirez, A.I., Magaña-Rueda, V., 2019. Building urban resilience and knowledge co-production in the face of weather hazards: flash floods in the Monterrey Metropolitan Area (Mexico). Environ. Sci. Policy 99, 37–47.

Aguilar-Ramírez, C.F., Camprubí, A., Fitz-Díaz, E., Cienfuegos-Alvarado, E., Morales-Puente, P., 2017. Variación en la composición isotópica del agua meteórica a lo largo de la sección centro-noreste de la Sierra Madre Oriental. Boletín la Soc. Geológica Mex. 69, 447–463.

Alcalá, F.J., Custodio, E., 2008. Using the Cl/Br ratio as a tracer to identify the origin of salinity in aquifers in Spain and Portugal. J. Hydrol. 359, 189–207.

Andersson, K.K., Hooper, A.B., 1983. O2 and H2O are each the source of one O in NO−2 produced from NH3 by Nitrosomonas : 15 N-NMR evidence. FEBS Lett. 164, 236–240.

APHA, (American Public Health Association), 2012. Standard Methods for the Examination of Water and Wastewater, 22nd ed, Standard Methods. APHA/AWWA/WEF.

Aravena, R., Evans, M.L., Cherry, J.A., 1993. Stable Isotopes of Oxygen and Nitrogen in Source Identification of Nitrate from Septic Systems. Ground Water 31, 180–186.

Aravena, R., Mayer, B., 2010. Isotopes and processes in the nitrogen and sulfur cycles. In: Aelion, M.C., Höhener, P., Hunkeler, D., Aravena, R. (Eds.), Environmental Isotopes in Biodegradation and Bioremediation. CRC Press, pp. 201–246.

Aravena, R., Robertson, W.D., 1998. Use of Multiple Isotope Tracers to Evaluate Denitrification in Ground Water: Study of Nitrate from a Large-Flux Septic System Plume. Ground Water 36, 975–982.

Archana, A., Thibodeau, B., Geeraert, N., Xu, M.N., Kao, S.J., Baker, D.M., 2018. Nitrogen sources and cycling revealed by dual isotopes of nitrate in a complex urbanized environment. Water Res. 142, 459–470.

Awaleh, M.O., Baudron, P., Soubaneh, Y.D., Boschetti, T., Hoch, F.B., Egueh, N.M., Mohamed, J., Dabar, O.A., Masse-Dufresne, J., Gassani, J., 2017. Recharge, groundwater flow pattern and contamination processes in an arid volcanic area: Insights from isotopic and geochemical tracers (Bara aquifer system, Republic of Djibouti). J. Geochemical Explor. 175, 82–98.

Azpilcueta Pérez, M.E., Pedroza Sandoval, A., Sanchez Cohen, I., Salcedo Jacobo, M. del R., Trejo Calzada, R., 2017. Calidad química del agua en un área agrícola de maíz forrajero (Zea mays L.) en la Comarca Lagunera, México. Rev. Int. Contam. Ambient. 33, 75–83.

Backer, L.C., 2000. Assessing the acute gastrointestinal effects of ingesting naturally occurring, high levels of sulfate in drinking water. Crit. Rev. Clin. Lab. Sci. 37, 389–400.

Bajaj, K., Thomas, R., Yadav, A., Datye, A., Chakraborty, S., 2019. Hydrological linkages between different water resources from two contrasting ecosystems of western peninsular India: a stable isotope perspective. Isotopes Environ. Health Stud. 55, 532–549.

Beltrán-Morales, F.A., Nieto-Garibay, A., Murillo-Chollet, J.S.A., Ruiz-Espinoza, F.H., Troyo-Dieguez, E., Alcala-Jauregui, J.A., Murillo-Amador, B., 2019. Contenido inorgánico de nitrógeno, fósforo y potasio de abonos de origen natural para su uso en agricultura orgánica. Rev. TERRA Latinoam. 37, 371–378.

Berman, E.S.F., Levin, N.E., Landais, A., Li, S., Owano, T., 2013. Measurement of δ 18 O, δ 17 O, and 17 O-excess in Water by Off-Axis Integrated Cavity Output Spectroscopy and Isotope Ratio Mass Spectrometry. Anal. Chem. 85, 10392–10398.

Bernhard, A., 2010. The Nitrogen Cycle: Processes, Players, and Human Impact. Nat. Educ. Knowl.

Biddau, R., Cidu, R., Da Pelo, S., Carletti, A., Ghiglieri, G., Pittalis, D., 2019. Source and fate of nitrate in contaminated groundwater systems: Assessing spatial and temporal variations by hydrogeochemistry and multiple stable isotope tools. Sci. Total Environ. 647, 1121–1136.

Blaisdell, J., Turyk, M.E., Almberg, K.S., Jones, R.M., Stayner, L.T., 2019. Prenatal exposure to nitrate in drinking water and the risk of congenital anomalies. Environ. Res. 176, 108553.

Blake, W.H., Boeckx, P., Stock, B.C., Smith, H.G., Bodé, S., Upadhayay, H.R., Gaspar, L., Goddard, R., Lennard, A.T., Lizaga, I., Lobb, D.A., Owens, P.N., Petticrew, E.L., Kuzyk, Z.Z.A., Gari, B.D., Munishi, L., Mtei, K., Nebiyu, A., Mabit, L., Navas, A., Semmens, B.X., 2018. A deconvolutional Bayesian mixing model approach for river basin sediment source apportionment. Sci. Rep. 8, 13073.

Boretti, A., Rosa, L., 2019. Reassessing the projections of the World Water Development Report. npj Clean Water 2, 15.

Boshers, D.S., Granger, J., Tobias, C.R., Böhlke, J.K., Smith, R.L., 2019. Constraining the Oxygen Isotopic Composition of Nitrate Produced by Nitrification. Environ. Sci. Technol. 53, 1206–1216.

Böttcher, J., Strebel, O., Voerkelius, S., Schmidt, H.-L., 1990. Using isotope fractionation of nitrate-

nitrogen and nitrate-oxygen for evaluation of microbial denitrification in a sandy aquifer. J. Hydrol. 114, 413–424.

Bottrell, S., Tellam, J., Bartlett, R., Hughes, A., 2008. Isotopic composition of sulfate as a tracer of natural and anthropogenic influences on groundwater geochemistry in an urban sandstone aquifer, Birmingham, UK. Appl. Geochemistry 23, 2382–2394.

Brandes, J.A., Devol, A.H., 1997. Isotopic fractionation of oxygen and nitrogen in coastal marine sediments. Geochim. Cosmochim. Acta 61, 1793–1801.

Brouste, L., Marlin, C., Dever, L., 1997. Geochemistry and residence time estimation of groundwater from the upper aquifer of the Chihuahua desert (Comarca Lagunera, Northern Mexico). Appl. Geochemistry 12, 775–786.

Burow, K.R., Nolan, B.T., Rupert, M.G., Dubrovsky, N.M., 2010. Nitrate in Groundwater of the United States, 1991−2003. Environ. Sci. Technol. 44, 4988–4997.

Camargo, J.A., Alonso, Á., 2006. Ecological and toxicological effects of inorganic nitrogen pollution in aquatic ecosystems: A global assessment. Environ. Int. 32, 831–849.

Camargo, J.A., Alonso, A., Salamanca, A., 2005. Nitrate toxicity to aquatic animals: a review with new data for freshwater invertebrates. Chemosphere 58, 1255–1267.

Canfield, D.E., 2018. Biogeochemistry of sulfur isotopes. In: Valley, J.W., Cole, D.R. (Eds.), Stable Isotope Geochemistry. Mouton de Gruyter, pp. 607–636.

Cardona, A., Carrillo-Rivera, J.J., Huizar-Álvarez, R., Graniel-Castro, E., 2004. Salinization in coastal aquifers of arid zones: an example from Santo Domingo, Baja California Sur, Mexico. Environ. Geol. 45, 350–366.

CEA, (Comisión Estatal del Agua), 2015. Programa hídrico estatal de Baja California Sur 2015-2021. La Paz.

Céréghino, R., Park, Y.-S., 2009. Review of the Self-Organizing Map (SOM) approach in water resources: Commentary. Environ. Model. Softw. 24, 945–947.

Ceseña, F.M.R., 2015. Current state of agriculture in Todos Santos and El Pescadero region. Todos Santos.

Chadha, D.K., 1999. A proposed new diagram for geochemical classification of natural waters and interpretation of chemical data. Hydrogeol. J. 7, 431–439.

Chae, G.-T., Yun, S.-T., Mayer, B., Kim, K.-H., Kim, S.-Y., Kwon, J.-S., Kim, K., Yong-Kwon Koh e, 2007. Fluorine geochemistry in bedrock groundwater of South Korea. Sci. Total Environ. 385, 272–283.

Charizopoulos, N., Zagana, E., Psilovikos, A., 2018. Assessment of natural and anthropogenic impacts in groundwater, utilizing multivariate statistical analysis and inverse distance weighted interpolation modeling: the case of a Scopia basin (Central Greece). Environ. Earth Sci. 77, 380.

Chen, X., Zheng, L., Dong, X., Jiang, C., Wei, X., 2020. Sources and mixing of sulfate contamination in the water environment of a typical coal mining city, China: evidence from stable isotope characteristics. Environ. Geochem. Health 42, 2865–2879.

Choi, W.-J., Kwak, J.-H., Lim, S.-S., Park, H.-J., Chang, S.X., Lee, S.-M., Arshad, M.A., Yun, S.-I., Kim, H.-Y., 2017. Synthetic fertilizer and livestock manure differently affect δ15N in the agricultural landscape: A review. Agric. Ecosyst. Environ. 237, 1–15.

Clark, I.D., Fritz, P., 1997. Environmental Isotopes in Hydrogeology. CRC Press/Lewis Publishers, Boca Raton, FL.

Clark, S., Sisson, S.A., Sharma, A., 2020. Tools for enhancing the application of self-organizing maps in water resources research and engineering. Adv. Water Resour. 143, 103676.

Clemens, M., Khurelbaatar, G., Merz, R., Siebert, C., van Afferden, M., Rödiger, T., 2020. Groundwater protection under water scarcity; from regional risk assessment to local wastewater treatment solutions in Jordan. Sci. Total Environ. 706, 136066.

CONAGUA, 2015a. Actualización de la disponibilidad media anual de agua en el acuífero Campo Buenos Aires (1907), Estado de Nuevo León. Mexico.

CONAGUA, 2015b. Actualización de la disponibilidad media anual de agua en el acuífero Campo Mina (1908), Estado de Nuevo León. Mexico.

CONAGUA, 2015c. Actualización de la disponibilidad media anual de agua en el acuífero Área Metropolitana de Monterrey (1906), Estado de Nuevo León. Mexico.

CONAGUA, (Comision Nacional del Agua), 2010. Manejo integrado de las aguas subterráneas en el acuífero La Paz, Baja California Sur. La Paz.

CONAGUA, (Comisión Nacional del Agua), 1997. Censo de captaciones de aguas subterráneas y colección de datos geohidrológicos en la zona La Paz-El Carrizal, BCS. Mexico City.

CONAGUA, (Comisión Nacional del Agua), 2001. Estudio de caracterización y modelación de la intrusión marina en el acuífero de La Paz. Mexico City.

CONAGUA, (Comisión Nacional del Agua), 2018. Estadísticas del agua en México 2018. Mexico City.

CONAGUA, (Comisión Nacional del Agua), 2019. Manual de Agua Potable, Alcantarillado y Saneamiento: Captación de pozos profundos. Secretaría de Medio Ambiente y Recursos Naturales, Mexico City.

CONAPO, (Consejo Nacional de Población), 2015. Delimitación de las áreas metropolitanas de México 2015 / Delimitation of the metropolitan areas of Mexico 2015. Mexico.

Cruz-Falcón, A., 2007. Caracterización y diagnóstico del acuífero de La Paz, B.C.S. mediante estudios geofísicos y geohidrológicos.

Cruz-Falcón, A., Troyo-Diéguez, E., Murillo-Jiménez, J.M., García-Hernández, J.L., Murillo-Amador, B., 2017. Familias de agua subterránea y distribución de sólidos totales disueltos en el acuífero de La Paz Baja California Sur, México. Terra Latinoam. 36, 39–48.

Cruz-Falcón, A., Vázquez-González, R., Ramírez-Hernández, J., Salinas-González, F., Nava-Sánchez, E., Troyo-Diéguez, E., 2010. Depth estimation to crystalline basement in the valley of La Paz, Baja California Sur, Mexico. Geofísica Int. 49, 213–224.

Cui, R., Fu, B., Mao, K., Chen, A., Zhang, D., 2020. Identification of the sources and fate of NO3−-N in shallow groundwater around a plateau lake in southwest China using NO3− isotopes (δ15N and δ18O) and a Bayesian model. J. Environ. Manage. 270, 110897.

Dang, D.H., Evans, R.D., Durrieu, G., Layglon, N., El Houssainy, A., Mullot, J.-U., Lenoble, V., Mounier, S., Garnier, C., 2018. Quantitative model of carbon and nitrogen isotope composition to highlight phosphorus cycling and sources in coastal sediments (Toulon Bay, France). Chemosphere 195, 683–692.

Dansgaard, W., 1964. Stable isotopes in precipitation. Tellus 16, 436–468.

Das, A., Pawar, N.J., Veizer, J., 2011. Sources of sulfur in Deccan Trap rivers: A reconnaissance isotope study. Appl. Geochemistry 26, 301–307.

Das, N., Das, A., Sarma, K.P., Kumar, M., 2018. Provenance, prevalence and health perspective of co-occurrences of arsenic, fluoride and uranium in the aquifers of the Brahmaputra River floodplain. Chemosphere 194, 755–772.

Dávila Pórcel, R.A., 2011. Desarrollo sostenible de usos de suelo en ciudades en crecimiento, aplicando hidrogeología urbana como parámetrro de planificación territorial: Caso de estudio Linares, N.L., México (Sustainable development of soiluses in growing cities, applying urban hy. Universidad Autónoma de Nuevo León.

Degnan, J.R., Böhlke, J.K., Pelham, K., Langlais, D.M., Walsh, G.J., 2016. Identification of Groundwater Nitrate Contamination from Explosives Used in Road Construction: Isotopic, Chemical, and Hydrologic Evidence. Environ. Sci. Technol. 50, 593–603.

Del Razo, L.M., Arellano, M.A., Cebrián, M.E., 1990. The oxidation states of arsenic in well-water from a chronic arsenicism area of Northern Mexico. Environ. Pollut. 64, 143–153.

Divers, M.T., Elliott, E.M., Bain, D.J., 2013. Constraining Nitrogen Inputs to Urban Streams from Leaking Sewers Using Inverse Modeling: Implications for Dissolved Inorganic Nitrogen (DIN) Retention in Urban Environments. Environ. Sci. Technol. 47, 1816–1823.

DOF, (Diario Oficial de la Federación), 2011. Acuerdo por el que se dan a conocer los estudios técnicos de las aguas nacionales de los acuíferos Área Metropolitana de Monterrey, Campo Buenos Aires, Campo Mina, Campo Durazno, Campo Topo Chico, Diario Oficial de la Federación. Mexico City, Mexico.

DOF, (Diario Oficial de la Federación), 2015. Acuerdo por el que se da a conocer el resultado de los estudios técnicos de las aguas nacionales subterráneas del Acuífero Nazas, clave 1025, en el Estado de Durango, Región Hidrológico-Administrativa Cuencas Centrales del Norte.

Ducci, D., Della Morte, R., Mottola, A., Onorati, G., Pugliano, G., 2019. Nitrate trends in groundwater of the Campania region (southern Italy). Environ. Sci. Pollut. Res. 26, 2120–2131.

Dutton, C.L., Subalusky, A.L., Hill, T.D., Aleman, J.C., Rosi, E.J., Onyango, K.B., Kanuni, K., Cousins, J.A., Staver, A.C., Post, D.M., 2019. A 2000-year sediment record reveals rapidly changing sedimentation and land use since the 1960s in the Upper Mara-Serengeti Ecosystem. Sci. Total Environ. 664, 148–160.

Einsiedl, F., Maloszewski, P., Stichler, W., 2009. Multiple isotope approach to the determination of the natural attenuation potential of a high-alpine karst system. J. Hydrol. 365, 113–121.

Erostate, M., Huneau, F., Garel, E., Ghiotti, S., Vystavna, Y., Garrido, M., Pasqualini, V., 2020. Groundwater dependent ecosystems in coastal Mediterranean regions: Characterization, challenges and management for their protection. Water Res. 172, 115461.

Escolero, O., Torres-Onofre, S., 2007. Análisis de la intrusión de agua de mar en el acuífero de La Paz (México). Bol. Geológico y Min. 118, 637–647.

Fenech, C., Rock, L., Nolan, K., Tobin, J., Morrissey, A., 2012. The potential for a suite of isotope and chemical markers to differentiate sources of nitrate contamination: A review. Water Res. 46, 2023–2041.

Fernandes, R., Millard, A.R., Brabec, M., Nadeau, M.-J., Grootes, P., 2014. Food Reconstruction Using Isotopic Transferred Signals (FRUITS): A Bayesian Model for Diet Reconstruction. PLoS One 9, e87436.

Fernando, W.A.M., Ilankoon, I.M.S.K., Syed, T.H., Yellishetty, M., 2018. Challenges and opportunities in the removal of sulphate ions in contaminated mine water: A review. Miner. Eng. 117, 74–90.

Fienen, M.N., Arshad, M., 2016. The International Scale of the Groundwater Issue. In: Jakeman, A.J., Barreteau, O., Hunt, R.J., Rinaudo, J.-D., Ross, A. (Eds.), Integrated Groundwater Management. Springer International Publishing, Cham, pp. 21–48.

Figueroa Viramontes, U., Núñez Hernández, G., Reta Sánchez, D.G., Flores López, H.E., 2015. Balance regional de nitrógeno en el sistema de producción leche-forraje de la Comarca Lagunera, México. Rev. Mex. Ciencias Pecu. 6, 377.

Flipse Jr., W.J., Bonner, F.T., 1985. Nitrogen-Isotope Ratios of Nitrate in Ground Water Under

Fertilized Fields, Long Island, New York. Ground Water 23, 59–67.

Fukada, T., Hiscock, K.M., Dennis, P.F., 2004. A dual-isotope approach to the nitrogen hydrochemistry of an urban aquifer. Appl. Geochemistry 19, 709–719.

Fukada, T., Hiscock, K.M., Dennis, P.F., Grischek, T., 2003. A dual isotope approach to identify denitrification in groundwater at a river-bank infiltration site. Water Res. 37, 3070–3078.

Galhardi, J.A., Bonotto, D.M., 2016. Hydrogeochemical features of surface water and groundwater contaminated with acid mine drainage (AMD) in coal mining areas: a case study in southern Brazil. Environ. Sci. Pollut. Res. 23, 18911–18927.

Galloway, J.N., 2003. The Global Nitrogen Cycle. In: Treatise on Geochemistry. Elsevier, pp. 557–583.

García-Salazar, J.A., Mora-Flores, J.S., 2008. Tarifas y consumo de agua en el sector residencial de la Comarca Lagunera. Región y Soc. 20, 119–132.

Gibrilla, A., Fianko, J.R., Ganyaglo, S., Adomako, D., Anornu, G., Zakaria, N., 2020. Nitrate contamination and source apportionment in surface and groundwater in Ghana using dual isotopes (15N and 18O-NO3) and a Bayesian isotope mixing model. J. Contam. Hydrol. 233, 103658.

Giménez-Forcada, E., 2010. Dynamic of Sea Water Interface using Hydrochemical Facies Evolution Diagram. Ground Water 48, 212–216.

Gomez Isaza, D.F., Cramp, R.L., Franklin, C.E., 2020. Living in polluted waters: A meta-analysis of the effects of nitrate and interactions with other environmental stressors on freshwater taxa. Environ. Pollut. 261, 114091.

González Sánchez, F., Puente Solís, R., González Partida, E., Camprubí, A., 2007. Estratigrafía del Noreste de México y su relación con los yacimientos estratoligados de fluorita, barita, celestina y Zn-Pb (Stratigraphy of Northeast Mexico and its relationship with stratified deposits of fluorite, barite, celestine and Zn-Pb). Bol. la Soc. Geol. Mex. 59, 43–62.

Granger, J., Sigman, D.M., Prokopenko, M.G., Lehmann, M.F., Tortell, P.D., 2006. A method for nitrite removal in nitrate N and O isotope analyses. Limnol. Oceanogr. Methods 4, 205–212.

Griffiths, N.A., Jackson, C.R., McDonnell, J.J., Klaus, J., Du, E., Bitew, M.M., 2016. Dual nitrate isotopes clarify the role of biological processing and hydrologic flow paths on nitrogen cycling in subtropical low-gradient watersheds. J. Geophys. Res. Biogeosciences 121, 422–437.

Grimm, N.B., Faeth, S.H., Golubiewski, N.E., Redman, C.L., Wu, J., Bai, X., Briggs, J.M., 2008. Global Change and the Ecology of Cities. Science (80-.). 319, 756–760.

Grimmeisen, F., Lehmann, M.F., Liesch, T., Goeppert, N., Klinger, J., Zopfi, J., Goldscheider, N., 2017. Isotopic constraints on water source mixing, network leakage and contamination in an

urban groundwater system. Sci. Total Environ. 583, 202–213.

Guo, H., Du, Y., Kah, L.C., Hu, C., Huang, J., Huang, H., Yu, W., Song, H., 2015. Sulfur isotope composition of carbonate-associated sulfate from the Mesoproterozoic Jixian Group, North China: Implications for the marine sulfur cycle. Precambrian Res. 266, 319–336.

Guo, Z., Yan, C., Wang, Z., Xu, F., Yang, F., 2020. Quantitative identification of nitrate sources in a coastal peri-urban watershed using hydrogeochemical indicators and dual isotopes together with the statistical approaches. Chemosphere 243, 125364.

Gutiérrez, M., Biagioni, R.N., Alarcón-Herrera, M.T., Rivas-Lucero, B.A., 2018. An overview of nitrate sources and operating processes in arid and semiarid aquifer systems. Sci. Total Environ. 624, 1513–1522.

Han, D., Song, X., Currell, M.J., 2016. Identification of anthropogenic and natural inputs of sulfate into a karstic coastal groundwater system in northeast China: evidence from major ions, δ 13 C DIC and δ 34 S SO 4. Hydrol. Earth Syst. Sci. 20, 1983–1999.

Harter, T., Lund, J.R., Darby, J., Fogg, G.E., Howitt, R., Jessoe, K.K., Pettygrove, G.S., Quinn, J.F., Viers, J.H., Boyle, D.B., Canada, H.E., DeLaMora, N., Dzurella, K.N., Fryjoff-Hung, A., Hollander, A.D., Honeycutt, K.L., Jenkins, M.W., Jensen, V.B., King, A.M., Kourakos, G., Liptzin, D., Lopez, E.M., Mayzelle, M.M., McNally, A., Medellin-Azuara, J., Rosenstock., T.S., 2012. Addressing Nitrate in California's Drinking Water with a Focus on Tulare Lake Basin and Salinas Valley Groundwater. Davis.

Held, I., Wolf, L., Eiswirth, M., Hötzl, H., 2007. IMPACTS OF SEWER LEAKAGE ON URBAN GROUNDWATER - Review of a case study in Germany. In: Urban Groundwater Management and Sustainability. Springer Netherlands, Dordrecht, pp. 189–204.

Hirales Rochin, J., Urcadiz Cazares, F.J., 2019. Geo-hazards associated with the urban geology of the city of La Paz, B.C.S. AEG News 62, 32–37.

Hopkins, J.B., Ferguson, J.M., 2012. Estimating the Diets of Animals Using Stable Isotopes and a Comprehensive Bayesian Mixing Model. PLoS One 7, e28478.

Horst, A., Mahlknecht, J., López-Zavala, M.A., Mayer, B., 2011. The origin of salinity and sulphate contamination of groundwater in the Colima State, Mexico, constrained by stable isotopes. Environ. Earth Sci. 64, 1931–1941.

Hosono, T., Delinom, R., Nakano, T., Kagabu, M., Shimada, J., 2011a. Evolution model of δ34S and δ18O in dissolved sulfate in volcanic fan aquifers from recharge to coastal zone and through the Jakarta urban area, Indonesia. Sci. Total Environ. 409, 2541–2554.

Hosono, T., Ikawa, R., Shimada, J., Nakano, T., Saito, M., Onodera, S., Lee, K.-K., Taniguchi, M., 2009. Human impacts on groundwater flow and contamination deduced by multiple isotopes in Seoul City, South Korea. Sci. Total Environ. 407, 3189–3197.

Hosono, T., Tokunaga, T., Tsushima, A., Shimada, J., 2014. Combined use of δ13C, δ15N, and δ34S tracers to study anaerobic bacterial processes in groundwater flow systems. Water Res. 54, 284–296.

Hosono, T., Wang, C.-H., Umezawa, Y., Nakano, T., Onodera, S., Nagata, T., Yoshimizu, C., Tayasu, I., Taniguchi, M., 2011b. Multiple isotope (H, O, N, S and Sr) approach elucidates complex pollution causes in the shallow groundwaters of the Taipei urban area. J. Hydrol. 397, 23–36.

Huang, T., Pang, Z., 2012. The role of deuterium excess in determining the water salinisation mechanism: A case study of the arid Tarim River Basin, NW China. Appl. Geochemistry 27, 2382–2388.

IANL, (Instituto del Agua de Nuevo León), 2007. Estudio para el manejo integrado de la Cuenca del Río San Juan (Study for integrated management of the San Juan river basin). Monterrey, México.

IBM, 2017. IBM SPSS Statistics 25. Ibm.

INEGI, (Instituto Nacional de Estadística Geografía e Informática), 1995. Síntesis Geográfica del Estado de Baja California Sur. Aguascalientes.

INEGI, (Instituto Nacional de Estadística Geografía e Informática), 2017. Anuario Estadístico y Geográfico de Baja California Sur 2017. Aguascalientes.

Jahangir, M.M.R., Fenton, O., Carolan, R., Harrington, R., Johnston, P., Zaman, M., Richards, K.G., Müller, C., 2020. Application of 15N tracing for estimating nitrogen cycle processes in soils of a constructed wetland. Water Res. 183, 116062.

Jalali, M., 2009. Geochemistry characterization of groundwater in an agricultural area of Razan, Hamadan, Iran. Environ. Geol. 56, 1479–1488.

Janža, M., Prestor, J., Pestotnik, S., Jamnik, B., 2020. Nitrogen Mass Balance and Pressure Impact Model Applied to an Urban Aquifer. Water 12, 1171.

Jensen, V.B., Darby, J.L., Seidel, C., Gorman, C., 2014. Nitrate in Potable Water Supplies: Alternative Management Strategies. Crit. Rev. Environ. Sci. Technol. 44, 2203–2286.

Ji, X., Xie, R., Hao, Y., Lu, J., 2017. Quantitative identification of nitrate pollution sources and uncertainty analysis based on dual isotope approach in an agricultural watershed. Environ. Pollut. 229, 586–594.

Jia, Y., Guo, H., Xi, B., Jiang, Y., Zhang, Z., Yuan, R., Yi, W., Xue, X., 2017. Sources of groundwater salinity and potential impact on arsenic mobility in the western Hetao Basin, Inner Mongolia. Sci. Total Environ. 601–602, 691–702.

Jin, Z., Zheng, Q., Zhu, C., Wang, Y., Cen, J., Li, F., 2018. Contribution of nitrate sources in surface water in multiple land use areas by combining isotopes and a Bayesian isotope mixing model.

Appl. Geochemistry 93, 10–19.

Jørgensen, P.R., Urup, J., Helstrup, T., Jensen, M.B., Eiland, F., Vinther, F.P., 2004. Transport and reduction of nitrate in clayey till underneath forest and arable land. J. Contam. Hydrol. 73, 207–226.

Kalteh, A.M., Hjorth, P., Berndtsson, R., 2008. Review of the self-organizing map (SOM) approach in water resources: Analysis, modelling and application. Environ. Model. Softw. 23, 835–845.

Kaown, D., Koh, D.-C., Mayer, B., Lee, K.-K., 2009. Identification of nitrate and sulfate sources in groundwater using dual stable isotope approaches for an agricultural area with different land use (Chuncheon, mid-eastern Korea). Agric. Ecosyst. Environ. 132, 223–231.

Katz, B.G., Eberts, S.M., Kauffman, L.J., 2011. Using Cl/Br ratios and other indicators to assess potential impacts on groundwater quality from septic systems: A review and examples from principal aquifers in the United States. J. Hydrol. 397, 151–166.

Kazakis, N., Matiatos, I., Ntona, M.-M., Bannenberg, M., Kalaitzidou, K., Kaprara, E., Mitrakas, M., Ioannidou, A., Vargemezis, G., Voudouris, K., 2020. Origin, implications and management strategies for nitrate pollution in surface and ground waters of Anthemountas basin based on a δ15N-NO3− and δ18O-NO3− isotope approach. Sci. Total Environ. 724, 138211.

Kendall, C., 1998. Tracing Nitrogen Sources and Cycling in Catchments. In: Kendall, C., McDonnell, J.J. (Eds.), Isotope Tracers in Catchment Hydrology. Elsevier, Amsterdam, pp. 519–576.

Kendall, C., Elliott, E.M., Wankel, S.D., 2008. Tracing Anthropogenic Inputs of Nitrogen to Ecosystems. In: Michener, R., Lajtha, K. (Eds.), Stable Isotopes in Ecology and Environmental Science: Second Edition. Blackwell Publishing Ltd, Oxford, UK, pp. 375–449.

Khazaei, E., Milne-Home, W., 2017. Applicability of geochemical techniques and artificial sweeteners in discriminating the anthropogenic sources of chloride in shallow groundwater north of Toronto, Canada. Environ. Monit. Assess. 189, 218.

Kim, H., Kaown, D., Mayer, B., Lee, J.-Y., Hyun, Y., Lee, K.-K., 2015. Identifying the sources of nitrate contamination of groundwater in an agricultural area (Haean basin, Korea) using isotope and microbial community analyses. Sci. Total Environ. 533, 566–575.

Kim, K.-H., Yun, S.-T., Mayer, B., Lee, J.-H., Kim, T.-S., Kim, H.-K., 2015. Quantification of nitrate sources in groundwater using hydrochemical and dual isotopic data combined with a Bayesian mixing model. Agric. Ecosyst. Environ. 199, 369–381.

Kim, K.-H., Yun, S.-T., Yu, S., Choi, B.-Y., Kim, M.-J., Lee, K.-J., 2020. Geochemical pattern recognitions of deep thermal groundwater in South Korea using self-organizing map: Identified pathways of geochemical reaction and mixing. J. Hydrol. 589, 125202.

King, A., Boyle, D., Jensen, V., Fogg, G.E., Harter, T., 2012. Groundwater Remediation and Management for Nitrate, Technical Report 5: Addressing Nitrate in California's Drinking Water

with a Focus on Tulare Lake Basin and Salinas Valley Groundwater.

Kinnunen, P., Kyllönen, H., Kaartinen, T., Mäkinen, J., Heikkinen, J., Miettinen, V., 2018. Sulphate removal from mine water with chemical, biological and membrane technologies. Water Sci. Technol. 2017, 194–205.

Knappett, P.S.K., Li, Y., Loza, I., Hernandez, H., Avilés, M., Haaf, D., Majumder, S., Huang, Y., Lynch, B., Piña, V., Wang, J., Winkel, L., Mahlknecht, J., Datta, S., Thurston, W., Terrell, D., Kirk Nordstrom, D., 2020. Rising arsenic concentrations from dewatering a geothermally influenced aquifer in central Mexico. Water Res. 185, 116257.

Koba, K., Tokuchi, N., Wada, E., Nakajima, T., Iwatsubo, G., 1997. Intermittent denitrification: The application of a 15N natural abundance method to a forested ecosystem. Geochim. Cosmochim. Acta 61, 5043–5050.

Kohn, J., Soto, D.X., Iwanyshyn, M., Olson, B., Kalischuk, A., Lorenz, K., Hendry, M.J., 2015. Groundwater nitrate and chloride trends in an agriculture-intensive area in southern Alberta, Canada. Water Qual. Res. J. Canada 51, wqrjc2015132.

Kohonen, T., 1982. Self-organized formation of topologically correct feature maps. Biol. Cybern. 43, 59–69.

Kohonen, T., 2013. Essentials of the self-organizing map. Neural Networks 37, 52–65.

Kong, J., Guo, Q., Wei, R., Strauss, H., Zhu, G., Li, S., Song, Z., Chen, T., Song, B., Zhou, T., Zheng, G., 2018. Contamination of heavy metals and isotopic tracing of Pb in surface and profile soils in a polluted farmland from a typical karst area in southern China. Sci. Total Environ. 637–638, 1035–1045.

Kreitler, C.W., 1979. Nitrogen-isotope ratio studies of soils and groundwater nitrate from alluvial fan aquifers in Texas. J. Hydrol. 42, 147–170.

Kruk, M.K., Mayer, B., Nightingale, M., Laceby, J.P., 2020. Tracing nitrate sources with a combined isotope approach (δ15NNO3, δ18ONO3 and δ11B) in a large mixed-use watershed in southern Alberta, Canada. Sci. Total Environ. 703, 135043.

Lasagna, M., De Luca, D.A., 2019. Evaluation of sources and fate of nitrates in the western Po plain groundwater (Italy) using nitrogen and boron isotopes. Environ. Sci. Pollut. Res. 26, 2089–2104.

Lassaletta, L., García-Gómez, H., Gimeno, B.S., Rovira, J. V., 2009. Agriculture-induced increase in nitrate concentrations in stream waters of a large Mediterranean catchment over 25years (1981–2005). Sci. Total Environ. 407, 6034–6043.

Ledesma-ruiz, R., Pastén-zapata, E., Parra, R., Harter, T., Mahlknecht, J., 2015. Investigation of the geochemical evolution of groundwater under agricultural land : A case study in northeastern Mexico. J. Hydrol. 521, 410–423.

Leslie, D., Lyons, W., 2018. Variations in Dissolved Nitrate, Chloride, and Sulfate in Precipitation, Reservoir, and Tap Waters, Columbus, Ohio. Int. J. Environ. Res. Public Health 15, 1752.

Li, C., Li, S.-L., Yue, F.-J., Liu, J., Zhong, J., Yan, Z.-F., Zhang, R.-C., Wang, Z.-J., Xu, S., 2019. Identification of sources and transformations of nitrate in the Xijiang River using nitrate isotopes and Bayesian model. Sci. Total Environ. 646, 801–810.

Li, X., Gan, Y., Zhou, A., Liu, Y., 2015. Relationship between water discharge and sulfate sources of the Yangtze River inferred from seasonal variations of sulfur and oxygen isotopic compositions. J. Geochemical Explor. 153, 30–39.

Li, X., Tang, C., Cao, Y., Li, D., 2020. A multiple isotope (H, O, N, C and S) approach to elucidate the hydrochemical evolution of shallow groundwater in a rapidly urbanized area of the Pearl River Delta, China. Sci. Total Environ. 724, 137930.

Lis, G., Wassenaar, L.I., Hendry, M.J., 2008. High-Precision Laser Spectroscopy D/H and 18 O/ 16 O Measurements of Microliter Natural Water Samples. Anal. Chem. 80, 287–293.

Liu, J., Shen, Z., Yan, T., Yang, Y., 2018. Source identification and impact of landscape pattern on riverine nitrogen pollution in a typical urbanized watershed, Beijing, China. Sci. Total Environ. 628–629, 1296–1307.

Liu, K., Lobb, D.A., Miller, J., Owens, P., Caron, M., 2017. Determining sources of fine-grained sediment for a reach of the Lower Little Bow River, Alberta, using a colour-based sediment fingerprinting approach. Can. J. Soil Sci. 69, CJSS-2016-0131.

Longman, J., Veres, D., Ersek, V., Phillips, D.L., Chauvel, C., Tamas, C.G., 2018. Quantitative assessment of Pb sources in isotopic mixtures using a Bayesian mixing model. Sci. Rep. 8, 6154.

López-Méndez, A., Armenta-López, C., Armenta-Bojórquez, A.D., Fraga-Palomino, H.C., Félix-Herrán, J.A., 2013. Localización de zonas aptas para la agricultura protegida en Baja California Sur, México. Agron. Mesoam. 24, 401–409.

Lu, L., Cheng, H., Pu, X., Liu, X., Cheng, Q., 2015. Nitrate behaviors and source apportionment in an aquatic system from a watershed with intensive agricultural activities. Environ. Sci. Process. Impacts 17, 131–144.

Mader, M., Schmidt, C., van Geldern, R., Barth, J.A.C., 2017. Dissolved oxygen in water and its stable isotope effects: A review. Chem. Geol. 473, 10–21.

Mahlknecht, J., Horst, A., Hernández-Limón, G., Aravena, R., 2008. Groundwater geochemistry of the Chihuahua City region in the Rio Conchos Basin (northern Mexico) and implications for water resources management. Hydrol. Process. 22, 4736–4751.

Mahlknecht, J., Merchán, D., Rosner, M., Meixner, A., Ledesma-Ruiz, R., 2017. Assessing seawater intrusion in an arid coastal aquifer under high anthropogenic influence using major constituents,

Sr and B isotopes in groundwater. Sci. Total Environ. 587–588, 282–295.

Man, K., Ma, Z.M., Xu, X.J., 2014. Research on the Mechanism of Sulfate Pollution of Groundwater in Jiaozuo Area. Appl. Mech. Mater. 665, 436–439.

Mariotti, A., Landreau, A., Simon, B., 1988. 15N isotope biogeochemistry and natural denitrification process in groundwater: Application to the chalk aquifer of northern France. Geochim. Cosmochim. Acta 52, 1869–1878.

Mariotti, A., Létolle, R., 1977. Application de l'étude isotopique de l'azote en hydrologie et en hydrogéologie — Analyse des résultats obtenus sur un exemple précis: Le Bassin de Mélarchez (Seine-et-Marne, France). J. Hydrol. 33, 157–172.

Matiatos, I., 2016. Nitrate source identification in groundwater of multiple land-use areas by combining isotopes and multivariate statistical analysis: A case study of Asopos basin (Central Greece). Sci. Total Environ. 541, 802–814.

Mattern, S., Sebilo, M., Vanclooster, M., 2011. Identification of the nitrate contamination sources of the Brusselian sands groundwater body (Belgium) using a dual-isotope approach. Isotopes Environ. Health Stud. 47, 297–315.

McArthur, J.M.M., Sikdar, P.K.K., Hoque, M.A. a., Ghosal, U., 2012. Waste-water impacts on groundwater: Cl/Br ratios and implications for arsenic pollution of groundwater in the Bengal Basin and Red River Basin, Vietnam. Sci. Total Environ. 437, 390–402.

McIlvin, M.R., Altabet, M.A., 2005. Chemical Conversion of Nitrate and Nitrite to Nitrous Oxide for Nitrogen and Oxygen Isotopic Analysis in Freshwater and Seawater. Anal. Chem. 77, 5589–5595.

McMahon, P.B., Chapelle, F.H., 2008. Redox Processes and Water Quality of Selected Principal Aquifer Systems. Ground Water 46, 259–271.

Meghdadi, A., Javar, N., 2018a. Quantification of spatial and seasonal variations in the proportional contribution of nitrate sources using a multi-isotope approach and Bayesian isotope mixing model. Environ. Pollut. 235, 207–222.

Meghdadi, A., Javar, N., 2018b. Evaluation of nitrate sources and the percent contribution of bacterial denitrification in hyporheic zone using isotope fractionation technique and multi-linear regression analysis. J. Environ. Manage. 222, 54–65.

Mejía-González, M.Á., González-Hita, L., Briones-Gallardo, R., Cardona-Benavides, A., Soto-Navarro, P., 2014. Mechanisms that release arsenic to the groundwater of the Laguna Region, states of Coahuila and Durango, Mexico. Tecnol. y Ciencias del Agua V, 71–82.

Mekonnen, M.M., Hoekstra, A.Y., 2015. Global Gray Water Footprint and Water Pollution Levels Related to Anthropogenic Nitrogen Loads to Fresh Water. Environ. Sci. Technol. 49, 12860–12868.

Merchán, D., Sanz, L., Alfaro, A., Pérez, I., Goñi, M., Solsona, F., Hernández-García, I., Pérez, C., Casalí, J., 2020. Irrigation implementation promotes increases in salinity and nitrate concentration in the lower reaches of the Cidacos River (Navarre, Spain). Sci. Total Environ. 706, 135701.

Minet, E., Coxon, C.E., Goodhue, R., Richards, K.G., Kalin, R.M., Meier-Augenstein, W., 2012. Evaluating the utility of 15N and 18O isotope abundance analyses to identify nitrate sources: A soil zone study. Water Res. 46, 3723–3736.

Minet, E.P.P., Goodhue, R., Meier-Augenstein, W., Kalin, R.M.M., Fenton, O., Richards, K.G.G., Coxon, C.E.E., 2017. Combining stable isotopes with contamination indicators: A method for improved investigation of nitrate sources and dynamics in aquifers with mixed nitrogen inputs. Water Res. 124, 85–96.

Mingzhu, L., Seyf-Laye, A.-S.M., Ibrahim, T., Gbandi, D., Honghan, C., 2014. Tracking sources of groundwater nitrate contamination using nitrogen and oxygen stable isotopes at Beijing area, China. Environ. Earth Sci. 72, 707–715.

Mizutani, Y., Rafter, T.A., 1973. Isotopic behaviour of sulphate oxygen in the bacterial reduction of sulphate. Geochem. J. 6, 183–191.

Monzalvo, M., 2010. Simulación hidrodinámica del acuífero de La Paz y su aprovechamiento como fuente de desalación. MSc Thesis, Univ. Nac. Autónoma México.

Moore, J.W., Semmens, B.X., 2008. Incorporating uncertainty and prior information into stable isotope mixing models. Ecol. Lett. 11, 470–480.

Mora, A., Mahlknecht, J., Rosales-Lagarde, L., Hernández-Antonio, A., 2017. Assessment of major ions and trace elements in groundwater supplied to the Monterrey metropolitan area, Nuevo León, Mexico. Environ. Monit. Assess. 189, 394.

Morales-Arredondo, J.I., Esteller-Alberich, M.V., Armienta Hernández, M.A., Martínez-Florentino, T.A.K., 2018. Characterizing the hydrogeochemistry of two low-temperature thermal systems in Central Mexico. J. Geochemical Explor. 185, 93–104.

Murgulet, D., Tick, G.R., 2013. Understanding the sources and fate of nitrate in a highly developed aquifer system. J. Contam. Hydrol. 155, 69–81.

Neumann, B., Ott, K., Kenchington, R., 2017. Strong sustainability in coastal areas: a conceptual interpretation of SDG 14. Sustain. Sci. 12, 1019–1035.

Nikolenko, O., Jurado, A., Borges, A. V., Knöller, K., Brouyère, S., 2018. Isotopic composition of nitrogen species in groundwater under agricultural areas: A review. Sci. Total Environ. 621, 1415–1432.

Oakley, S.M., Gold, A.J., Oczkowski, A.J., 2010. Nitrogen control through decentralized wastewater treatment: Process performance and alternative management strategies. Ecol. Eng. 36, 1520–

1531.

Oesterreich, D.M., Medina Aleman, J.J., 2002. Groundwater Resources Management for the City of Monterrey, NE-Mexico:The Buenos Aires Wellfield in the Huasteca Canyon. In: International Symposium on Resource Utilization: Globalization and Local Structure. p. 6.

Ogrinc, N., Tamše, S., Zavadlav, S., Vrzel, J., Jin, L., 2019. Evaluation of geochemical processes and nitrate pollution sources at the Ljubljansko polje aquifer (Slovenia): A stable isotope perspective. Sci. Total Environ. 646, 1588–1600.

Olds, H.T., Corsi, S.R., Dila, D.K., Halmo, K.M., Bootsma, M.J., McLellan, S.L., 2018. High levels of sewage contamination released from urban areas after storm events: A quantitative survey with sewage specific bacterial indicators. PLOS Med. 15, e1002614.

Ortega-Gaucin, D., 2012. Sequía en Nuevo León: vulnerabilidad, impactos y estrategias de mitigación (Drought in Nuevo León: vulnerability, impacts and mitigation strategies), 1st ed. Instituto del Agua del Estado de Nuevo León, Apodaca.

Ortega-Guerrero, A., 2003. Origin and geochemical evolution of groundwater in a closed-basin clayey aquitard, Northern Mexico. J. Hydrol. 284, 26–44.

Ortega-Guerrero, A., 2017. Evaporative concentration of arsenic in groundwater: health and environmental implications, La Laguna Region, Mexico. Environ. Geochem. Health 39, 987–1003.

Otero, N., Torrentó, C., Soler, A., Menció, A., Mas-Pla, J., 2009. Monitoring groundwater nitrate attenuation in a regional system coupling hydrogeology with multi-isotopic methods: The case of Plana de Vic (Osona, Spain). Agric. Ecosyst. Environ. 133, 103–113.

Panno, S.V., Hackley, K.C., Hwang, H.H., Greenberg, S.E., Krapac, I.G., Landsberger, S., O'Kelly, D.J., 2006. Characterization and Identification of Na-Cl Sources in Ground Water. Ground Water 44, 176–187.

Parnell, A.C., Inger, R., Bearhop, S., Jackson, A.L., 2010. Source Partitioning Using Stable Isotopes: Coping with Too Much Variation. PLoS One 5, e9672.

Pastén-Zapata, E., Ledesma-Ruiz, R., Harter, T., Ramírez, A.I., Mahlknecht, J., 2014. Assessment of sources and fate of nitrate in shallow groundwater of an agricultural area by using a multi-tracer approach. Sci. Total Environ. 470–471, 855–864.

Pereau, J.-C., Pryet, A., Rambonilaza, T., 2019. Optimality Versus Viability in Groundwater Management with Environmental Flows. Ecol. Econ. 161, 109–120.

Peters, M., Guo, Q., Strauss, H., Zhu, G., 2015. Geochemical and multiple stable isotope (N, O, S) investigation on tap and bottled water from Beijing, China. J. Geochemical Explor. 157, 36–51.

Phillips, D.L., Gregg, J.W., 2003. Source partitioning using stable isotopes: coping with too many

sources. Oecologia 136, 261–269.

Pittalis, D., Carrey, R., Da Pelo, S., Carletti, A., Biddau, R., Cidu, R., Celico, F., Soler, A., Ghiglieri, G., 2018. Hydrogeological and multi-isotopic approach to define nitrate pollution and denitrification processes in a coastal aquifer (Sardinia, Italy). Hydrogeol. J. 26, 2021–2040.

Popescu, R., Mimmo, T., Dinca, O.R., Capici, C., Costinel, D., Sandru, C., Ionete, R.E., Stefanescu, I., Axente, D., 2015. Using stable isotopes in tracing contaminant sources in an industrial area: A case study on the hydrological basin of the Olt River, Romania. Sci. Total Environ. 533, 17–23.

Puig, R., Folch, A., Menció, A., Soler, A., Mas-Pla, J., 2013. Multi-isotopic study (15N, 34S, 18O, 13C) to identify processes affecting nitrate and sulfate in response to local and regional groundwater mixing in a large-scale flow system. Appl. Geochemistry 32, 129–141.

Puig, R., Soler, A., Widory, D., Mas-Pla, J., Domènech, C., Otero, N., 2017. Characterizing sources and natural attenuation of nitrate contamination in the Baix Ter aquifer system (NE Spain) using a multi-isotope approach. Sci. Total Environ. 580, 518–532.

R Core Team, 2019. R: A language and environment for statistical computing.

Ramírez Gutiérrez, J.G., 2011. Marco geológico-estratigráfico del Valle de Cuatro Ciénegas, Coahuila, México (Geological-stratigraphic framework of the Cuatro Ciénegas Valley, Coahuila, Mexico). Universidad Autónoma de Nuevo León.

Ransom, K.M., Grote, M.N., Deinhart, A., Eppich, G., Kendall, C., Sanborn, M.E., Souders, A.K., Wimpenny, J., Yin, Q., Young, M., Harter, T., 2016. Bayesian nitrate source apportionment to individual groundwater wells in the Central Valley by use of elemental and isotopic tracers. Water Resour. Res. 52, 5577–5597.

Rao, N.S., 2006. Nitrate pollution and its distribution in the groundwater of Srikakulam district, Andhra Pradesh, India. Environ. Geol. 51, 631–645.

Ritchie, H., Rose, M., 2020. Water Use and Stress [WWW Document]. OurWorldInData.org. URL https://ourworldindata.org/water-use-stress

Rivas Sada, E., 2011. Agua subterránea, electrificación rural y agricultura del algodón en el norte de México - La Comarca Lagunera (1920-1955). In: Sheridan Prieto, C., Cerutti, M. (Eds.), Usos y Desusos Del Agua En Cuencas Del Norte de México. CIESAS, Mexico City, p. 205.

Rivett, M.O., Buss, S.R., Morgan, P., Smith, J.W.N., Bemment, C.D., 2008. Nitrate attenuation in groundwater: A review of biogeochemical controlling processes. Water Res. 42, 4215–4232.

Robinson, B.W., Al Ruwaih, F., 1985. The stable-isotopic composition of water and sulfate from the Raudhatain and Umm Al Aish freshwater fields, Kuwait. Chem. Geol. Isot. Geosci. Sect. 58, 129–136.

Rodrigues Braga, A.C., Serrao-Neumann, S., de Oliveira Galvão, C., 2020. Groundwater Management in Coastal Areas through Landscape Scale Planning: A Systematic Literature Review. Environ. Manage. 65, 321–333.

Romanelli, A., Soto, D.X., Matiatos, I., Martínez, D.E., Esquius, S., 2020. A biological and nitrate isotopic assessment framework to understand eutrophication in aquatic ecosystems. Sci. Total Environ. 715, 136909.

Rozanski, K., Araguás-Araguás, L., Gonfiantini, R., 1993. Isotopic Patterns in Modern Global Precipitation. In: Swart, P.K., Lohmann, K.C., Mckenzie, J., Savin, S. (Eds.), Climate Change in Continental Isotopic Records. American Geophysical Union, Washington, DC, pp. 1–36.

Ruiz-Beviá, F., Fernández-Torres, M.J., 2019. Effective catalytic removal of nitrates from drinking water: An unresolved problem? J. Clean. Prod. 217, 398–408.

Ryabenko, E., Altabet, M.A., Wallace, D.W.R., 2009. Effect of chloride on the chemical conversion of nitrate to nitrous oxide for δ 15 N analysis. Limnol. Oceanogr. Methods 7, 545–552.

Saccon, P., Leis, A., Marca, A., Kaiser, J., Campisi, L., Böttcher, M.E., Savarino, J., Escher, P., Eisenhauer, A., Erbland, J., 2013. Determination of Nitrate Pollution Sources in the Marano Lagoon (Italy) by using a Combined Approach of Hydrochemical and Isotopic Techniques. Procedia Earth Planet. Sci. 7, 758–761.

Saldarriaga-Noreña, H., Garza-Rodríguez, I. de la, Waliszewski, S., Colunga-Urbina, E., Amador-Muñoz, O., Moreno-Dávila, M., Morales-Cueto, R., 2014. Chemical Evaluation of Groundwater from Supply Wells in the State of Coahuila, México. J. Water Resour. Prot. 06, 49–54.

Salinas Jasso, J.A., 2014. Estudio geotécnico-geofísico del comportamiento dinámico del subsuelo para el área metropolitana de Monterrey, Nuevo León, México (Geotechnical-geophysical study of the subsoil's dynamic behavior for the metropolitan area of Monterrey, Nuevo León, Mexico). Universidad Autónoma de Nuevo León.

Samborska, K., Halas, S., Bottrell, S.H., 2013. Sources and impact of sulphate on groundwaters of Triassic carbonate aquifers, Upper Silesia, Poland. J. Hydrol. 486, 136–150.

Sanchez, R., Rodriguez, L., Tortajada, C., 2018. Transboundary aquifers between Chihuahua, Coahuila, Nuevo Leon and Tamaulipas, Mexico, and Texas, USA: Identification and categorization. J. Hydrol. Reg. Stud. 20, 74–102.

Selvakumar, A., Field, R., Burgess, E., Amick, R., 2004. Exfiltration in sanitary sewer systems in the US. Urban Water J. 1, 227–234.

SEMARNAP, (Secretaria de Medio Ambiente Recursos Naturales y Pesca), 1997. Norms Oficial Mexicana NOM-003-CNA-1996.

Serhal, H., Bernard, D., Khattabi, J. El, Sabine, B.-L., Shahrour, I., 2009. Impact of fertilizer application and urban wastes on the quality of groundwater in the Cambrai Chalk aquifer,

Northern France. Environ. Geol. 57, 1579–1592.

SGM, (Servicio Geológico Mexicano), 2007. Inventario físico de los recursos minerales en áreas del municipio de La Paz, Edo. Baja California Sur. Pachuca.

Shalev, N., Burg, A., Gavrieli, I., Lazar, B., 2015. Nitrate contamination sources in aquifers underlying cultivated fields in an arid region – The Arava Valley, Israel. Appl. Geochemistry 63, 322–332.

Shang, X., Huang, H., Mei, K., Xia, F., Chen, Z., Yang, Y., Dahlgren, R.A., Zhang, M., Ji, X., 2020. Riverine nitrate source apportionment using dual stable isotopes in a drinking water source watershed of southeast China. Sci. Total Environ. 724, 137975.

Sharma, M.K., Kumar, M., 2020. Sulphate contamination in groundwater and its remediation: an overview. Environ. Monit. Assess. 192.

Shelton, J.L., Engle, M.A., Buccianti, A., Blondes, M.S., 2018. The isometric log-ratio (ilr)-ion plot: A proposed alternative to the Piper diagram. J. Geochemical Explor. 190, 130–141.

SIAP, (Sistema de Información Agroalimentaria y Pesquera), 2018a. Anuario Estadístico de la Producción Ganadera [WWW Document]. Secr. Agric. y Desarro. Rural. URL https://nube.siap.gob.mx/cierre_pecuario/ (accessed 4.10.20).

SIAP, (Sistema de Información Agroalimentaria y Pesquera), 2018b. Anuario Estadístico de la Producción Agrícola [WWW Document]. Secr. Agric. y Desarro. Rural. URL https://nube.siap.gob.mx/cierreagricola/ (accessed 4.10.20).

Singaraja, C., Chidambaram, S., Jacob, N., Johnson Babu, G., Selvam, S., Anandhan, P., Rajeevkumar, E., Balamurugan, K., Tamizharasan, K., 2018. Origin of high fluoride in groundwater of the Tuticorin district, Tamil Nadu, India. Appl. Water Sci. 8, 54.

Sisto, N.P., Ramírez, A.I., Aguilar-Barajas, I., Magaña-Rueda, V., 2016. Climate threats, water supply vulnerability and the risk of a water crisis in the Monterrey Metropolitan Area (Northeastern Mexico). Phys. Chem. Earth, Parts A/B/C 91, 2–9.

Smith, H.G., Karam, D.S., Lennard, A.T., 2018. Evaluating tracer selection for catchment sediment fingerprinting. J. Soils Sediments 18, 3005–3019.

Snider, D.M., Spoelstra, J., Schiff, S.L., Venkiteswaran, J.J., 2010. Stable Oxygen Isotope Ratios of Nitrate Produced from Nitrification: 18 O-Labeled Water Incubations of Agricultural and Temperate Forest Soils. Environ. Sci. Technol. 44, 5358–5364.

Soucek, D.J., Kennedy, A.J., 2005. EFFECTS OF HARDNESS, CHLORIDE, AND ACCLIMATION ON THE ACUTE TOXICITY OF SULFATE TO FRESHWATER INVERTEBRATES. Environ. Toxicol. Chem. 24, 1204.

Spalding, R.F., Hirsh, A.J., Exner, M.E., Little, N.A., Kloppenborg, K.L., 2019. Applicability of the dual isotopes δ15N and δ18O to identify nitrate in groundwater beneath irrigated cropland. J.

Contam. Hydrol. 220, 128–135.

Stein, L.Y., Klotz, M.G., 2016. The nitrogen cycle. Curr. Biol. 26, R94–R98.

Sterzel, T., Lüdeke, M.K.B., Walther, C., Kok, M.T., Sietz, D., Lucas, P.L., 2020. Typology of coastal urban vulnerability under rapid urbanization. PLoS One 15, e0220936.

Stock, B., Semmens, B., 2016. MixSIAR GUI User Manual. Version 3.1.

Stock, B.C., Jackson, A.L., Ward, E.J., Parnell, A.C., Phillips, D.L., Semmens, B.X., 2018. Analyzing mixing systems using a new generation of Bayesian tracer mixing models. PeerJ 6, e5096.

Strebel, O., Böttcher, J., Fritz, P., 1990. Use of isotope fractionation of sulfate-sulfur and sulfate-oxygen to assess bacterial desulfurication in a sandy aquifer. J. Hydrol. 121, 155–172.

Sun, J., Takahashi, Y., Strosnider, W.H.J., Kogure, T., Wang, B., Wu, P., Zhu, L., Dong, Z., 2021. Identification and quantification of contributions to karst groundwater using a triple stable isotope labeling and mass balance model. Chemosphere 263, 127946.

Szynkiewicz, A., Borrok, D.M., Ganjegunte, G.K., Skrzypek, G., Ma, L., Rearick, M.S., Perkins, G.B., 2015. Isotopic studies of the Upper and Middle Rio Grande. Part 2 — Salt loads and human impacts in south New Mexico and west Texas. Chem. Geol. 411, 336–350.

Szynkiewicz, A., Medina, M.R., Modelska, M., Monreal, R., Pratt, L.M., 2008. Sulfur isotopic study of sulfate in the aquifer of Costa de Hermosillo (Sonora, Mexico) in relation to upward intrusion of saline groundwater, irrigation pumping and land cultivation. Appl. Geochemistry 23, 2539–2558.

Tamez-Meléndez, C., Hernández-Antonio, A., Gaona-Zanella, P.C., Ornelas-Soto, N., Mahlknecht, J., 2016. Isotope signatures and hydrochemistry as tools in assessing groundwater occurrence and dynamics in a coastal arid aquifer. Environ. Earth Sci. 75, 830.

Thivya, C., Chidambaram, S., Thilagavathi, R., Prasanna, M. V., Singaraja, C., Nepolian, M., Sundararajan, M., 2014. Identification of the geochemical processes in groundwater by factor analysis in hard rock aquifers of Madurai District, South India. Arab. J. Geosci. 7, 3767–3777.

Thomas, B.F., Gibbons, A.C., 2018. Sustainable Water Resources Management: Groundwater Depletion. In: Brinkmann, R., Garren, S.J. (Eds.), The Palgrave Handbook of Sustainability. Springer International Publishing, Cham, pp. 53–77.

Ti, C., Wang, X., Yan, X., 2018. Determining $\delta^{15}N$-NO_3^- values in soil, water, and air samples by chemical methods. Environ. Monit. Assess. 190, 341.

Tilman, D., Cassman, K.G., Matson, P.A., Naylor, R., Polasky, S., 2002. Agricultural sustainability and intensive production practices. Nature 418, 671–677.

Tiwari, A.K., Pisciotta, A., De Maio, M., 2019. Evaluation of groundwater salinization and pollution

level on Favignana Island, Italy. Environ. Pollut.

Torres-Martínez, J.A., Mahlknecht, J., Hernández-Antonio, A., Mora, A., 2017. Origin of the Salinity in the Coastal Aquifer of La Paz, Mexico. Procedia Earth Planet. Sci. 17, 520–523.

Torres-Martínez, J.A., Mora, A., Knappett, P.S.K., Ornelas-Soto, N., Mahlknecht, J., 2020a. Tracking nitrate and sulfate sources in groundwater of an urbanized valley using a multi-tracer approach combined with a Bayesian isotope mixing model. Water Res. 182, 115962.

Torres-Martínez, J.A., Mora, A., Mahlknecht, J., Daesslé, L.W., Cervantes-Avilés, P.A., Ledesma-Ruiz, R., 2020b. Estimation of nitrate pollution sources and transformations in groundwater of an intensive livestock-agricultural area (Comarca Lagunera), combining major ions, stable isotopes and MixSIAR model. Environ. Pollut. 703, 115445.

Torres-Martinez, J.A., Mora, A., Ramos-Leal, J.A., Morán-Ramírez, J., Arango-Galván, C., Mahlknecht, J., Ramos-Leal, J.A., Morán-Ramírez, J., Arango-Galván, C., 2019. Constraining a density-dependent flow model with the transient electromagnetic method in a coastal aquifer in Mexico to assess seawater intrusion. Hydrogeol. J. 27, 2955–2972.

Tuttle, M.L.W., Breit, G.N., Cozzarelli, I.M., 2009. Processes affecting δ34S and δ18O values of dissolved sulfate in alluvium along the Canadian River, central Oklahoma, USA. Chem. Geol. 265, 455–467.

Umezawa, Y., Hosono, T., Onodera, S., Siringan, F., Buapeng, S., Delinom, R., Yoshimizu, C., Tayasu, I., Nagata, T., Taniguchi, M., 2008. Sources of nitrate and ammonium contamination in groundwater under developing Asian megacities. Sci. Total Environ. 404, 361–376.

Upadhayay, H.R., Bodé, S., Griepentrog, M., Bajracharya, R.M., Blake, W., Cornelis, W., Boeckx, P., 2018. Isotope mixing models require individual isotopic tracer content for correct quantification of sediment source contributions. Hydrol. Process. 32, 981–989.

Utom, A.U., Werban, U., Leven, C., Müller, C., Knöller, K., Vogt, C., Dietrich, P., 2020. Groundwater nitrification and denitrification are not always strictly aerobic and anaerobic processes, respectively: an assessment of dual-nitrate isotopic and chemical evidence in a stratified alluvial aquifer. Biogeochemistry 147, 211–223.

Valiente, N., Carrey, R., Otero, N., Gutiérrez-Villanueva, M.A., Soler, A., Sanz, D., Castaño, S., Gómez-Alday, J.J., 2017. Tracing sulfate recycling in the hypersaline Pétrola Lake (SE Spain): A combined isotopic and microbiological approach. Chem. Geol. 473, 74–89.

Vengosh, A., 2014. Salinization and Saline Environments. In: Treatise on Geochemistry. Elsevier, pp. 325–378.

Vesanto, J., Alhoniemi, E., 2000. Clustering of the self-organizing map. IEEE Trans. Neural Networks 11, 586–600.

Vitòria, L., Otero, N., Soler, A., Canals, À., 2004. Fertilizer Characterization: Isotopic Data (N, S, O,

C, and Sr). Environ. Sci. Technol. 38, 3254–3262.

Vitòria, L., Soler, A., Canals, À., Otero, N., 2008. Environmental isotopes (N, S, C, O, D) to determine natural attenuation processes in nitrate contaminated waters: Example of Osona (NE Spain). Appl. Geochemistry 23, 3597–3611.

Vystavna, Y., Schmidt, S.I., Diadin, D., Rossi, P.M., Vergeles, Y., Erostate, M., Yermakovych, I., Yakovlev, V., Knöller, K., Vadillo, I., 2019. Multi-tracing of recharge seasonality and contamination in groundwater: A tool for urban water resource management. Water Res. 161, 413–422.

Wang, H., Zhang, Q., 2019. Research Advances in Identifying Sulfate Contamination Sources of Water Environment by Using Stable Isotopes. Int. J. Environ. Res. Public Health 16, 1914.

Wang, Mei, Yu, Li, Meng, Hu, 2019. Anthropogenic Effects on Hydrogeochemical Characterization of the Shallow Groundwater in an Arid Irrigated Plain in Northwestern China. Water 11, 2247.

Ward, M., Jones, R., Brender, J., de Kok, T., Weyer, P., Nolan, B., Villanueva, C., van Breda, S., 2018. Drinking Water Nitrate and Human Health: An Updated Review. Int. J. Environ. Res. Public Health 15, 1557.

Wehrens, R., Buydens, L.M.C., 2007. Self- and Super-organizing Maps in R : The kohonen Package. J. Stat. Softw. 21, 19.

Whaley-Martin, K.J., Mailloux, B.J., van Geen, A., Bostick, B.C., Ahmed, K.M., Choudhury, I., Slater, G.F., 2017. Human and livestock waste as a reduced carbon source contributing to the release of arsenic to shallow Bangladesh groundwater. Sci. Total Environ. 595, 63–71.

WHO, (World Health Organization), 2017. Guidelines for drinking-water quality: Fourth edition incorporating the first addendum, 4th ed. Geneva.

Widory, D., Petelet-Giraud, E., Négrel, P., Ladouche, B., 2005. Tracking the sources of nitrate in groundwater using coupled nitrogen and boron isotopes: A synthesis. Environ. Sci. Technol. 39, 539–548.

Xia, X., Zhang, S., Li, S., Zhang, L.L., Wang, G., Zhang, L.L., Wang, J., Li, Z., 2018. The cycle of nitrogen in river systems: sources, transformation, and flux. Environ. Sci. Process. Impacts 20, 863–891.

Xiao, Y., Gu, X., Yin, S., Pan, X., Shao, J., Cui, Y., 2017. Investigation of Geochemical Characteristics and Controlling Processes of Groundwater in a Typical Long-Term Reclaimed Water Use Area. Water 9, 800.

Xie, X., Wang, Y., Ellis, A., Li, J., Su, C., Duan, M., 2013. Multiple isotope (O, S and C) approach elucidates the enrichment of arsenic in the groundwater from the Datong Basin, northern China. J. Hydrol. 498, 103–112.

Xin, J., Liu, Y., Chen, F., Duan, Y., Wei, G., Zheng, X., Li, M., 2019. The missing nitrogen pieces: A critical review on the distribution, transformation, and budget of nitrogen in the vadose zone-groundwater system. Water Res. 165, 114977.

Xu, Z., Wang, L., Yin, H., Li, H., Schwegler, B.R., 2016. Source apportionment of non-storm water entries into storm drains using marker species: Modeling approach and verification. Ecol. Indic. 61, 546–557.

Xue, D., Botte, J., De Baets, B., Accoe, F., Nestler, A., Taylor, P., Van Cleemput, O., Berglund, M., Boeckx, P., 2009. Present limitations and future prospects of stable isotope methods for nitrate source identification in surface- and groundwater. Water Res. 43, 1159–1170.

Xue, D., De Baets, B., Van Cleemput, O., Hennessy, C., Berglund, M., Boeckx, P., 2012. Use of a Bayesian isotope mixing model to estimate proportional contributions of multiple nitrate sources in surface water. Environ. Pollut. 161, 43–49.

Yang, X., Liu, Q., Fu, G., He, Y., Luo, X., Zheng, Z., 2016. Spatiotemporal patterns and source attribution of nitrogen load in a river basin with complex pollution sources. Water Res. 94, 187–199.

Yuan, F., Mayer, B., 2012. Chemical and isotopic evaluation of sulfur sources and cycling in the Pecos River, New Mexico, USA. Chem. Geol. 291, 13–22.

Yue, F.-J., Li, S.-L., Liu, C.-Q., Zhao, Z.-Q., Ding, H., 2017. Tracing nitrate sources with dual isotopes and long term monitoring of nitrogen species in the Yellow River, China. Sci. Rep. 7, 8537.

Zeng, H., Wu, J., 2014. Tracing the Nitrate Sources of the Yili River in the Taihu Lake Watershed: A Dual Isotope Approach. Water 7, 188–201.

Zhang, H., Xu, Y., Cheng, S., Li, Q., Yu, H., 2020. Application of the dual-isotope approach and Bayesian isotope mixing model to identify nitrate in groundwater of a multiple land-use area in Chengdu Plain, China. Sci. Total Environ. 717, 137134.

Zhang, M., Zhi, Y., Shi, J., Wu, L., 2018. Apportionment and uncertainty analysis of nitrate sources based on the dual isotope approach and a Bayesian isotope mixing model at the watershed scale. Sci. Total Environ. 639, 1175–1187.

Zhang, Q., Wang, H., 2020. Assessment of sources and transformation of nitrate in the alluvial-pluvial fan region of north China using a multi-isotope approach. J. Environ. Sci. 89, 9–22.

Zhang, Q., Wang, H., Lu, C., 2020. Tracing sulfate origin and transformation in an area with multiple sources of pollution in northern China by using environmental isotopes and Bayesian isotope mixing model. Environ. Pollut. 265, 115105.

Zhang, Y., Shi, P., Li, F., Wei, A., Song, J., Ma, J., 2018a. Quantification of nitrate sources and fates in rivers in an irrigated agricultural area using environmental isotopes and a Bayesian isotope mixing model. Chemosphere 208, 493–501.

Zhang, Y., Shi, P., Song, J., Li, Q., 2018b. Application of Nitrogen and Oxygen Isotopes for Source and Fate Identification of Nitrate Pollution in Surface Water: A Review. Appl. Sci. 9, 18.

Zhao, Y., Zheng, B., Jia, H., Chen, Z., 2019. Determination sources of nitrates into the Three Gorges Reservoir using nitrogen and oxygen isotopes. Sci. Total Environ. 687, 128–136.

Zhu, A., Chen, J., Gao, L., Shimizu, Y., Liang, D., Yi, M., Cao, L., 2019. Combined microbial and isotopic signature approach to identify nitrate sources and transformation processes in groundwater. Chemosphere 228, 721–734.

Zuo, K., Kim, J., Jain, A., Wang, T., Verduzco, R., Long, M., Li, Q., 2018. Novel Composite Electrodes for Selective Removal of Sulfate by the Capacitive Deionization Process. Environ. Sci. Technol. 52, 9486–9494.

Appendix 1

Table A1.1. Physical, chemical and isotopic parameter of sampling points in the study area

| Group | ID | UTM coordinates | | altitude | meters | m.a.s.l. | T | pH | mg/L | mg/L | mg/L | mg/L | mg/L | mg/L | mg/L | mg/L | mmol/L |
		x	y		Sampling depth				Ca^{2+}	Mg^{2+}	Na^+	K^+	F^-	Cl^-	NO_3^-	SO_4^{-2}	HCO_3^-
1	BA01	360397.01	2827670.17	848.00	24.00	824.00	22.00	7.46	73.60	9.48	2.22	0.43	0.24	3.21	1.06	31.87	4.12
1	BA02	359868.01	2828331.15	831.00	10.00	821.00	21.84	7.28	73.45	8.27	2.03	0.40	0.21	2.55	1.04	25.32	4.07
1	BA03	358446.56	2828770.74	820.00	70.00	750.00	21.99	7.24	75.40	8.84	2.16	0.41	0.24	3.07	1.07	33.93	4.10
1	BA04	357523.34	2829343.74	810.00	25.00	785.00	21.50	7.21	72.50	8.04	1.63	0.39	0.20	2.82	0.98	22.10	4.02
1	BA05	357124.45	2829621.84	801.00	23.00	778.00	22.33	7.21	74.50	8.98	2.28	0.44	0.28	3.59	1.14	29.10	4.04
1	BA06	353064.97	2833256.93	757.00	10.00	747.00	23.65	7.26	71.80	10.95	3.00	0.47	0.39	4.49	1.12	38.46	3.95
1	BA07	352537.14	2833453.52	766.00	7.00	759.00	25.00	7.24	70.10	14.50	0.95	0.62	0.56	6.24	1.55	60.64	4.03
1	BA08	355053.99	2835278.22	750.00	34.00	716.00	22.96	7.07	82.00	9.04	2.81	0.48	0.25	3.82	1.52	61.81	3.94
1	BA09	354433.50	2837718.92	680.00	6.00	674.00	25.61	7.35	79.50	11.59	3.92	0.63	0.34	5.41	1.96	78.07	3.80
1	ST04	372340.80	2826052.20	715.00	-	-	21.82	8.19	71.85	2.28	2.10	0.33	0.1	2.14	0.34	33.56	3.18
2	MN01	346133.35	2878503.02	622.00	32.00	590.00	30.15	7.22	110.50	12.40	61.90	1.03	0.55	129.02	1.38	143.69	4.18
2	MN02	344748.58	2879202.50	622.00	30.00	592.00	29.92	7.42	102.10	11.47	65.38	1.19	0.54	138.26	1.46	121.51	4.14
2	MN03	343363.03	2879825.37	624.00	29.00	595.00	30.14	7.19	111.20	12.88	60.15	1.01	0.57	121.64	1.33	156.44	4.20
2	MN04	343288.52	2878712.20	617.00	33.00	584.00	30.29	7.17	105.30	12.13	51.60	1.69	0.53	100.74	1.53	153.19	4.18
2	MN05	343516.90	2877813.99	614.00	20.00	594.00	30.40	7.14	126.20	15.03	68.60	0.95	0.67	145.79	0.83	206.86	4.31
2	MN06	342439.12	2878134.70	629.00	36.00	593.00	31.04	7.12	107.50	12.25	53.10	1.06	0.55	94.55	2.00	155.73	4.26
2	MN07	342635.93	2878550.76	631.00	39.00	592.00	30.68	7.12	107.50	12.49	54.15	1.22	0.55	106.99	1.67	156.88	4.28
3	ZM04	362111.82	2840157.02	602.00	38.00	564.00	28.13	7.51	93.95	9.84	7.76	0.01	0.56	19.83	3.53	73.22	4.12
3	ZM05	362906.40	2839881.17	590.00	30.00	560.00	29.71	7.31	93.80	9.69	6.83	0.56	0.63	18.57	4.03	75.52	4.13
3	ZM07	363960.47	2840971.82	579.00	35.00	544.00	32.05	7.35	92.05	9.65	7.21	0.57	0.62	18.62	3.04	70.03	4.10
3	ZM08	363712.88	2841297.48	588.00	44.00	544.00	30.17	7.32	94.30	9.69	5.85	0.52	0.59	16.31	3.74	64.53	4.24
4	ZM01	361340.49	2839466.65	602.00	19.00	583.00	23.62	7.36	102.20	15.54	20.86	1.59	0.29	42.45	10.13	89.02	4.87
4	ZM02	361565.11	2839605.76	598.00	21.00	577.00	24.95	7.07	103.40	19.14	30.20	1.09	0.37	46.03	11.59	90.75	5.17
4	ZM03	362047.25	2839585.45	588.00	20.00	568.00	23.54	7.08	107.90	13.87	18.26	0.56	0.27	36.26	9.70	84.46	4.97
4	ZM06	363071.10	2840442.52	587.00	29.00	558.00	24.50	7.25	106.90	16.75	25.29	1.56	0.33	48.55	11.10	94.33	5.10

4	ZM09	364327.36	2844405.03	550.00	32.00	518.00	25.83	7.22	133.75	13.82	22.02	1.08	0.19	50.84	18.64	139.10	5.84
4	ZM10	364811.15	2841818.49	568.00	30.00	538.00	25.27	7.12	121.10	13.30	21.97	0.20	0.34	42.72	13.23	120.08	5.26
4	ZM11	368610.77	2839528.05	533.00	12.00	521.00	24.72	7.06	110.60	12.94	20.39	1.29	0.21	32.24	8.28	86.31	4.14
4	ZM12	368316.84	2839417.10	539.00	18.00	521.00	24.92	7.14	112.80	13.59	22.24	1.20	0.25	36.65	10.83	105.33	4.30
4	ZM13	368651.91	2839739.99	530.00	9.00	521.00	24.79	7.12	112.90	14.71	22.98	1.24	0.22	34.65	9.07	90.49	4.91
4	ZM14	367601.16	2840067.34	541.00	20.00	521.00	25.44	7.09	108.30	16.17	24.87	1.46	0.21	37.49	10.20	106.32	4.70
4	ZM15	368157.66	2844154.02	534.00	30.00	504.00	25.44	6.97	113.00	17.30	26.50	1.05	0.25	41.69	12.01	98.45	5.08
4	ZM20	368087.38	2845219.31	532.00	25.00	507.00	25.73	7.20	100.30	23.60	21.74	0.69	0.25	37.94	9.86	114.79	4.48
5	ZM16	373018.98	2847937.18	486.00	10.00	476.00	26.04	7.02	155.00	18.75	52.90	1.04	0.42	106.04	21.79	224.50	5.54
5	ZM17	368914.84	2847715.68	511.00	7.00	504.00	27.05	6.88	123.75	33.23	50.05	0.36	0.32	63.38	19.25	199.60	5.51
5	ZM18	371265.38	2853852.53	479.00	14.00	465.00	26.07	6.94	217.00	12.40	110.30	0.40	0.66	224.28	30.81	539.40	5.58
5	ZM19	362201.95	2853627.13	591.00	46.00	545.00	30.79	7.30	180.70	14.00	65.45	0.43	0.52	184.53	11.28	245.43	4.46
5	ZM21	372800.12	2843428.64	498.00	11.00	487.00	26.27	6.94	234.00	23.69	41.90	0.69	0.26	167.70	12.45	321.32	5.71
5	ZM22	382109.19	2851419.07	424.00	16.00	408.00	26.07	7.01	173.10	25.48	145.60	0.73	0.49	169.55	14.73	420.60	6.44
5	ZM23	382779.53	2850674.65	421.00	18.00	403.00	25.56	6.75	189.65	22.27	97.20	1.75	0.35	146.71	8.84	340.90	6.88

Group	ID	$\delta^{18}O$ (H$_2$O)	δ^2H (H$_2$O)	$\delta^{15}N$-NO$_3$ AIR ± 0.3‰	$\delta^{18}O$-NO$_3$ VSMOW ± 0.8‰	$\delta^{18}O$-SO$_4$ VSMOW ± 0.5‰	$\delta^{34}S$-SO$_4$ VCDT ± 0.3‰	Br μg/L	B μg/L	I μg/L
1	BA01	-9.28	-62.82	3.93	-0.27	8.26	5.03	23.000	13.000	2.300
1	BA02	-9.22	-62.49	4.46	1.32	8.19	3.88	19.000	10.000	2.000
1	BA03	-9.48	-63.15	4.31	0.54	8.59	5.98	22.000	13.000	2.300
1	BA04	-9.10	-61.42	3.97	0.95	7.88	3.65	18.000	10.000	1.900
1	BA05	-9.36	-62.03	3.46	3.05	7.57	1.03	18.000	10.000	1.700
1	BA06	-9.16	-61.94	3.74	2.00	8.84	5.06	23.000	13.000	2.100
1	BA07	-9.54	-63.89	4.45	2.54	7.74	1.09	37.000	29.000	3.300
1	BA08	-9.17	-61.53	3.75	2.50	8.93	9.10	22.000	17.000	2.700
1	BA09	-8.83	-59.40	3.55	3.14	10.48	7.14	29.000	18.000	2.100
1	ST04	-8.94	-57.66	2.04	1.03	8.85	6.92	20.000	13.000	2.300
2	MN01	-7.59	-48.34	5.89	4.60	11.35	10.94	64.000	44.000	2.200
2	MN02	-7.34	-47.71	6.15	4.87	11.13	10.27	59.000	40.000	2.200

2	MN03	-7.46	-48.46	6.23	4.73	11.52	10.58	75.000	51.000	2.200
2	MN04	-7.53	-49.73	6.86	5.47	10.75	8.40	100.000	83.000	4.200
2	MN05	-7.45	-46.74	6.92	4.82	12.12	12.16	84.000	56.000	4.000
2	MN06	-7.86	-49.98	8.27	6.55	9.87	6.49	133.000	105.000	4.000
2	MN07	-7.53	-49.10	7.40	5.34	10.75	8.05	80.000	58.000	1.700
3	ZM04	-7.39	-44.55	4.42	4.92	8.15	6.83	17.000	16.000	1.600
3	ZM05	-7.01	-43.65	3.54	7.74	7.50	5.66	21.000	22.000	1.900
3	ZM07	-7.23	-45.02	3.88	1.90	9.00	8.04	23.000	19.000	2.100
3	ZM08	-6.98	-43.04	3.69	1.60	7.87	6.07	24.000	27.000	2.600
4	ZM01	-8.71	-58.07	9.26	4.08	6.75	6.29	82.000	40.000	2.300
4	ZM02	-8.38	-56.56	9.03	1.39	5.79	6.30	165.000	124.000	5.000
4	ZM03	-8.38	-56.58	8.66	2.50	7.24	6.40	82.000	47.000	4.700
4	ZM06	-8.25	-53.78	9.63	1.55	6.43	6.47	124.000	106.000	5.600
4	ZM09	-6.80	-43.84	9.66	2.32	6.49	7.53	157.000	63.000	7.600
4	ZM10	-7.77	-50.07	8.90	1.76	6.70	4.77	139.000	86.000	4.800
4	ZM11	-7.26	-48.33	9.93	2.83	8.28	6.55	88.000	55.000	3.600
4	ZM12	-6.02	-39.55	10.57	3.58	8.82	7.55	86.000	41.000	3.400
4	ZM13	-7.48	-50.07	10.09	2.35	7.84	6.84	89.000	61.000	3.200
4	ZM14	-6.86	-47.19	10.13	2.13	7.92	6.82	115.000	99.000	6.000
4	ZM15	-7.71	-51.00	10.33	2.15	8.02	6.48	139.000	103.000	5.000
4	ZM20	-7.04	-45.97	9.48	2.08	8.96	7.82	64.000	83.000	8.400
5	ZM16	-5.85	-37.68	10.07	3.33	9.13	7.06	252.000	154.000	9.900
5	ZM17	-6.34	-42.20	10.22	2.30	8.94	7.54	175.000	133.000	7.600
5	ZM18	-5.37	-35.26	13.16	5.49	9.60	10.02	809.000	419.000	70.300
5	ZM19	-6.48	-39.91	11.18	4.06	9.41	8.43	234.000	67.000	4.100
5	ZM21	-8.59	-56.48	13.97	9.86	9.98	8.04	18.000	11.000	1.700
5	ZM22	-8.61	-57.81	14.79	7.19	9.01	6.15	22.000	13.000	2.100
5	ZM23	-7.11	-42.49	14.44	6.80	9.57	6.46	13.000	12.000	0.800
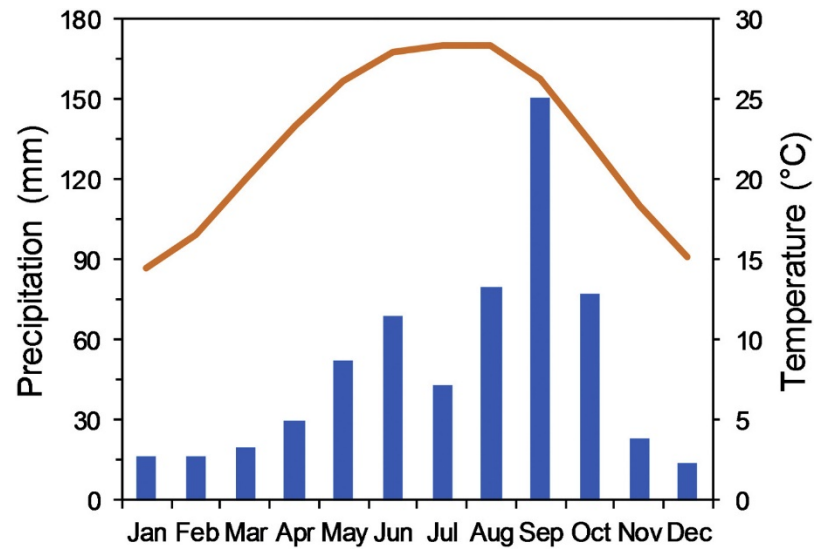
Fig. A1.1. Average total annual precipitation (mm) and average temperature in the study area

Table A1.2. Isotopic composition used in the MixSIAR for the different pollution sources

Source	Meand15N	SDd15N	n	Mean d18O	SDd18O	n	reference	Study Area
Industrial sewage	-8.6	10.6	12				Popescu et al 2015	Romania
Industrial sewage	8.5	0.9	3	38.5	18.9	3	Jin et al 2018	China
Manure	9.7	4.7	70				Li et al 2007	China
Manure	3.7	2.1	65				Li et al 2007	China
Manure	14	0	1				Heaton et al, 1983	South Africa
Manure	6.8	0.3	3				Choi et al, 2007	Korea
Manure	9.6	0.4	3				Choi et al, 2007	Korea
Manure	17.1	0.9	3				Choi et al, 2007	Korea
Manure	17.8	1.2	3				Choi et al, 2007	Korea
Manure	20.9	0.7	3				Choi et al, 2007	Korea
Manure	40.1	3.4	3				Choi et al, 2007	Korea
Manure	45.2	4.1	3				Choi et al, 2007	Korea
Manure	7.6	0.1	3				Choi et al, 2007	Korea
Manure	15.23	0.68	3				Girard & Hillaire-Marcel, 1997	Niger
Manure	7	3.2	5				Liu et al 2006	China
Manure	8.7	1.3	3				Chen et al 2014	China
Manure	9.6	3.68	6				Wassenaar 1995	Canada
Manure	10.6	5.6	4				Fun-Jun et al 2013	China
Manure	6.25	3.71	4				Rogers et al 2012	France
Manure	8.9	9.28	4	3.5	4.98	4	Widory et al 2013	France
Manure	6.45	3.6	2				Briand et al 2017	France
Manure	10.73	2.15	4				Shomar et al , 2008	Gaza strip
Manure	5.69	2.5	3				Sacoon et al 2013	Italy
Manure	11.75	2.19	2				Nishikori et al 2012	Japan
Manure	8.57	1	9				Girard & Hillaire-Marcel, 1997	Niger
Manure	9.2	0.2	3				Choi et al, 2007	Korea

Type							Reference	Country
Manure	13.88	0	1	11.7	0	1	Mattern et al 2011	Belgium
Manure/Sewage	10.49	4.53	7	3.45	2.63	7	Ji et al 2017	China
Manure/Sewage	12.73	3.4	14	4.08	0.33	14	M. Zhang et al 2018	China
Sewage	4.98	0.67	4				Rogers et al 2012	France
Sewage	5.74	1.26	19	0.95	0.96	19	Minet et al 2012	Ireland
Sewage	9.9	1.5	13	3.5	1.4	16	Aravena et al, 1993	Canada
Manure	8.1	39	11				Bateman & Kelly	England
Sewage	27.89	8.89	9	10.87	4.52	9	Aravena & Robertson 1998	Canada
Sewage	4.39	3.62	4	1.24	2.03	4	Mattern et al 2011	Belgium
Sewage	11.4	2.3	9	2.5	2.2	9	Ding et al 2014	China
Sewage	5	5.75	3	5.43	9.98	3	Yue et al 2014	China
Sewage	15.32	0.83	6	9.11	0.93	6	Lu et al 2015	China
Sewage	24.25	7.14	4				Wilson et al, 1994	England
Sewage	24.45	7.71	2	1.7	8.77	2	Widory et al 2013	France
Sewage	14.05	0.21	2	3.35	1.35	2	Stoewer et al 2015	Germany
Sewage	14.15	2.69	7	8.73	2.18	7	Delconte et al 2014	Italy
Sewage	10.4	7.5	8	6	3.6	8	Jin et al 2018	China
Sewage	16.3	5.7	40	7	2.7	40	Zhang et al 2018	China
Sewage	3.7	0.8	3				Liu et al 2006	China
Sewage	9.9	2	7				Mariotti et al 1988	France
Sewage	14.4	3.8	10	7.6	1.5	7	El Gaouzi et al 2013	France
Sewage	13.3	3.7	3	7.6	1.08	3	Briand et al 2017	France
Sewage	13.37	2.25	2	10.45	2.76	2	Sacchi et al 2013	Italy
Sewage	9.3	6.29	6	2.9	6.32	6	Schmidt et al 2016	USA
Sewage	10.3	4.5	11	0.65	2.6	11	Anisfeld et al 2007	USA
Sewage	8.9	0	1	5.6	0	1	Li et al 2010	China
Sewage	20.28	9.03	8	9.29	6.99	8	Adebowie et al 2019	Australia
Sewage sludge	5.25	0.9	16				Shomar et al , 2008	Gaza strip
Precipitation	-1.49	1.75	6	58.18	14.22	6	Ji et al 2017	China

Precipitation	-6.2	1.24	5	53.76	4.04	5	Spoelstra et al , 2004	Canada
Precipitation	1.5		21	34.2	0	14	Liu et al 2006	China
Precipitation	4.6	3.9	8	54	13.2	8	Ding et al 2014	China
Precipitation	-4.15	2.75	2	54.4	10.04	2	Yue et al 2014	China
Precipitation	-0.7	2.41	4	43.85	4.93	4	Lu et al 2015	China
Precipitation	3.1	1.5	6	56.7	17.8	6	Yue et al 2015b	China
Precipitation	-2.2	0	1	82.7	0	1	Hosono et al 2011b	China
Precipitation	1.6	0	1	78.6	0	1	Briand et al 2017	France
Precipitation	4.3	1.1	8	64.5	4.8	8	Durka et al, 1994	Germany
Precipitation	-3.2	0.92	3	65.9	25.79	3	Stoewer et al 2017	Germany
Precipitation	-0.67	1.24	2	52.05	3.89	2	Lee et al, 2008	Korea
Precipitation	0.3	4.5	12				Popescu et al 2015	Romania
Precipitation	-2		24				Heaton et al, 1983	South Africa
Precipitation	0.6	1.5	6	57.2	6.9	6	Jin et al 2018	China
Precipitation	3.2	2.4	30	44	9.1	30	Zhang et al 2018	China
Precipitation	2.3	1.4	8	60.8	1.5	8	M. Zhang et al 2018	China
Precipitation	3.07	2.14	2	75.67	2.64	2	Mattern et al 2011	Belgium
Precipitation	5.6	1.7	3				Chen et al 2014	China
Precipitation	2.2	3.96	2	59.55	8.41	2	Itoh et al 2011	Mongolia
Precipitation	-2.3	1.7	26	62.2	8.5	26	Pardo et al 2004	USA
Precipitation	-2.4	2.5	13	70.5	6	13	Anisfeld et al 2007	USA
Precipitation	-7.57	1.89	6				Li et al 2007	China
Precipitation	-0.6	0	1	49.6	0	1	Umezawa et al, 2008	Manila (Philippines)
Soil	4.37	0.48	8				Wassenaar 1995	Canada
Soil	6.6	2.4	7				Fun-Jun et al 2013	China
Soil	4.7	0.3	4	-3	0	1	Ding et al 2014	China
Soil	5.81	1.51	12	1.24	3.13	12	Lu et al 2015	China
Soil	7.35	2.76	2				Wilson et al, 1994	England
Soil	-2.33	6.88	4	8.85	2.45	4	Briand et al 2017	France

Source	Meand34S	SDd34S	n	Meand18O	SDd18O	n	reference	Study Area
Soil	5.04	1.75	5				Shomar et al , 2008	Gaza strip
Soil	-6.1		6	13		6	Stoewer et al 2018	Germany
Soil	2.27	2.22	6	3.2	5.2	6	Stoewer et al 2019	Germany
Soil	1.8	1.4	4	-2.4	7.9	4	Stoewer et al 2020	Germany
Soil	6.18	0.83	5	0.9	0.69	5	Minet et al 2012	Ireland
Soil	2.63	0.31	3	-0.23	1.5	3	Minet et al 2012	Ireland
Soil	7.27	2.69	6				Girard & Hillaire-Marcel, 1997	Niger
Soil	2.18	2.59	6	0.63	2.01	6	Ji et al 2017	China
Soil	4.52	2.67	20	4.08	0.33	20	M. Zhang et al 2018	China
Soil	5.7	2	6				Liu et al 2006	China
Soil - Desert	0	2.2	20				Bohlke et al 1997	Chile-USA
Source	Meand34S	SDd34S	n	Meand18O	SDd18O	n	reference	Study Area
Gypsum	12.9	0.2	3	13.7	0.2	3	Bottrell et al 2008	England
Gypsum	23.8	2.84	35	15.41	3.72	26	Palmer et al 2004	Turkey
Gypsum	18.32	2.61	48	17.4	2.36	29	Fontes & Letolle 1976	France
Gypsum	16.29	6.04	79				Chivas et al 1991	Australia
Gypsum	14.72	1.46	54	10.45	1.33	54	Chen et al 2016	USA
Gypsum	12.5	0.61	8	10.85	0.77	8	Chen et al 2016	USA
Gypsum	-15.2	0	1				Moncaster et al 2000	England
Gypsum	12.9		9				Szynkiewickz et al 2012	USA
Gypsum	17.8	0.47	10	13.22	0.96	10	Lo Forte et al, 2005	Argentina
Gypsum	16.75	4.86	30	14.4	20.21	30	Cortecci et al 1981	Italy
Gypsum	14.99	0.95	37	12.54	2.09	36	Ortí et al 2014	Spain
Gypsum	-21.23	4.29	20	10.57	7.01	25	Valiente et al 2017	Spain
Gypsum	22.09	2	11				Sacks & Tihsanky, 1996	USA
Gypsum	22.48	0.25	6	16.61	0.54	6	Pierre 2018	France
Gypsum	17.92	2.44	17	15.62	0.89	14	Van Everdingen et al , 1982	Canada
Gypsum	29.23	1.94	21	13.96	1.21	9	Van Everdingen et al , 1982	Canada
Gypsum	22.07	7.48	19	14.04	2.12	17	Van Everdingen et al , 1982	Canada

Misisipian Anhydrite	11.54	2.99	8				Plummer et al, 1990	USA
Rus anhydrite	18.6	0	1	14.2		1	Robinson & Al Ruwaih, 1985	Kuwait
Wadi Al Batin getch	15.6	0	1	15.6		1	Robinson & Al Ruwaih, 1985	Kuwait
Halite	17.9	0.2	6	12.4	0.2	6	Bottrell et al 2008	England
Halite	24.7	34.7					Van Everdingen et al , 1982	Canada
Precipitaiton	4.89	0.83	24	6.86	2.99	24	Tichomirowa et al 2010	Germany
Precipitation	13.53	4.4	19				Bottrell & Novak 1997	England
Precipitation	4.67	1.77	10	12.19	0.61	9	Bottrell et al 2008	England
Precipitation	5.2	0.85	2	13.85	4.74	2	Brenot et al 2007	France
Precipitation	5.7	1.72	10	9.34	1.56	11	D. Zhang et al 2015	China
Precipitation	3.23	2.77	3	11.95	2.95	4	Einsield & Mayer 2005	Germany
Precipitation	3.01	1.51	11	12.12	2.39	13	Einsield et al 2007	Germany
Precipitation	2.5	0.7	34	13.3	1.7	34	Gorka et al 2008	Poland
Precipitation	5.04	0.64	14				Ingri et al 1997	Sweden
Precipitation	1.25	1.53	13	14.56	2.21	15	Jenkins & Bao 2006	USA
Precipitation	6.08	0	1	8.74	0	1	Jezierski et al 2005	Poland
Precipitaiton	4	0.53	3				Jiang 2012	China
Precipitation	0.98	1.56	5	10.47	1.4	3	Meyer et al 1995	Germany
Precipitation	1.97	1.12	6				Meyer et al 1995	Germany
Precipitation				14.2	0.5	24	Novak et al 2007	Czech Republic
Precipitation	7.7	0.5	38	13.1	0.3	23	Novak et al 2007	Czech Republic
Precipitation	3.2	0	1				Strebel et al, 1990	Germany
Precipitation	5.14	0.35	5	7.42	1.18	5	Tichomirowa & Heidel 2012	Germany
Precipitation	5.01	1.23	39	7.93	3.8	39	Tichomirowa & Heidel 2012	Germany
Precipitation	15.6	0	1	6		1	Van Donkelaar et al, 1994	Canada
Precipitation	6.6	1.8	70	11.1	2.4	66	Han et al 2016	China
Precipitation	-3.2	1.33	5	40.62	3	5	Sánchez et al 2017	USA
Manure	6.4	0	1				Bartlett et al 2010	England

Manure	3.7	0	1				Otero et al 2007	Spain
Manure	4	0	1				Bartlett et al 2010	England
Sewage	-2.31	1.94	9	-2.04	1.22	9	Aravena & Robertson 1998	Canada
Sewage	7.23	2.34	8	12.35	3.65	6	Bottrell et al 2008	England
Sewage	9.6	2	15	10	1	15	Otero et al 2008	Spain
Sewage	8.6	1.3	4	10.5			Jurado et al 2013	Spain
Sand	0.74	3.57	5	-1.16	3	5	Dowuona & Mermut, 1993	Canada
Soil	2.4	0.6	5				Mayer et al 1991	Germany
Soil	2.2	0.6	5	6.1	0.2	4	Mayer et al 1992	Germany
Soil	1.9	1.3	6				Mayer et al 1993	Germany
Soil	2.5	0.1	3	2.6	0.4	3	Mayer et al 1994	Germany
Granite	5.95	1.34	2				Mayer et al 1995	Germany
Soil	5.48	1.99	5	7.18	6.06	5	D. Zhang et al 2015	China

Table A1.3. Summary of proportional contribution sources for nitrate and sulfate, including the possible transformation process. The percentage in bold represent the main pollution source of each well.

Sample ID	Group	Land use	Surface geology	Probable source of nitrate			Possible nitrate transformation process	Probable source of sulfate				Possible sulfate transformation process
				Atmospheric deposition	Soil Organic Nitrogen	Manure/sewage		Atmospheric deposition	Soil sulfate	Manure/sewage	Marine evaporites	
				Mean±S.D.	Mean±S.D.	Mean±S.D.		Mean±S.D.	Mean±S.D.	Mean±S.D.	Mean±S.D.	
BA-01	1	Piedmont shrubland	Limestone	0.2%±0.3	**97.3%±2.4**	2.4%±2.4	Nitrification	28.7%±12.4	25.5%±19.4	**39.1%±26.2**	6.6%±4.5	Evaporative enrichment
BA-02	1	Piedmont shrubland	Shale	0.3%±0.5	**96.8%±4.4**	3.0%±4.4	Nitrification	27.6%±18.4	29.1%±24.5	**39.20%±30.8**	4.1%±4.1	Evaporative enrichment
BA-03	1	Piedmont shrubland	Limestone	0.3%±0.4	**97.3%±3.5**	2.5%±3.4	Nitrification	34.0%±19.8	20.5%±18.0	**38.1%±27.3**	7.4%±6.9	Evaporative enrichment/mixing
BA-04	1	Piedmont shrubland	Shale	0.2%±0.4	**97.1%±3.9**	2.7%±3.8	Nitrification	24.4%±17.0	31.7%±26.2	**40.0%±31.6**	3.9%±3.7	Evaporative enrichment
BA-05	1	Piedmont shrubland	Alluvium	0.4%±0.7	**96.3%±4.9**	3.3%±4.8	Denitrification	11.2%±9.4	42.1%±37.3	**44.4%±38.7**	2.3%±2.3	Evaporative enrichment/mixing
BA-06	1	Piedmont shrubland	Alluvium	0.3%±0.5	**96.7%±4.4**	2.9%±4.3	Denitrification	35.8%±20.4	22.4%±19.4	**36.0%±27.2**	5.8%±5.6	Evaporative enrichment/mixing
BA-07	1	Piedmont shrubland	Alluvium	0.4%±0.6	**96%±5.5**	3.6%±5.4	Denitrification	11.7%±9.9	41.4%±37.0	**44.5%±38.8**	2.4%±2.3	Evaporative enrichment/mixing
BA-08	1	Piedmont shrubland	Limestone	0.3%±0.6	**96.5%±4.7**	3.1%±4.6	Denitrification	23.2%±16.2	14.8%±13.7	**41.3%±29.0**	20.7%±15.0	Evaporative enrichment
BA-09	1	Piedmont shrubland	Limestone	0.4%±0.7	**96.4%±5.0**	3.2%±4.9	Denitrification	**46.8%±22.8**	13.2%±12.7	28.0%±22.9	12.0%±10.2	Evaporative enrichment
ST-04	1	Mixed woodland	Shale	0.2%±0.4	**97.7%±2.8**	2%±2.7	Nitrification	34.7%±20.4	17.2%±15.4	**38.0%±26.4**	10.2%±9.4	Evaporative enrichment/mixing
MN-01	2	Desert shrubland	Alluvium	3.1%±1.3	**75%±9.3**	21.9%±9.2	Denitrification	25.7%±10.6	10.2%±7.0	24.3%±12.6	**39.7%±7.5**	Evaporative enrichment
MN-02	2	Desert shrubland	Limestone	2.7%±1.9	**74.3%±15.8**	23%±15.8	Denitrification	24.6%±16.1	8.7%±8.6	20.8%±15.6	**45.9%±13.0**	Evaporative enrichment
MN-03	2	Secondary shrubland	Alluvium	2.5%±1.8	**74.5%±15.6**	22.9%±15.6	Denitrification	23.4%±15.6	8.7%±8.6	19.4%±14.4	**48.5%±13.1**	Evaporative enrichment
MN-04	2	Secondary shrubland	Alluvium	3.2%±2.1	**67.7%±16.9**	29.1%±17.1	Denitrification	34.7%±20.8	10.0%±9.9	24.4%±18.3	**30.9%±12.7**	Evaporative enrichment/mixing
MN-05	2	Desert shrubland	Alluvium	2.5%±1.8	**70.1%±17.1**	27.5%±17.2	Denitrification	18.2%±12.6	7.0%±6.8	16.0%±12.1	**58.8%±12.6**	Evaporative enrichment
MN-06	2	Desert shrubland	Alluvium	4.5%±2.6	**52.9%±18.7**	42.6%±19.2	Denitrification/mixing	**39.8%±22.4**	13.3%±13.3	28.7%±21.6	18.2%±10.3	Evaporative enrichment
MN-07	2	Desert shrubland	Limestone	3.1%±2.1	**64.7%±17.9**	32.2%±18.1	Denitrification	**36.6%±21.4**	10.3%±10.3	24.0%±18.2	29.1%±12.7	Evaporative enrichment
ZM-04	3	Urban area	Alluvium	2.7%±2.0	**82.1%±12.3**	15.1%±12.1	Denitrification	25.5%±17.7	16.9%±15.7	**38.6%±24.4**	19.0%±10.1	Evaporative enrichment
ZM-05	3	Urban area	Alluvium	7.9%±3.3	**77.2%±12.2**	14.9%±12.1	Denitrification	22.1%±16.3	22.5%±19.7	**41.8%±27.4**	13.6%±8.4	Evaporative enrichment
ZM-07	3	Urban area	Alluvium	1.0%±0.9	**90.3%±7.6**	8.7%±7.5	Nitrification	27.9%±18.2	12.8%±12.4	**32.8%±21.9**	26.5%±12.1	Evaporative enrichment/mixing
ZM-08	3	Urban area	Shale	0.2%±0.2	**64%±13.1**	35.8%±13.1	Nitrification	12.0%±18.2	18.6%±11.11	**60.2%±16.5**	9.2%±5.3	Evaporative enrichment
ZM-01	4	Urban area	Alluvium	0.3%±0.6	48.8%±18.5	**50.9%±18.6**	Denitrification/mixing	10.4%±10.0	20.5%±17.0	**61.2%±23.3**	7.9%±6.8	Evaporative enrichment
ZM-02	4	Urban area	Alluvium	0.2%±0.3	**59.6%±21.4**	40.2%±21.4	Nitrification/mixing	8.3%±8.1	22.9%±18.6	**61.3%±24.8**	7.6%±6.7	Evaporative enrichment
ZM-03	4	Urban area	Alluvium	0.2%±0.3	**59.1%±19.0**	40.7%±19.0	Denitrification/mixing	12.2%±11.6	18.4%±15.6	**60.9%±23.1**	8.5%±7.4	Evaporative enrichment

ZM-20	4	Urban area	Alluvium	0.2%±0.3	**56.4%±19.6**	45.3%±19.6	Nitrification/mixing	16.5%±15.2	13.1%±11.6	**55.3%±22.8**	15.2%±10.8	Evaporative enrichment
ZM-06	4	Urban area	Alluvium	0.2%±0.3	**54.2%±21.2**	45.7%±21.2	Nitrification/mixing	9.7%±9.2	20.4%±16.8	**61.9%±23.4**	8.1%±7.3	Evaporative enrichment
ZM-09	4	Urban area	Alluvium	0.2%±0.3	**52.2%±19.6**	47.6%±19.6	Nitrification/mixing	8.5%±8.0	16.5%±14.5	**64.5%±22.6**	10.4%±9.3	Evaporative enrichment
ZM-10	4	Urban area	Alluvium	0.2%±0.3	**59.2%±20.4**	40.7%±20.4	Nitrification/mixing	10.7%±10.6	25.6%±20.6	**58.2%±25.6**	5.5%±5.0	Evaporative enrichment
ZM-11	4	Urban area	Alluvium	0.2%±0.4	**48.3%±18.6**	51.5%±18.6	Nitrification/mixing	15.9%±14.8	16.8%±14.5	**57.3%±23.1**	10.0%±8.1	Evaporative enrichment
ZM-13	4	Urban area	Alluvium	0.2%±0.3	**48.9%±19.5**	50.9%±19.5	Nitrification/mixing	13.8%±13.0	16.3%±14.0	**59.7%±22.7**	10.2%±8.5	Evaporative enrichment
ZM-15	4	Urban area	Aluvium	0.8%±0.7	15.0%±9.6	**84.2%±9.6**	Nitrification	28.0%±10.9	11.2%±9.0	**45.4%±15.5**	15.5%±5.9	Evaporative enrichment
ZM-12	4	Urban area	Alluvium	0.7%±0.9	20.9%±16.9	**78.4%±17.0**	Nitrification	27.5%±17.6	10.7%±11.1	**46.5%±22.4**	15.3%±9.6	Evaporative enrichment
ZM-14	4	Urban area	Alluvium	0.6%±0.7	21.9%±19.1	**77.5%±19.1**	Nitrification	23.5%±16.1	13.1%±13.4	**51.6%±23.4**	11.8%±8.3	Evaporative enrichment
ZM-16	5	Urban area	Alluvium	0.7%±0.9	23.2%±18.9	76.1%±18.9	Nitrification	31.4%±19.4	10.6%±11.2	**43.9%±22.5**	14.1%±9.2	Evaporative enrichment
ZM-17	5	Urban area	Alluvium	0.6%±0.7	21.4%±18.3	78.0%±18.4	Nitrification	28.0%±17.7	10.8%±11.0	**45.1%±22.2**	16.1%±10.0	Evaporative enrichment
ZM-18	5	Urban area	Conglomerate	0.9%±1.2	12.0%±10.4	87.1%±10.6	Denitrification	21.1%±13.8	9.0%±8.9	**36.2%±20.2**	**33.7%±13.1**	Evaporative enrichment/mixing
ZM-19	5	Urban area	Limestone	0.8%±1.0	18.1%±15.0	81.1%±15.1	Denitrification	26.9%±17.2	9.4%±9.8	**41.7%±21.1**	22.0%±11.4	Evaporative enrichment
ZM-21	5	Urban area	Alluvium	3.2%±3.6	8.1%±6.9	88.6%±8.8	Denitrification	**32.6%±19.3**	9.0%±9.0	**37.6%±20.6**	20.8%±11.4	Evaporative enrichment/mixing
ZM-22	5	Urban area	Alluvium	1.2%±1.7	8.4%±7.3	90.4%±7.7	Denitrification	33.9%±19.9	11.8%±11.8	**43.9%±22.9**	10.4%±7.2	Evaporative enrichment
ZM-23	5	Urban area	Alluvium	1.1%±1.6	8.8%±7.5	90.1%±7.9	Denitrification	**38.6%±20.7**	10.7%±10.7	**39.0%±22.0**	11.7%±8.1	Evaporative enrichment/mixing

Appendix 2

A2. Hydrogeological characteristics

A.2.1 Principal-Lagunera Region

The Principal-Lagunera Region aquifer is included within an intermontane valley whose geological structure is mainly associated with folded sedimentary rocks (limestone, dolomite, gypsum, clayey sand, and conglomerate), eventually affected by intrusive igneous rocks (granite and volcanic deposits) (**Fig. A2.1**).
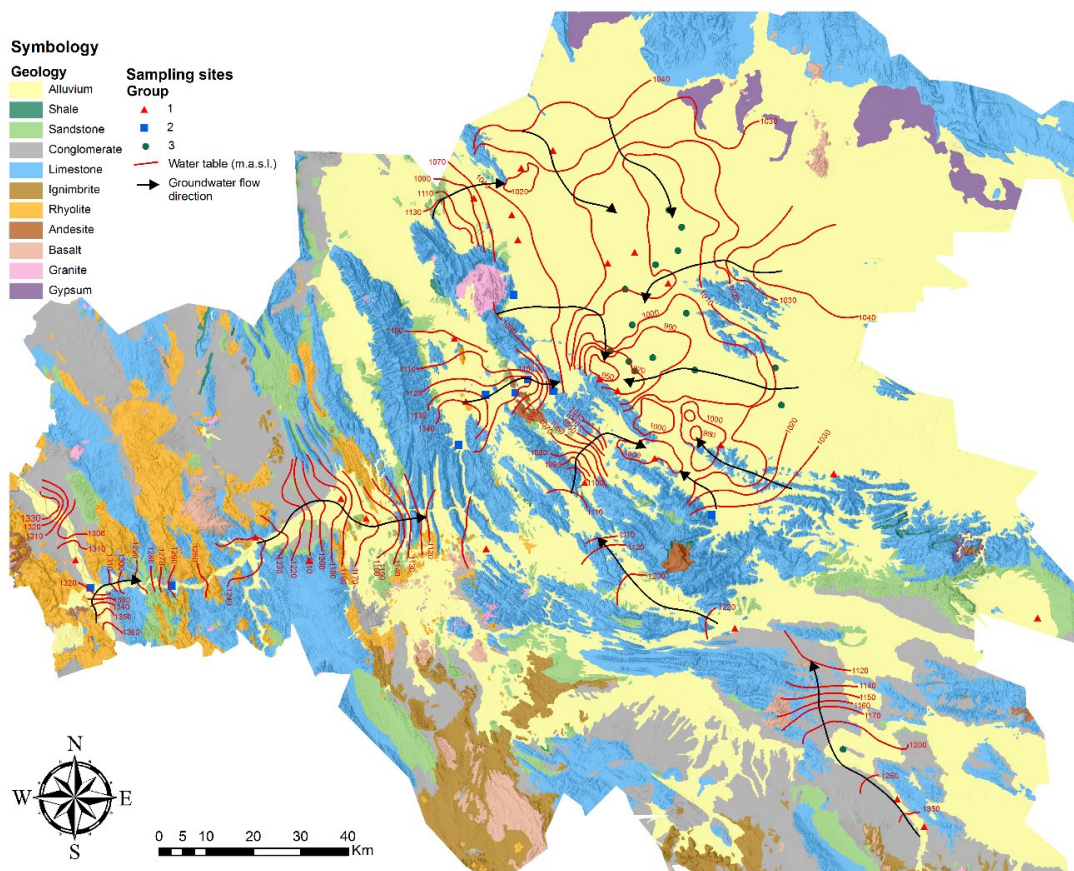
Fig. A2.1. Map showing the surface geology of the Comarca Lagunera Region, the groundwater table of 2017, and groundwater flow direction, including the location of the sampling sites in the CLR.

The geological succession in the Principal-Lagunera Region aquifer comprises (1) the Jurassic formation "Minas Viejas" which is composed of gypsum, lutites, and limestones; (2) the Cretaceous formations, "Aurora" formed by limestones and dolomites, "Indura" composed of lutites, limonites and limestones, and "Caracol" with lutites, clays, and sands; (3) the Tertiary formations, "Ahuichila" constituted of sandstones, limestones and conglomerates and "Santa Ines" which is also formed of limestones and conglomerates with a matrix of impermeable clay; finally (4) the Quaternary alluvium integrated by alluviums and terraces filling the stream channels and crowning older igneous rocks (This formation is considered the important aquifer).

The recent groundwater flow circulation has been modified from its natural condition (from the mountains near Torreón to the discharge areas in the Mayrán Lakes) by the increasing over-extraction from the around 3600 groundwater wells causing an inversion in the groundwater flow direction from the northeastern area in Los Remedios mountain range to the southwestern region where are situated the agricultural lands (CONAGUA, 2015a). The potentiometric surface in the area is around 100 m deep in the center of the depression and around 15 m deep in the areas near the mountains.

A2.2 Villa Juárez

The general geology of the Villa Juárez aquifer is represented by sedimentary and igneous extrusive and intrusive rocks whose stratigraphic record comprises from Triassic-Jurassic to Recent. According to the geological information, the aquifer is constituted, in its upper portion, by alluvial, fluvial, and forest foot sediments, due to the weathering of rocks that work as a free aquifer. Below this formation, it is found a fractured medium with karsticity ("Cuesta del Cura" and "Aurora" formations), followed by limestones from the "Cupido" and "Zuloaga" formations.

In this aquifer, there are 55 groundwater wells mainly used by agricultural activities. The groundwater flow direction is in the Nazas river's direction, with a typical depth oscillating between 5 and 10 m from the surface.

A2.3 Oriente-Aguanaval

The Oriente Aguanaval aquifer is made up of alluvial material and of sedimentary rocks, among which limestones and conglomerates stand out, which constitute 20% of the area each, whose rocks are of permeable to highly permeable characteristics. There are outcrops of extrusive igneous rocks in the center and south of the aquifer, such as basalt and acid tuff (CONAGUA, 2015b). The aquifer recharge is mainly derived from precipitation carried out on the mountains, plateaus, and hills, which infiltrates through the fractures in the volcanic rocks.

In this area, there are 310 groundwater wells whose exploitation generates an average depth to the water table is 55.3 m, and the groundwater flow follows the shape of the Aguanaval river in a direction from southeast to northwest leading to the Matamoros community.

A2.4 Nazas

The geological succession in Nazas aquifer comprises (1) the Jurassic formations "La Casita," "La Gloria" and "Zuloaga" composed of gypsum, sandstones, and limestones; (2) the Cretaceous formations, "Cuchillo" and "Aurora" formed by limestones and dolomites, and "Indura" composed of lutites, limonites, and limestones; (3) the Tertiary formations, "Ahuichila" constituted of sandstones, limestones and conglomerates and "Santa Ines" which is also formed of limestones and conglomerates with a matrix of impermeable clay; finally (4) the Quaternary alluvium integrated wich is made up clastic-granular materials of gravel, sand, and clay, and is considered the most permeable area from the region.

The Nazas aquifer is a shallow free-type aquifer with a typical depth oscillating between 15 and 24 m from surface and 211 groundwater wells. The groundwater flow direction is according to the direction of the Nazas river (CONAGUA, 2015c).

Table A2.1. Physical, chemical, and isotopic parameter of sampling points in the study area

			m.a.s.l.	m	m.a.s.l.			°C	mV		mg/L	µS-cm
Group	x	y	Elevation	Depth to the water table	Groundwater table	Surface geology	ID	T	ORP	pH	DO	CE
1	663053.7	2850240.6	1110	90.4	1019.6	Alluvium	B03	26.3	252.5	6.8	3.4	2400
1	670154.9	2843682.9	1112	88.2	1023.8	Alluvium	B04	25.5	448.6	7.1	2.3	1876
1	669462.7	2868023	1099	108.12	990.88	Alluvium	B06	28.9	230.7	7.9	7.3	1609
1	657401.5	2847978	1116	94.48	1021.52	Alluvium	B08	25.6	276.5	7.1	4.5	1966
1	681266.2	2809561.6	1132	139.81	991.97	Limestone	B10	29.8	232.7	7.1	4.6	1514
1	667308	2806715.7	1144	149.38	994.75	Limestone	B12	26.7	179.7	7.2	3.6	1309
1	624942.8	2832066.1	1261	158.64	1102.36	Limestone	B14	20.7	227.3	7.6	7.0	1560
1	627349.4	2818729.6	1184	44.70	1139.30	Rhyolite	B17	26.0	241.6	7.3	3.6	1533
1	633450.7	2816582.9	1211	90.5	1120.5	Alluvium	B18	25.2	306.1	7.2	2.9	1770
1	626835.5	2794726.5	1266	151.0	1115.0	Alluvium	B21	24.3	324.7	6.8	2.0	1732
1	631674.6	2787628.6	1269	159.9	1108.6	Alluvium	B22	24.1	375.5	7.1	5.4	1052
1	606242.4	2794013.6	1211	39.3	1171.7	Rhyolite	B24	26.1	331.0	7.0	1.8	1486
1	600929	2798224.5	1234	40.9	1193.1	Alluvium	B25	26.4	316.3	7.0	3.6	2564
1	637060.4	2858133.5	1123	66.9	1056.1	Alluvium	T01	28.4	208.0	7.6	6.6	1457
1	638354.5	2852894.5	1127	80.1	1046.9	Alluvium	T02	28.3	288.0	7.1	4.8	1815
1	639074.9	2868019.7	1109	78.2	1030.8	Alluvium	T03	29.3	264.4	7.0	3.8	3470
1	629097.9	2861690	1156	48.7	1107.3	Alluvium	T04	26.5	285.9	7.7	6.5	1217
1	645786.4	2871782.1	1099	61.8	1037.2	Alluvium	T05	26.7	190.3	7.4	6.2	4704
1	705231.6	2803470.4	1100	67.7	1032.3	Limestone	T10	28.9	206.7	7.7	5.7	1696
1	748372.2	2773018.4	1416	134.8	1281.2	Alluvium	T11	24.7	116.4	7.5	2.6	5957
1	652489.8	2801619.4	1189	64.9	1109.9	Alluvium	T12	26.2	114.7	7.6	4.5	966
1	684308.1	2770854.7	1397	58.4	1338.6	Alluvium	T13	22.4	228.7	7.6	3.7	1021
1	718676.2	2734749.8	1491	75.6	1415.4	Alluvium	T15	23.3	205.0	7.5	5.8	3298

1	724348.6	2728927.7	1516	68.3	1447.5	Alluvium	T16	34.4	192.5	7.2	4.4	2027
1	594232.5	2785154	1645	72.5	1210.7	Limestone	T17	22.9	275.5	7.3	5.0	1541
1	582864.9	2790137.1	1254	14.0	1239.8	Limestone	T18	23.3	241.3	7.5	5.9	904
1	544751.9	2785205.2	1328	12.6	1315.1	Alluvium	T21	23.6	170.1	7.5	6.4	1126
1	655672.5	2823530.9	1142	192.7	949.0	Limestone	T24	23.7	265.3	7.7	5.9	1352
1	659493.7	2821061.9	1125	154.5	970.5	Limestone	T25	26.1	192.0	7.5	3.7	1423
2	637444.7	2841247.8	1170	104.44	1065.56	Limestone	B07	33.6	227.4	6.99	1.85	730
2	679352.1	2794785.8	1207	174.86	1032.28	Limestone	B11	27.2	233.9	7.1	5.43	724
2	640465.8	2823393.1	1146	26.73	1119.27	Alluvium	B13	24.4	226	7.11	1.01	793
2	631527.7	2820117.6	1157	24.26	1133.19	Alluvium	B15	25.3	247.2	7.39	2.37	710
2	625801.8	2809543.3	1192	37.13	1155.20	Alluvium	B16	30	228.6	7.18	1.88	759
2	637822.9	2820584.1	1141	13.2	1127.8	Andesite	B19	25.8	305.3	7.25	3.57	852
2	645814.2	2820930.3	1140	39.8	1100.2	Limestone	B20	23.1	293.3	7.02	2.14	1019
2	565112.8	2779790.7	1280	22.9	1257.1	Alluvium	T19	22.7	274	7.15	3.28	532
2	547865.3	2779365.3	1323	3.2	1319.8	Alluvium	T20	24.3	264.2	7.27	1.78	677
3	672223.1	2850587.8	1109	116.0	993.0	Alluvium	B01	27.7	317.7	6	5.42	556
3	667498.3	2847612.7	1115	101.4	1013.6	Alluvium	B02	30.7	279	7.32	1.29	373
3	670332.1	2859127.9	1104	95.4	1008.6	Alluvium	B05	29.3	213.3	8.11	3.92	766
3	661020	2842405.5	1114	102.93	1011.07	Alluvium	B09	33.4	249.9	7.94	3.67	468.4
3	661810.6	2827148.8	1120	159.6	960.4	Alluvium	B27	26.6	298.2	7.64	5.33	463.7
3	666866.7	2827986.5	1119	134.9	984.1	Alluvium	B28	27.8	282.4	7.65	2.37	441.2
3	673005.5	2855534.3	1106	115.9	990.1	Alluvium	B29	29	283.8	8.01	1.47	814
3	673973.7	2837383.6	1108	120.2	987.8	Alluvium	B30	32.9	491.5	8.24	2.18	543
3	675800.5	2825362.4	1115	122.4	992.6	Alluvium	T07	32.4	211.9	8.56	1.69	332.1
3	692837.6	2825828.4	1132	120.3	1011.7	Alluvium	T08	29.8	205	8.15	4.06	565
3	694125	2817928	1107	96.0	1011.0	Alluvium	T09	28.3	144.6	7.97	2.02	1029
3	707169.8	2745200.2	1458	67.4	1390.6	Conglomerate	T14	26.2	206.1	8.64	6.69	677
3	662514.4	2834896.7	1120	110.4	1009.6	Alluvium	T22	33.1	272.1	8.2	6.8	824
3	657906.8	2829379.1	1116	152.6	963.4	Alluvium	T23	26.6	262.2	7.82	6.73	571

3	663063.2	2825148.4	1116	155.6	960.4	Alluvium	T26	29.3	196.8	7.93	4.6	531

Table A2.1. Physical, chemical, and isotopic parameter of sampling points in the study area (continued)

		mg/L	mg/L	mg/L	mg/L	mg/L	mg/L	mg/L	mg/L	mg/L	mg/L	µg/L	µg/L	µg/L				
Group	ID	Ca	Mg	Na	K	HCO_3	F	Cl	NO_3	SO_4	SDT	Br	I	Si	$\delta^{18}O_{H2O}$	δ^2H_{H2O}	$\delta^{15}N_{NO3}$	$\delta^{18}O_{NO3}$
1	B03	386.0	31.2	129.0	4.3	214.7	0.3	158.0	45.0	745.0	1744.6	2430	48.3	31100	-8.02	-61.34	13.95	9.64
1	B04	304.0	17.8	135.0	4.5	281.0	0.1	56.2	5.3	748.0	1580.1	858	22.1	28300	-7.80	-59.90	14.43	2.79
1	B06	117.0	3.9	215.0	3.1	118.3	0.6	42.9	6.8	325.0	857.7	857	196.0	25100	-8.17	-60.73	13.83	7.64
1	B08	233.0	20.7	142.0	3.9	202.5	0.2	130.0	39.9	485.0	1280.3	1920	24.8	23100	-7.73	-59.66	13.34	8.28
1	B10	191.0	41.6	55.5	4.5	194.0	1.6	21.5	2.3	493.0	1021.3	289	23.7	16300	-8.08	-62.34	12.84	7.01
1	B12	101.0	32.8	133.0	6.6	162.3	1.0	92.1	7.2	308.0	858.5	620	42.9	14500	-8.56	-65.74	16.85	9.24
1	B14	87.6	11.5	259.0	6.1	114.7	2.5	65.6	74.8	379.0	1020.2	1380	221.0	19400	-8.97	-64.22	20.52	12.39
1	B17	174.0	47.2	111.0	5.7	305.0	0.3	24.0	11.1	437.0	1135.7	411	95.4	20300	-8.01	-59.54	9.92	3.94
1	B18	179.0	62.5	137.0	6.0	357.5	0.2	46.7	8.3	274.0	1088.7	1110	49.5	17600	-7.42	-57.32	11.76	1.20
1	B21	253.0	29.2	120.0	7.1	218.4	0.3	51.0	34.1	360.0	1092.6	1280	20.6	19500	-8.06	-60.86	13.12	10.27
1	B22	86.1	17.2	119.0	9.1	242.8	0.9	51.4	18.7	227.0	798.5	854	77.4	26300	-9.07	-66.47	10.39	6.59
1	B24	148.0	24.9	171.0	3.7	377.0	0.6	48.7	12.3	401.0	1210.9	701	48.8	23700	-7.02	-54.84	12.54	8.24
1	B25	276.0	73.9	231.0	6.9	247.7	0.8	142.0	33.8	961.0	1994.2	2100	78.9	21200	-8.24	-62.26	9.22	7.81
1	T01	114.0	25.2	176.0	6.3	168.4	0.3	10.3	1.6	590.0	1108.1	143	144.0	16100	-8.92	-62.76	10.97	5.73
1	T02	307.0	46.2	59.9	6.3	160.6	2.1	44.9	19.6	734.0	1400.3	642	36.0	19700	-8.78	-62.82	10.14	7.26
1	T03	488.0	99.5	218.0	9.0	164.7	0.9	129.0	11.8	1710.0	2848.0	1310	170.0	17200	-7.86	-57.19	10.28	6.36
1	T04	133.0	29.3	106.0	4.2	179.3	0.5	48.2	14.7	374.0	904.7	727	105.0	15400	-7.18	-52.89	10.50	5.64
1	T05	526.0	41.7	691.0	6.0	139.1	0.6	88.2	1.6	2630.0	4148.3	882	1210.0	24100	-7.90	-57.90	39.67	12.04
1	T10	129.0	43.0	163.0	6.6	237.9	1.3	142.0	2.9	435.0	1176.8	662	63.9	16100	-8.19	-64.35	11.88	5.00
1	T11	591.0	43.7	969.0	5.6	113.5	0.2	180.0	109.0	2850.0	4874.4	1790	42.8	12500	-7.51	-58.51	10.84	10.56
1	T12	73.0	23.0	115.0	6.6	246.9	1.9	30.5	4.3	240.0	756.3	500	60.7	15100	-9.18	-68.41	10.49	3.49
1	T13	95.7	21.7	107.0	15.1	250.1	0.4	36.1	16.4	241.0	807.8	670	201.0	24300	-12.51	-86.72	25.13	14.89
1	T15	178.0	42.3	519.0	14.2	394.1	4.5	91.2	9.9	1490.0	2777.5	1650	1010.0	34300	-7.01	-56.61	11.63	3.76

1	T16	152.0	23.3	201.0	13.9	322.1	2.3	80.5	16.0	462.0	1293.0	1310	107.0	20000	-7.70	-61.40	14.78	8.34
1	T17	152.0	66.2	128.0	10.9	348.9	1.8	34.9	10.0	497.0	1274.9	379	35.5	25200	-6.85	-52.42	13.20	2.74
1	T18	103.0	17.3	94.1	5.2	398.9	1.5	19.6	2.9	145.0	813.7	253	22.1	26200	-6.87	-53.88	9.23	-0.93
1	T21	109.0	12.4	146.0	5.6	402.6	2.3	31.4	14.2	183.0	939.2	334	111.0	32700	-6.84	-53.29	13.63	1.24
1	T24	143.0	38.9	120.0	6.5	148.8	0.8	68.3	24.1	376.0	945.1	687	36.5	18700	-8.22	-61.58	12.14	5.40
1	T25	143.0	34.3	128.0	5.1	191.5	0.7	67.0	26.3	372.0	983.6	788	36.5	15700	-8.14	-62.05	11.27	6.88
2	B07	81.1	24	22	2.54	245	0.86	7.66	6.75	57.7	459.2	90	20.1	11700	-9.89	-67.45	8.86	8.82
2	B11	71.6	25	45.9	3.64	243	0.62	23.4	5.67	114	544.3	232	23.4	11700	-9.97	-71.54	9.74	4.66
2	B13	103	20	50.6	4.67	312	0.34	14.1	3.21	145	672.4	205	38.1	18800	-7.09	-54.94	15.34	10.25
2	B15	84.2	26	35	3.87	218	0.37	14.7	2.86	144	549.4	248	22.4	19800	-8.44	-63.15	11.68	7.15
2	B16	82	25	30.6	3.91	266	0.47	11.9	6.9	119	556.5	205	14.1	10900	-9.36	-66.49	8.94	4.41
2	B19	109	22	43.8	4.6	314	0.26	19.6	6.37	178	715.3	221	12.8	18300	-6.89	-54.13	10.13	2.16
2	B20	101	33	101	4.84	394	0.25	19.6	6.35	178	859.4	229	9.8	20900	-6.31	-50.82	9.59	-0.02
2	T19	62.8	4.9	50.1	3.91	329	1.04	5.46	0.15	32	505.9	88	20.8	16100	-6.92	-52.68		
2	T20	59.6	9.2	90.1	5.1	349	1.08	6.46	0.14	36.2	577.9	128	41.2	21100	-8.11	-59.32		
3	B01	49.4	1.6	67.2	1.47	166	0.62	8.48	2.42	105	423.1	176	29.6	20500	-8.05	-60.61	18.39	10.09
3	B02	21.8	0.3	52.9	1.04	134	0.6	4.2	0.97	49.6	284.9	79	16.5	19300	-7.90	-59.83		
3	B05	37.7	1	115	1.3	134	0.64	11.2	0.97	106	430.5	285	88.2	22500	-7.64	-58.36		
3	B09	15.4	0.3	75.3	1.81	162	3.09	12.6	0.54	41.6	332.4	61	37.2	19500	-8.21	-62.91		
3	B27	50.7	5.3	38.3	3.34	156	0.43	14.4	2.41	73	360.9	130	12.3	16900	-8.07	-61.20	10.21	-0.21
3	B28	42.1	1.6	35.1	2.51	143	0.31	13.9	1.77	67.1	322.8	138	10.2	15700	-7.70	-59.76	12.39	0.57
3	B29	43.1	1.3	120	1.4	120	0.62	29.6	2.15	230	570	556	95.8	22300	-7.96	-60.68	24.82	12.06
3	B30	28.3	0.4	70.7	1.21	105	0.69	12.6	0.32	125	363.3	158	34.9	19200	-7.65	-58.86		
3	T07	10.1	0.1	55.7	0.85	136	0.74	3.51	0.05	32.1	257.5	50	13.5	18500	-7.50	-58.00		
3	T08	26.7	0.7	87.7	1.27	137	2.46	5.93	0.01	123	406.3	71	180	21900	-9.40	-69.03		
3	T09	41.4	6.9	164	3.34	172	1.82	11.9	0.01	342	769.1	165	275	26000	-8.67	-66.52		
3	T14	3.76	0.7	151	2.17	288	1.43	17.4	0.4	75.2	554.7	328	65.5	14700	-8.34	-65.82		
3	T22	31.4	2	118	3.21	155	0.86	42.7	2.58	64.9	439.1	316	43.6	18500	-8.08	-61.60	12.43	0.09
3	T23	54.8	6.7	51.2	3.31	160	0.41	41.2	2.59	70.8	406.7	176	26.3	15900	-7.88	-59.88	10.23	1.16

3	T26	43.6	2.9	56.9	3.03	221	0.5	13	0.7	97	454.6	91	37	16200	-7.97	-61.24

Table A2.2. Proportional contributions of the different pollution sources result of MixSIAR model

Units			AD		SON		NO3-F		NH4-F		Manure		Sewage		Main N source
ID	$\delta^{15}N_{NO3}$	$\delta^{18}O_{NO3}$	Mean	SD	Mean	SD	Mean	SD	Mean	SD	Mean	SD	Mean	SD	
B03	13.95	9.64	1.7%	1.4%	2.6%	2.7%	2.0%	2.0%	2.1%	2.2%	**45.8%**	**2.1%**	45.8%	2.1%	Manure/sewage
B04	14.43	2.79	0.9%	1.1%	2.3%	3.8%	1.3%	1.9%	1.9%	3.1%	**93.5%**	**5.7%**	0.0%	0.0%	Manure
B06	13.83	7.64	1.6%	2.0%	3.0%	4.6%	2.3%	3.2%	2.4%	3.8%	**90.8%**	**7.5%**	0.0%	0.0%	Manure
B08	13.34	8.28	1.8%	2.2%	3.1%	4.8%	2.5%	3.7%	2.5%	4.0%	0.0%	0.0%	**90.1%**	**8.1%**	Sewage
B10	12.84	7.01	1.5%	1.9%	3.1%	4.9%	2.2%	3.1%	2.5%	4.2%	0.0%	0.0%	**90.6%**	**7.9%**	Sewage
B12	16.85	9.24	1.8%	2.2%	2.3%	3.3%	2.1%	3.1%	1.8%	2.7%	0.0%	0.0%	**92.0%**	**6.2%**	Sewage
B14	20.52	12.39	2.4%	3.1%	1.7%	2.2%	1.9%	2.8%	1.4%	1.9%	**92.6%**	**5.5%**	0.0%	0.0%	Manure
B17	9.92	3.94	1.2%	1.4%	3.8%	6.8%	1.8%	2.4%	2.9%	5.2%	**72.2%**	**7.5%**	18.5%	1.1%	Manure
B18	11.76	1.20	0.8%	1.0%	2.7%	4.8%	1.3%	1.7%	2.1%	3.8%	18.6%	1.3%	**74.5%**	**5.4%**	Sewage
B21	13.12	10.27	2.6%	3.1%	3.0%	4.3%	3.2%	4.6%	2.4%	3.6%	**88.8%**	**8.5%**	0.0%	0.0%	Manure
B22	10.39	6.59	1.6%	1.9%	3.9%	6.5%	2.4%	3.5%	3.3%	5.4%	0.0%	0.0%	**88.8%**	**9.9%**	Sewage
B24	12.54	8.24	1.9%	2.3%	3.3%	5.0%	2.7%	3.8%	2.6%	4.0%	0.0%	0.0%	**89.6%**	**8.5%**	Sewage
B25	9.22	7.81	2.0%	2.3%	4.6%	7.3%	3.1%	4.4%	3.7%	6.1%	**86.7%**	**11.5%**	0.0%	0.0%	Manure
T01	10.97	5.73	0.6%	0.6%	2.2%	2.5%	0.9%	1.0%	1.8%	1.9%	**94.4%**	**3.3%**	0.0%	0.0%	Manure
T02	10.14	7.26	1.1%	1.7%	4.0%	6.7%	1.8%	3.2%	3.1%	5.5%	0.0%	0.0%	90.0%	10.1%	Sewage
T03	10.28	6.36	1.0%	1.5%	4.0%	6.7%	1.5%	2.6%	3.2%	5.6%	**90.4%**	**10.0%**	0.0%	0.0%	Manure
T04	10.50	5.64	0.8%	1.3%	3.7%	6.6%	1.4%	2.4%	2.8%	4.9%	0.0%	0.0%	**91.3%**	**9.3%**	Sewage
T05	39.67	12.04	0.4%	0.6%	0.7%	0.9%	0.4%	0.7%	0.6%	0.8%	**97.9%**	**1.6%**	0.0%	0.0%	Manure
T10	11.88	5.00	0.7%	1.1%	3.5%	5.9%	1.2%	2.0%	2.7%	4.6%	**91.8%**	**8.3%**	0.0%	0.0%	Manure
T11	10.84	10.56	1.8%	2.9%	3.1%	4.7%	2.4%	4.6%	2.7%	4.2%	**89.9%**	**9.4%**	0.0%	0.0%	Manure
T12	10.49	3.49	0.6%	0.9%	3.5%	6.3%	1.1%	1.7%	2.9%	5.0%	0.0%	0.0%	91.8%	8.7%	Sewage
T13	25.13	14.89	1.2%	2.2%	1.2%	1.6%	0.9%	1.6%	1.0%	1.4%	**95.7%**	**3.8%**	0.0%	0.0%	Manure
T15	11.63	3.76	0.6%	0.9%	3.2%	5.9%	1.0%	1.7%	2.6%	4.6%	**92.6%**	**8.2%**	0.0%	0.0%	Manure

|															
T16	14.78	8.34	1.0%	1.6%	2.6%	3.9%	1.4%	2.4%	2.2%	3.5%	0.0%	0.0%	92.8%	6.6%	Sewage
T17	13.20	2.74	0.6%	0.9%	2.9%	5.1%	0.9%	1.5%	2.2%	3.9%	**93.4%**	**7.0%**	0.0%	0.0%	Manure
T18	9.23	-0.93	0.4%	0.6%	2.3%	4.1%	0.7%	1.1%	1.8%	3.4%	**75.8%**	**4.6%**	19.0%	1.1%	Manure
T21	13.63	1.24	0.5%	0.7%	2.4%	4.1%	0.8%	1.2%	1.9%	3.4%	**75.5%**	**4.6%**	18.9%	1.2%	Manure
T24	12.14	5.40	0.8%	1.2%	3.4%	5.9%	1.3%	2.2%	2.7%	4.6%	0.0%	0.0%	**91.9%**	**8.3%**	Sewage
T25	11.27	6.88	1.0%	1.5%	3.7%	6.3%	1.5%	2.6%	3.0%	4.9%	0.0%	0.0%	**90.9%**	**9.3%**	Sewage
B07	8.86	8.82	1.7%	1.7%	9.1%	8.0%	3.0%	3.2%	7.1%	6.5%	**79.2%**	**9.7%**	0.0%	0.0%	Manure
B11	9.74	4.66	1.1%	1.3%	9.8%	11.8%	2.2%	2.7%	7.2%	9.0%	**79.7%**	**14.6%**	0.0%	0.0%	Manure
B13	15.34	10.25	1.9%	2.7%	4.6%	5.1%	2.8%	4.1%	3.7%	4.2%	**39.0%**	**8.1%**	39.0%	8.1%	Sewage/Manure
B15	11.68	7.15	1.4%	1.8%	7.3%	8.4%	2.8%	3.7%	6.0%	7.1%	**42.2%**	**6.2%**	42.2%	6.2%	Sewage/Manure
B16	8.94	4.41	1.1%	1.3%	10.8%	13.6%	2.2%	2.8%	8.0%	10.3%	**78.0%**	**16.2%**	0.0%	0.0%	Manure
B19	10.13	2.16	0.8%	1.0%	7.5%	9.9%	1.6%	2.1%	5.7%	7.9%	**84.4%**	**12.3%**	0.0%	0.0%	Manure
B20	9.59	-0.02	0.6%	0.8%	5.9%	7.9%	1.3%	1.6%	5.0%	7.2%	0.0%	0.0%	**87.1%**	**10.7%**	Sewage
T19															Manure
T20															Manure
B01	18.39	10.09	1.2%	1.4%	3.2%	3.2%	1.6%	1.9%	2.9%	2.9%	18.2%	1.0%	**72.9%**	**3.8%**	Sewage
B02															Manure
B05															Manure
B09															Manure
B27	10.21	-0.21	0.6%	0.8%	3.1%	5.2%	1.0%	1.4%	2.5%	4.2%	0.0%	0.0%	**92.8%**	**7.1%**	Sewage
B28	12.39	0.57	0.6%	0.8%	2.9%	4.7%	1.0%	1.4%	2.5%	4.0%	0.0%	0.0%	**93.1%**	**6.7%**	Sewage
B29	24.82	12.06	1.1%	1.9%	1.4%	1.7%	1.0%	1.6%	1.3%	1.7%	**95.1%**	**3.8%**	0.0%	0.0%	Manure
B30															Manure
T07															Sewage
T08															Manure
T09															Manure
T14															Manure
T22	12.43	0.09	0.6%	0.8%	2.6%	4.1%	1.0%	1.4%	2.4%	4.2%	0.0%	0.0%	**93.4%**	**6.2%**	Sewage

| T23 | 10.23 | 1.16 | 0.7% | 1.0% | 3.4% | 5.9% | 1.1% | 1.6% | 3.2% | 5.5% | 0.0% | 0.0% | **91.6%** | **8.6%** | Sewage |
| T26 | | | | | | | | | | | | | | | Sewage |

Appendix 3
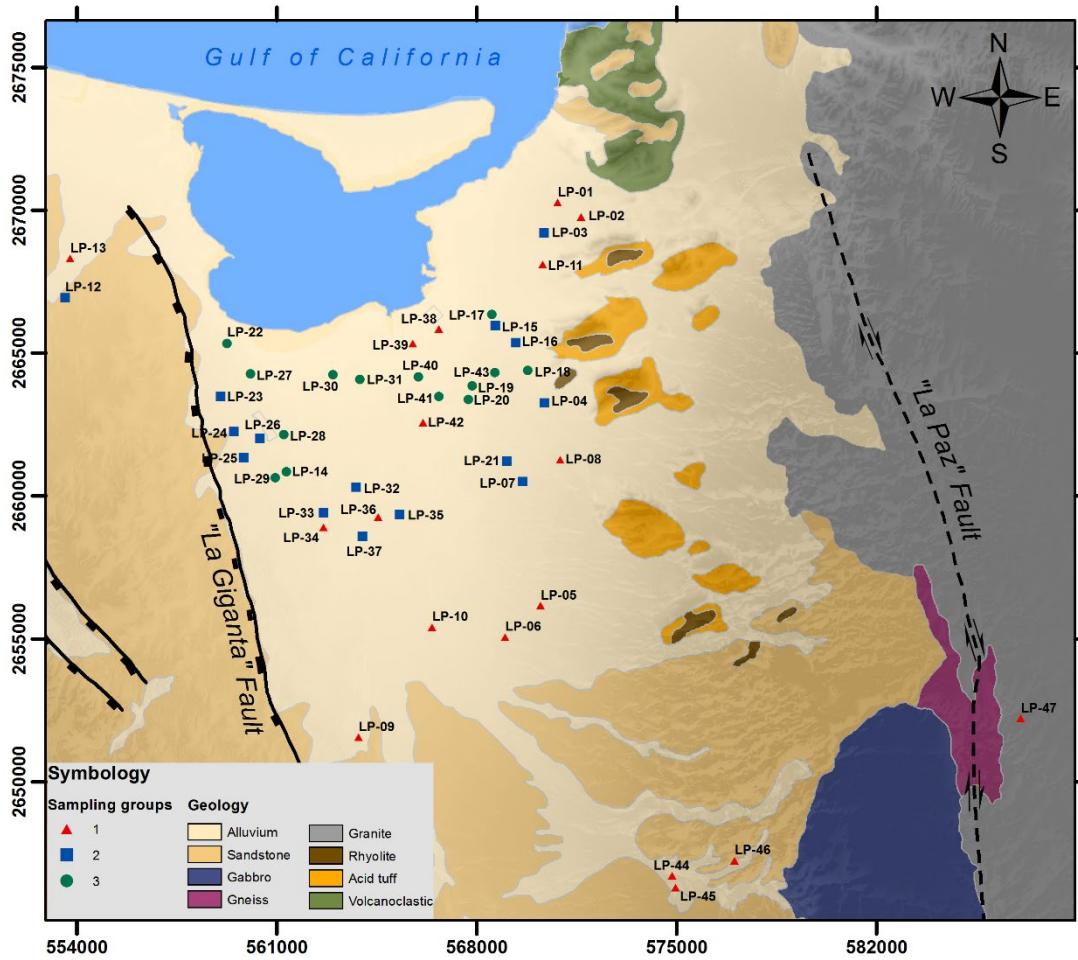
Figure A3.1. Geology of the La Paz aquifer in northeastern Mexico, including locations of the sampled sites.

Table A3.1. Physical, chemical, and isotopic parameter of sampling points in the study area

Units	UTM (m)	UTM (m)	m	°C		mg/L	µS-cm	mg/L	mg/L	mg/L	mg/L	mg/L	mg/L	mg/L
ID	x	y	Depth to the water table	T	pH	DO	EC	Ca	Mg	Na	K	HCO$_3$	Si	Cl
LP-01	570842	2670257	-	28.9	6.8	8.3	893	51.0	16.5	67.5	4.1	166.0	19.6	159.0
LP-02	571664	2669761	-	30.1	7.1	8.1	702	40.8	14.0	53.2	3.9	175.0	21.9	107.0
LP-03	570367	2669200	-	29.2	6.9	7.8	1537	103.0	33.7	99.9	5.5	185.0	21.9	385.0
LP-04	570374	2663253	76	31.5	7.2	8.6	1566	82.5	39.5	137.0	4.4	305.0	30.4	342.0
LP-05	570242	2656151	201	32.5	7.1	7.8	642	44.7	15.9	40.6	2.3	215.0	26.8	80.8
LP-06	569005	2655058	201	32.5	7.4	7.7	701	46.8	14.7	44.6	1.7	175.0	37.3	111.0
LP-07	569616	2660497	150	31.1	7.1	7.7	2109	155.0	60.3	80.9	4.9	190.0	30.7	521.0
LP-08	570927	2661256	57	29.9	7.8	8.2	1142	52.3	23.0	96.9	3.7	210.0	27.8	206.0
LP-09	563872	2651544	201	30.5	7.4	6.7	865	52.7	20.0	81.7	2.7	280.0	27.4	118.0
LP-10	566450	2655401	156	33.0	7.7	7.3	561	34.0	11.4	67.1	3.8	254.0	28.7	69.4
LP-11	570323	2668091	80	25.0	7.4	7.9	998	41.1	17.0	105.0	4.0	232.0	27.5	168.0
LP-12	553602	2666923	80	25.0	7.4	6.1	1150	38.7	10.5	223.0	5.6	325.0	42.0	284.0
LP-13	553777	2668299	60	31.8	7.6	7.1	1155	43.6	10.1	141.0	5.5	250.0	39.0	188.0
LP-14	561136	2660711	60	29.6	7.1	5.6	3480	263.0	90.7	228.0	4.9	370.0	39.0	936.0
LP-15	568653	2665957	200	30.6	7.2	6.6	2868	134.0	50.7	327.0	8.3	402.0	36.2	700.0
LP-16	569371	2665353	30	29.9	7.3	7.9	2552	104.0	40.8	299.0	7.8	395.0	35.7	567.0
LP-17	568535	2666344	50	29.5	7.1	6.8	3320	182.0	63.7	658.0	9.8	540.0	38.4	833.0
LP-18	569801	2664378	64	31.0	7.0	6.3	5100	335.0	186.0	391.0	9.1	578.0	37.9	1400.0
LP-19	567844	2663845	64	29.6	6.9	6.4	5570	500.0	162.0	354.0	10.2	372.0	43.5	1690.0
LP-20	567715	2663365	60	29.3	7.1	7.2	3840	347.0	120.0	233.0	7.7	432.0	42.4	1120.0
LP-21	569066	2661212	130	33.4	7.1	7.8	2124	199.0	68.5	117.0	5.6	406.0	33.8	550.0
LP-22	559262	2665334	15	30.7	7.0	7.5	7520	356.0	131.0	1080.0	10.2	498.0	45.0	2260.0

LP-23	559035	2663477	-	30.0	7.3	8.3	2603	205.0	60.8	343.0	6.0	512.0	43.9	744.0
LP-24	559501	2662250	35	31.0	7.5	4.5	1295	66.3	18.4	187.0	2.6	426.0	43.2	264.0
LP-25	559854	2661330	38	32.7	7.4	7.7	1292	81.6	23.5	144.0	4.5	406.0	33.5	266.0
LP-26	560420	2662001	-	29.1	7.2	8.1	3080	164.0	61.1	395.0	3.9	724.0	42.9	728.0
LP-27	560089	2664261	69	28.2	7.2	4.8	2944	147.0	56.8	443.0	3.2	442.0	51.1	590.0
LP-28	561256	2662144	15	29.0	7.0	8.6	6880	421.0	186.0	763.0	8.9	634.0	47.9	2030.0
LP-29	561142	2660711	20	29.7	7.1	5.6	3460	261.0	110.0	283.0	5.9	476.0	44.9	934.0
LP-30	562975	2664232	22	27.9	6.77	3.85	5160	422	157	395	7.03	568	42.8	1590
LP-31	563921	2664065	30	27.1	7.06	5.18	4770	189	110	693	3.49	1290	43.5	1140
LP-32	563778	2660294	70	29	7.2	5.75	2589	237	55.9	134	3.59	325	33.2	731
LP-33	562650	2659405	70	29.3	7.4	8.69	1777	131	38.7	122	3.13	340	32.6	398
LP-34	562646	2658893	75	29.7	7.59	8.35	1023	64.1	21.1	80.1	2.58	250	26.4	183
LP-35	565310	2659338	70	31.3	7.17	6.09	2751	255	74.5	102	2.97	276	29.3	793
LP-36	564566	2659248	35	31	7.44	7.08	1207	91.1	23.2	70.6	2.64	236	28	245
LP-37	564005	2658582	60	29.4	7.27	5.92	1658	106	26.7	138	3.16	260	31.5	380
LP-38	566692	2665834	24	29.5	7.78	7.31	799	44.5	20.7	59.8	2.05	186	36.2	164
LP-39	565779	2665324	-	29.9	7.64	7.02	683	33.3	15.2	58.4	2.25	218	35.9	95.6
LP-40	565970	2664157	28	28.7	7.18	7.05	8920	658	344	583	14	984	36.2	2960
LP-41	566687	2663468	5	29.4	7.03	5.72	6000	342	159	562	7.75	656	39.7	1840
LP-42	566128	2662563	50	30.2	7.42	7.26	1182	79.3	39.7	59.2	3.54	206	38.8	289
LP-43	568638	2664303	60	30.3	7.31	7.35	4250	311	105	325	9.55	528	37.5	1140
LP-44	574854	2646697	80	30.2	7.23	7.14	630	33.5	15.6	50.1	1.54	198	25.8	89.7
LP-45	574967	2646285	50	28.5	7.18	7.84	610	39.1	21.6	36.7	2.1	275	20.9	61.9
LP-46	577039	2647235	21	28.1	7.13	6.31	924	49.1	27.6	80.9	2.32	398	26.7	107
LP-47	587059	2652205	-	27.4	8.27	14.7	479	27.8	9.31	39.3	4.14	182	21.1	54.5

Table A2.1. Physical, chemical and isotopic parameter of sampling points in the study area (continued)

Units	mg/L	mg/L	mg/L	mg/L	ug/L	‰ VSMOW	‰ VSMOW	‰ Air	‰ VSMOW	‰ VSMOW	‰ VCDT
ID	NO$_3$ as N	SO$_4$	SDT	Br	As	δ^{18}O$_{H2O}$	δ^{2}H$_{H2O}$	δ^{15}N$_{NO3}$	δ^{18}O$_{NO3}$	δ^{18}O$_{SO4}$	δ^{34}S$_{SO4}$
LP-01	10.1	37.1	530.9	0.38	4.05	-10.99	-81.56	11.15	-1.07	4.50	14.81
LP-02	8.8	27.9	452.5	0.17	4.59	-11.15	-81.08	9.89	-1.04	5.41	13.64
LP-03	4.8	34.3	873.1	1.09	4.27	-11.04	-82.07	9.87	-1.26	6.46	18.07
LP-04	3.7	43.9	988.5	1.01	12.80	-9.38	-69.79	7.76	-0.73	3.60	14.04
LP-05	2.9	14.4	443.5	0.25	3.26	-10.74	-73.56	7.90	0.09	5.83	9.56
LP-06	3.0	10.8	444.9	0.37	3.76	-9.98	-68.05	6.62	-0.51	6.28	15.36
LP-07	6.9	77.1	1126.9	1.33	440.00	-10.07	-68.98	7.05	-1.20	4.26	17.56
LP-08	3.6	32.7	656.1	0.60	10.20	-10.49	-73.17	7.12	-0.94	3.90	7.49
LP-09	1.4	47.5	631.4	0.33	4.55	-9.01	-61.42	7.23	-0.50	6.79	1.50
LP-10	1.5	9.8	479.6	0.17	5.31	-9.49	-62.96	6.90	0.37	6.85	9.80
LP-11	8.9	36.8	640.3	0.43	10.00	-11.61	-81.11	9.94	-0.89	8.76	15.84
LP-12	5.5	75.1	1009.4	0.84	43.10	-7.72	-52.11	6.82	1.27	5.11	19.34
LP-13	5.0	53.5	735.7	0.53	33.80	-8.16	-54.97	8.26	0.63	12.49	19.01
LP-14	9.6	136.0	2077.2	3.57	13.50	-8.39	-57.91	8.73	-0.06	3.85	12.36
LP-15	11.8	166.0	1836.0	1.91	15.20	-9.67	-69.03	11.75	-0.57	3.60	15.94
LP-16	10.4	169.0	1628.7	1.86	19.70	-8.63	-63.97	11.21	-0.04	8.77	16.94
LP-17	12.9	180.0	2517.8	1.96	10.90	-9.60	-72.03	12.08	-0.33	5.60	16.05
LP-18	27.8	195.0	3159.8	3.39	12.20	-8.18	-62.61	13.39	2.42	3.69	16.67
LP-19	6.1	290.0	3427.8	5.01	8.09	-8.79	-67.07	9.89	-0.88	3.62	14.84
LP-20	4.0	148.0	2454.2	2.94	6.18	-9.11	-67.01	8.48	-1.34	3.90	15.35
LP-21	6.4	107.0	1493.3	1.40	6.05	-9.31	-67.68	7.54	-0.71	4.14	17.28
LP-22	12.4	490.0	4882.6	6.78	26.30	-7.20	-53.81	12.14	0.17	4.97	14.74
LP-23	4.8	152.0	2071.5	1.91	21.80	-7.41	-53.50	9.27	0.75	4.07	15.78
LP-24	3.9	42.3	1053.7	0.86	20.40	-8.03	-55.58	9.10	1.75	5.75	12.48

LP-25	2.1	37.9	999.0	0.84	12.10	-7.07	-57.75	7.66	-0.80	6.71	9.21
LP-26	11.2	160.0	2290.1	2.27	19.10	-8.15	-53.72	23.89	8.62	6.10	14.26
LP-27	45.8	316.0	2094.9	< 1	16.80	-9.49	-62.62	13.33	2.47	4.60	13.84
LP-28	17.0	441.0	4548.8	6.46	21.50	-9.08	-58.71	13.21	2.15	4.62	11.96
LP-29	9.4	137.0	2261.2	2.04	13.70	-9.25	-58.68	9.17	0.06	9.81	12.15
LP-30	9.91	143	3334.7	3.96	9.79	-8.84	-62.36	13.93	0.00	4.99	13.71
LP-31	48.8	228	3745.8	2.32	23.70	-8.48	-64.38	14.66	0.56	3.90	14.64
LP-32	10.6	50.3	1580.6	2.96	6.68	-8.51	-63.12	9.26	1.48	5.78	9.46
LP-33	6.3	69.4	1141.1	1.24	8.31	-8.63	-61.70	13.08	2.86	5.16	9.21
LP-34	1.99	42.6	671.9	0.50	6.11	-8.29	-61.20	11.69	2.11	8.09	4.23
LP-35	8.15	64.3	1605.2	2.56	5.14	-8.98	-66.51	8.15	1.27	6.24	16.03
LP-36	3.15	29.1	728.8	0.61	3.21	-8.60	-63.39	8.66	-0.28	15.77	7.26
LP-37	2.4	65.9	1013.7	1.13	6.27	-8.55	-63.11	8.20	-1.17	7.76	7.91
LP-38	1.52	11.5	526.3	0.46	5.84	-9.56	-68.03	6.71	-0.57	2.19	11.49
LP-39	1.78	14	474.4	0.30	6.01	-8.27	-65.90	6.13	-2.19	4.78	16.85
LP-40	5.63	243	5827.8	7.16	12.00	-8.11	-65.90	10.56	1.68	2.65	16.52
LP-41	0.15	176	3782.6	5.18	8.10	-8.35	-64.60	-	-	4.46	15.59
LP-42	2.86	19.6	738.0	0.90	5.00	-9.25	-68.29	7.16	-0.57	5.41	16.57
LP-43	8.77	292	2756.8	2.93	7.07	-8.98	-66.66	11.69	0.92	4.16	14.85
LP-44	8.07	14.5	436.8	0.33	4.14	-9.42	-65.59	9.68	1.69	9.38	14.37
LP-45	2.93	11.6	471.8	0.16	1.97	-10.17	-71.01	9.14	2.13	8.69	15.62
LP-46	2.4	14.6	708.6	0.30	6.24	-9.06	-62.91	9.28	-0.12	11.01	17.49
LP-47	1.76	7.86	347.8	0.13	1.16	-8.96	-64.08	7.88	3.72	4.28	14.22

Curriculum Vitae

Juan Antonio Torres Martínez was born in Ciudad Madero, Tamaulipas, Mexico, on March 8th, 1990. He obtained a bachelor's degree in Civil Engineering at the Universidad Michoacana de San Nicolás de Hidalgo in 2014. During his bachelor's education, he worked on the characterization of historical drought events and estimation of its effects, considering climate change predictions. In 2016, he obtained a Master's in Science degree in Environmental Systems from the Tecnológico de Monterrey. During his Master's education, he worked on a groundwater flow model in Mexico's coastal aquifer at the Water Center for Latin America and the Caribbean. In 2017 he joined the doctoral program of the School of Engineering and Sciences at Tecnológico de Monterrey. His research was focused on groundwater quality issues (nitrate and sulfate pollution) in semi-arid zones of Northern Mexico, mainly using isotopic tools and Bayesian models. Throughout his Ph.D., he (co-) authored five articles and five conference papers in international peer-reviewed journals.

Publication list

Torres-Martínez, J.A., Mahlknecht, J., Hernández-Antonio, A., Mora, A., 2017. *Origin of the salinity in the coastal aquifer of La Paz, Mexico*. Procedia Earth and Planetary Science, Vol. 17, 520-523. DOI: 10.1016/j.proeps.2016.12.131

Hernández-Antonio, A., Mahlknecht, J., Mora, A., **Torres-Martínez, J.A.**, Ramírez-Orozco, A.I., 2017. *Geochemistry and Hydrothermal Contamination of the Atemajac-toluquilla Groundwater System (Guadalajara, Mexico).* Procedia Earth and Planetary Science, Vol. 17, 822-825. DOI: 10.1016/j.proeps.2017.01.051

Mahlknecht, J., Daesslé, L.W., Esteller, M.V., **Torres-Martínez, J.A.**, Mora, A., 2018. *Groundwater Flow Processes and Human Impact along the Arid US-Mexican Border, Evidenced by Environmental Tracers: The Case of Tecate, Baja California*. International Journal of Environmental Research and Public Health, Vol. 15 (5), 887. DOI: 10.3390/ijerph15050887

Mora, A., Mahlknecht, J., **Torres-Martínez, A.**, 2018. *Evolution and multivariable analysis of trace elements in groundwater of an agricultural area in a semi-arid region of Mexico*. Energy Procedia, Vol. 153, 196-201. DOI: 10.1016/j.egypro.2018.10.007

Torres-Martinez, J.A., Mora, A., Ramos-Leal, J.A., Morán-Ramírez, J., Arango-Galván, C., Mahlknecht, J., 2019. *Constraining a density-dependent flow model with the transient electromagnetic method in a coastal aquifer in Mexico to assess seawater intrusion*. Hydrogeology Journal, Vol. 27, 2955-2972. DOI: 10.1007/s10040-019-02024-w

Torres-Martínez, J.A., Dorjderem, B., Mahlknecht, J., 2020. *Revisiting groundwater chemical processes in a rapidly urbanizing basin*. Energy Reports, Vol. 6, 868-873. DOI: 10.1016/j.egyr.2019.11.021

Dorjderem, B., **Torres-Martínez, J.A.**, Mahlknecht, J., 2020. *Intensive long-term pumping in the Principal-Lagunera Region aquifer (Mexico) causing heavy impact on groundwater quality.* Energy Reports, Vol. 6, 862-867. DOI: 10.1016/j.egyr.2019.11.020

Torres-Martínez, J.A., Mora, A., Knappett, P.S.K., Ornelas-Soto, N., Mahlknecht, J., 2020. *Tracking nitrate and sulfate sources in groundwater of an urbanized valley using a multi-tracer approach combined with a Bayesian isotope mixing model*. Water Research, Vol. 182, 115962. DOI: 10.1016/j.watres.2020.115962

Torres-Martínez, J.A., Mora, A., Mahlknecht, J., Daesslé, L.W., Cervantes-Avilés, P.A., Ledesma-Ruiz, R., 2020. Estimation of nitrate pollution sources and transformations in groundwater of an intensive livestock-agricultural area (Comarca Lagunera), combining major ions, stable isotopes and MixSIAR model. Environmental Pollution, In Press, 115445. DOI: 10.1016/j.envpol.2020.115445

Torres-Martínez, J.A., Mora, A., Mahlknecht, J., Kaown, D., Barceló, D., 2020. *Determining nitrate and sulfate pollution sources and transformations in a coastal aquifer impacted by seawater intrusion—A multi-isotopic approach combined with self-organizing maps and a Bayesian mixing model.* In review.